REPORT

OF

PORT AND HARBOUR TECHNICAL RESEARCH INSTITUTE

REPORT NO. 8

Wave Forces on a Vertical Circular Cylinder :
Experiments and a Proposed Method
of Waev Force Computation.

by

Yoshimi Goda

August 1964

PORT AND HARBOUR TECHNICAL RESEARCH INSTITUTE
MINISTRY OF TRANSPORTATION

162 Kawama Yokosuka-City Kanagawa-Prefecture, Japan

TABLE OF CONTENTS

Page

SYNOPSIS 5

I. INTRODUCTION 7

1.1 Background of the Study 7

1.2 Basic Concepts of Wave Forces on a Cylinder 8

1.3 Brief Discussions of Previous Studies 9

II. EXPERIMENTAL APPARATUS AND PROCEDURE 11

2.1 Purposes and Scope of the Experiment 11

2.2 Experimental Apparatus 12

2.3 Experimental Runs and Procedure of Data Analysis 17

III. PRESENTATION AND DISCUSSION OF EXPERIMENTAL RESULTS 18

3.1 Breaking Wave Heights on Gently Inclined Bottom 18

3.2 Height of Wave Crest Elevation 22

3.3 Magnitudes and Distributions of Horizontal Particle Velocities 26

3.4 Drag Coefficient of a Circular Cylinder 30

3.5 Virtual Mass Coefficient of a Circular Cylinder 33

3.6 Maximum Wave Force Moment 36

IV. A COMPUTATION METHOD OF WAVE FORCE ON A VERTICAL CIRCULAR CYLINDER 37

4.1 Selection of Design Wave and Water Depth 37

4.2 Drag Force and Its Moment 39

4.3 Virtual Mass Force and Its Moment 44

4.4 Total Wave Force and Its Moment 47

4.5 An Example of Wave Force Design 49

4.6 Remarks on the Design of Piling Subject to Wave Action 52

V. CONCLUSIONS 55

ACKNOWLEDGEMENT 56

REFERENCES 56

APPENDICES: Tables of Experimental Data 60

Figures of Typical Wave Profiles and Orbital Velocity Distributions under Wave Crests and Troughs 66

LIST OF FIGURES*, PHOTOGRARHS, AND TABLES

Figure No. **Page**

1. Sketch of Stream Lines around a Circular Cylinder 8
2. Sketch of Wave Channel and Instrumentations 12
3. Test Pile Arrangement 15
4. Wave Gages Arrangement for Test of Breaking Waves 19
5. Profiles of Breaking Waves 20
6. Relative Breaking Wave Height H_b/h_b vs. Relative Depth h_b/L_A 22
7. Ratio of Wave Crest Height to Wave Height η_c/H vs. Wave Steepness H/L_A 23
8. Relative Height of Wave Crest above the Bottom h_c/h vs. Relative Wave Height H/h ... 24
9. Comparison of Proposed Index for Wave Crest Elevation with BEB Data (after Bretschneider 1958) 25
10. Lake Okeechobee Data on Wave Crest Elevation (after Bretschneider 1958) 25
11. Comparison of Measured Orbital Velocities with Calculated Ones under Wave Crests at Mean Water Level 29
12. Drag Coefficient Based on Actual Velocity Distributions C_D vs. Reynolds Number R_e ... 30
13. Apparent Drag Coefficient associated with Small Amplitude Wave Theory C_D' vs. Relative Depth h/L_A 32
14. Virtual Mass Coefficient C_M vs. Relative Depth h/L_A 34
15. Comparison of Maximum Moment with Moments of Maximum Drag and Virtual Mass Forces 37
16. Limiting Wave Height for a Given Wave Period at a Given Water Depth 39
17. Design Diagram for Orbital Velocity under Wave Crest at $z=0$ and $0.5h$ 40
18. Design Diagram for Orbital Velocity under Wave Creast at $z=h$ 41
19. Design Diagram for Orbital Velocity at Wave Crest, $z=h_c$ 42
20. Drag Force Factor K_D for a Uniform Vertical Cylinder 43
21. Effective Lever Arm S_D for Maximum Drag Force 43
22. Design Diagram for Water Particle Acceleration 45
23. Virtual Mass Force Factor K_M for a Uniform Vertical Cylinder 46
24. Effectiye Lever Arm S_M for Maximum Virtual Mass Force 47
25. Comparison of Calculated Maximum Moments with Measured Ones 48
26. Comparison of Calculated Maximum Forces with Experimental Ones (after Harleman and Shapiro 1955) 49
27. Design Diagram for Relative Depth, h/L_A 50
28. Critical Value of H/D for $(F_D)_{max}=(F_M)_{max}$ 55

A-1 through A-18

Typical Wave Profiles and Orbital Velocity Distributions under Wave Crests and Troughs ..... 66～74

Photo. No. **Page**

1. Miniature Current Meter and Holding Frame ····13
2. Arrangement of Wave Gage, Test Pile, and Current Meters····14
3. A View of Experimental Run ····14
4. Pivot Bearing for Test Pile ····15
5. Records of Wave Profile, Orbital Velocities, and Wave Force Moment (Case No. 4 6)···16
6. Breaking Wave of Spilling Type with a Small Curling ····21

Table No. **Page**

1. Proposed Breaker Index and Maximum Velocity Factor····28
2. Virtual Mass Coefficient Based on Diffraction Theory ····54

A-1 Wave Characteristics and Wave Force Data ····60

A-2 Breaking Wave Characteristics ····64

A-3 Harmonic Analysis of Test Wave for Determination of Virtual Mass Coefficient. ····65

LIST OF SYMBOLS*

a_n=amplitude of n-th component wave of cosine terms
b_n=amplitude of n-th component wave of sine terms
C_D=drag coefficient
C_M=virtual mass coefficient
D=diameter of cylinder
F_D=drag force
F_M=virtual mass force
F_T=total force
g=acceleration of gravity ($=9.80\ \mathrm{m/sec^2}$)
h=water depth
h_1=initial water depth at uniform section of wave channel
h_b=water depth at breaking point
h_c=height of wave crest above sea bottom
H=wave height
H_b=breaking wave height

* Only the most commonly used notations are defined here. Notations not generaly used throughout the study are defined only in their place of usage.

i =slope of sea bottom
k =wave number $(=2\pi/L)$
K =velocity correction factor
K_D=non-dimensional factor for maximum drag force
K_M=non-dimensional factor for maximum virtual mass force
L_A=wave length of small amplitude wave
M_D=moment of drag force
M_M=moment of virtual mass force
R_e=Reynolds number $(=u^*D/\nu)$
S_D=arm length of maximum drag force measured from sea bottom
S_M=arm length of maximum virtual mass force measured from sea bottom
t =time
T =wave period
u =horizontal component of water particle orbital velocity
u^*=orbital velocity under wave crest at mean water level
w =specific weight of water
x =horizontal coordinate
z =vertical coordinate measured upward from sea bottom
α =depth factor for velocity correction factor
η =elevation of water surface from mean water level
ν =kinematic viscosity of water
π =constant $(=3.14159\cdots\cdots)$
σ =angular frequency $(=2\pi/T)$

Wave Forces on a Vertical Circular Cylinder: Experiments and a Proposed Method of Wave Force Computation

By Yoshimi Goda*

Synopsis

The analysis of the wave forces acting on piles is very important for the design of offshore structures such as oil-drilling platforms. Since the analysis requires good informations on the orbital velocities of water particles and the drag coefficient of cylinders, large scale tests have been conducted in a wave channel of 105 m in length with test piles of 7.62 and 13.98 cm in diameter. The drag coefficient of a circular cylinder under the wave action was determined from the moments of wave forces with the actual orbital velocities directly measured, showing almost the same value with the drag coefficient in steady state flow. The limiting wave height on a gently inclined bottom of 1 to 100, the elevations of wave crests above the mean water level, and the virtual mass coefficient of a circular cylinder were also investigated in the experiment.

Based upon the results of the experiment and other investigations, a computation method of the wave forces on a vertical cylinder has been prepared and presented in this report. The wave forces calculated with this method showed good agreements with experimental data of the present author and others. For a vertical pile of uniform section, several design diagrams are available for convenience of the wave force design.

* Chief of Model Test Section, Hydraulics Division, Sc. M

要　　旨

直円柱に作用るす波力の実験ならびに波力算定方式(試案)について

水工部　　合　田　良　実

近年，海底資源の開発や洋上の燈標建設などの目的で，鋼管やコンクリート管を使った柱状構造物が洋上に建設されることが多く見られる。こうした構造物は，一般に激しい波力を受けるので，波力に対して十分安全なように設計されなければならないが，その基礎となる波力の算定方式は未だ十分に確立されているとは言い難い。波力の算定にあたっては，波による水粒子の運動速度や円柱，角柱などの抗力・質量係数の値を正確に知る必要がある。このため，当所においては数年前より長さ 105mの大型造波水路を使用して，直径 7.62 及び 13.98cmの直円柱に作用する波力の実験を行なって来た。この実験においては，数台の小型プロペラ流速計を鉛直に並べて，水粒子速度の同時測定を行ない，これによって得られた実際の水粒子速度の鉛直分布と直円柱に作用する波力との比較から，波浪中の円柱の抗力係数を決定した。この結果，レイノルズ数が1×10^4から2.1×10^5 の範囲では，波浪中の円柱の抗力係数も定常流における値とほぼ等しい値を取ることが判明した。質量係数については，微小振幅波としての粒子加速度を用いた値として平均1.71を得たが，構造物の設計ではポテンシャル理論による 2.0 の値の採用が望ましいと考えられる。

一方波力と同時に得られた波形記録から，波峯の上昇高が求められ，水深波長比が0.05から 0.5 までの中間領域については，波峯の上昇高が波高水深比でほぼ一義的に与えられことが示された。また，設計外力として必要な最大波高の資料として，勾配 1/100 の斜面上における砕波高についても実験が行なわれ，種々の理論値などと比較検討することによって，限界波高が水深波長比の関数として求められた。

これらの実験データや他の研究成果などに基いて，直円柱に作用する波力の算定方式の一試案が作成された。この試案は，ゆるやかな勾配の海底面から直立した円柱に，砕波限界以下の波高の波が作用した時に生ずる最大波力及びそのモーメントを求めるためのものである。この方式によって算定された波力の最大値は，当所及び他機関で得られた実験値とほぼ一致した。なお，一様断面の直柱については数種の設計図表が示されている。

I. INTRODUCTION

1.1 Background of the Study

Since the end of the World War II, many new structures have been erected in the sea off the shore. Best examples are oil-drilling platforms which have been constructed to explore the petroleum resources under the ocean bottoms. One of these movable platforms for the oil-drilling, called the Hakuryu (white dragon in Japanese), has been under operation along the northern coast of the Sea of Japan since 1958. Other examples of offshore structures are the platforms for radar stations and those for lighthouses amid the ocean. Such a movement of structure building into the ocean is a big challenge for engineers, because these structures in the sea are frequently attacked by strong winds and huge waves and they must be designed strong enough to withstand the combined forces of winds and waves with moderate construction costs. A failure of an offshore structures often results in the loss of tremendous amount of money and in some cases in the loss of human lives as illustrated in the collapse of Texas Tower No. 4 off the Atlantic Coast of the United States.

An offsore structure is mostly constructed with circular cylinders, vertical, horizontal, and diagonal, which are combined into spatial frame works. One of the advantages of a circular cylinder is the fact that it experiences less forces under the wave action than a cylinder of other shape does, in addition to its equal strength against the force applied from any direction. For example, Morison, Johnson, and O'Brien 1953 showed experimentally that the moment of the wave force on a H-section pile is $1.42 \sim 3.50$ times the moment on a circular pile with the same projected area.

Among many cylindrical members for an offshore structure, the most important ones are the vertical cylinders which are employed to withstand the bending moment of the wave force principally. The use of a single vertical pile is also common for a stove pipe to protect an oil pipe from wave actions or for other purposes. Hence it becomes very important to analyse the wave force on a vertical cylinder correctly and to estimate its magnitude properly, before one can design an offshore structure successfully. The present report is intended to provide a reasonable designing method for a vertical circular cylinder subject to severe wave actions. The materials presented herein are mostly based on the resulte of the experiments conducted in a large wave channel (105 m long) at the Port and Harbour Technical Research Institute, supplemented with theoretical and experimental data obtained by other investigators.

1.2 Basic Concepts of Wave Forces on a Cylinder

The nature of wave force on a cylinder is quite different from the nature of wave pressure on a veritcal wall. The wave pressure on a vertical wall is either due to hydrostatic pressure of standing waves caused by the reflection of waves at the wall, or due to dynamic pressure of breaking waves caused by the collision of water mass to the wall. In the case of cylindrical objects, however, waves continue to propagate by the cylinders with only partial reflection or partial collision.

The wave force on a cylinder is primarily originated from the fact that the stream lines around a cylinder are deformed by the presence of the cylinder itself. The deformation of stream lines causes the occurrence of two types of forces.

The first force is the result of the wake zone formation behind the cylinder and the frictional stress around it. In the ideal fluid, the flow pattern is symmetric

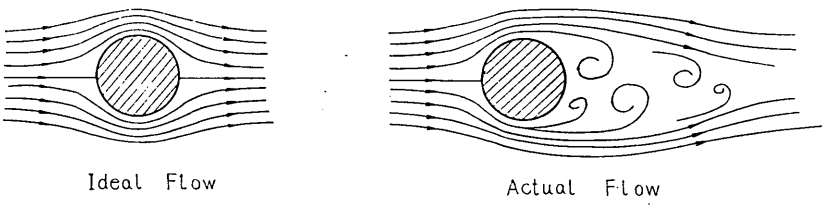

Fig. 1. Sketch of Stream Lines around a Circular Cylinder

around the cylinder, producing no net force on the cylinder in the steady state flow. In the actual flow, however, the stream lines tend to be separated from the periphery of the cylinder because of the viscosity presented, thus forming a wake zone in the rear of the cylinder as sketched in Fig. 1. Since the pressure is lower in the wake zone than in the front and the frictional force is also present, a net force is produced toward the downstream. This force is called the drag force and denoted by F_D in this report. For a cylinder of diameter D and length ds, the drag force is expressed as:

$$dF_D=C_D\frac{w}{2g}Du^2ds \quad \cdots\cdots(1)$$

where C_D is called the drag coefficient, w is the specific weight of water, g is acceleration of gravity, and u is the undisturbed velocity of the flow. As might be seen from the nature of the drag force, the magnitude of C_D depends upon the shape of the cylinder and a Reynolds Number, uD/ν, where ν is the kinematic viscosity of the fluid.

The second force is the result of the stream lines deformation itself. When the flow is accelerated or decelerated, the stream lines are deformed from time to time. Since some force is required to deform stream lines or to vary velocity vectors around a cylinder, the force must be worked out by the cylinder and the cylinder in turn

must experience that force. Such force is called the intertia force or virtual mass force and denoted by F_M in this report. For a cirular cylinder of diameter D and length of ds, the virtual mass force is expressed as:

$$dF_M = C_M \frac{w}{g} \frac{\pi D^2}{4} \frac{\partial u}{\partial t} ds \quad \cdots\cdots (2)$$

where C_M is a coefficient called the virtual mass coefficient.

As seen in the nature of these forces, the drag force appears in its pure form in a steady state flow, whereas the pure form of the virtual mass force is seen in the flow with pure acceleration or in a potential flow. The motion of a water particles under the wave action is that of unsteady oscillating flow, however. Both vectors of velocity and acceleration vary from time to time and from point to point. To handle such a complicated kinematic field, Morison et. al. 1950 analysed the wave force on a vertical circular pile as the sum of the drag force and the virtual mass force with the instantaneous velocity and acceleration: i.e.,

$$dF_T = dF_D + dF_M \quad \cdots\cdots (3)$$

Once the coefficients of drag and virtual mass are properly evaluated, this method can give a reasonable estimate for the wave forces on cylinders. For this reason the method to separate the total wave force into the drag force and the virtual mass force have heen employed by many investigators for the analysis of laboratory and field data of wave force measurements, and it is also the approach taken in this study.

1.3 Brief Discussions of Previous Studies

The first systematic study of the wave force on piles was undertaken by Morison et. al. 1950 at the University of California. Separating the total wave force into the drag force and virtual mass force, they employed the theory of small amplitude waves to estimate the velocities and accelerations of water particles under the wave action. The coefficients of drag and virtual mass were then evaluated with these velocities and accelerations of small amplitude waves. The results of this study yielded a design method of piling which was presented by Morison 1951 at the First Conference on Coastal Engineering. The study was then continued to investigate the effect of the cross sectional shape of a cylinder on the wave force acting on it, the influence of neighboring cylinders, and the wave forces on a cylinder with a varying diameter (see Morison et. al. 1953). Although these studies were the great step forward for the analysis of the wave force problems on piles, the inherent weakness of this approach was the employment of the small amplitude wave theory as its theoretical basis. The design waves against which piles are to be designed are very large in heights, far beyond the range of the wave height in which the small amplitude wave theory may reasonably be applied. The effects of high amplitude

were all included in the terms of the drag and virtual mass coefficients.

In order to take the effect of finite amplitude into consideration for the design of piling, Reid and Bretschneider 1953, and Bretschneider 1958 prepared several design diagrams with which engineers may estimate the rise of the water surface at the wave crest, the increase of wave length with the increasing wave height, and maximum values of total drag and virtual mass forces on a vertical circular cylinder. These informations are essentially dependent upon the characteristics of finite amplitude waves. Reid and Bretschneider applied the method of interpolation ingeneously to construct their diagrams from then-available theories of finite amplitude waves: i. e., Michell-Havelock's highest wave in deep water, Stokes' waves with relatively small amplitudes and the solitary wave in shallow water. Because of the broad coverages and convenient forms for practical design applications, the use of these design diargams seems to be accepted as the standard design method in the United States (see References 1 and 26). These design diagrams, however, are to be refined with the results of developements of finite amplitude wave theories and laboratory investigations. The computation of Stokes' wave to higher order terms such as the fifth order wave table by Skjelbreia and Hendrickson 1962 will be very helpful for this purpose.

The remaining question in the problem of piling is the magnitudes of the drag coefficient and virtual mass coefficient. Since most of pile diameters are quite small in comparison to the design wave heights, the drag force is predominant in most cases. Thus much emphasis have been placed on the determination of the drag coefficient for a circular cylinder under the wave action. The drag coefficient associated with the small amplitude wave theory has been studied by Wiegel, Beebe, and Moon 1957 after Morison et. al. Wiegel and others conducted field tests of wave forces on circular piles of which diameters ranged from 16.6 cm to 1.52 m. The analysis of the drag coefficient with a Stokes wave theory was carried out by Harleman and Shapiro 1955. Reid 1957 correlated the record of the wave force on a prototype pile to the irregular water level variation with an elaborate technique to find out the drag coefficient. Other types of tests to investigate the effect of acceleration on the drag coefficient have also been conducted by Laird, Johnson, and Walker 1959, showing almost the same drag coefficient in accelerated flow as that in steady flow.

Despite of these field and laboratory tests, no attempt seems to have been made to correlate the drag coefficient with the actual velocities of water particles under wave actions. Once the record of wave forces were correlated with the wave profile and the actual velocity distribution directly measured, the true nature of the drag coefficient of a circular cylinder under the wave action would have been revealed. To

obtain the actual drag coefficient, a large scale test has been conducted in the present study with six miniature current meters.

It may be worth while to mention that a different approach to the problem of wave forces on a cylinder has been taken by Crook 1955 after Iversen and Balent 1951; they proposed the use of a single resistance coefficient for a cylinder in accelerated flow. The practical application of this approach for the actual designs of pilings has not been fully explored and it does not seem to be promising to the present author.

II. EXPERIMENTAL APPARATUS AND PROCEDURE

2.1 Purposes and Scope of the Experiment

As discussed in the preceding section, the experiment was primarily concerned with the determination of the actual drag coefficient based upon the measurements of velocity distributions in a large wave channel.

The use of the large wave channel was also decided from the standpoint of the high Reynolds number possible in the channel. In prototype conditions the Reynolds number is in the range of 10^6 to 10^7, but few informations in such supercritical range of the Reynolds number were then available at the planning stage of the study. Thus the value of the Reynolds number as high as possible was sought in the experiment. With test cylinders of 7.62 cm and 13.98 cm in diameter, the Reynolds number of 10^4 to 2×10^5 was obtained.

The second purpose of the experiment was to make a comprehensive test of the wave force on a vertical cylinder for the full range of water waves so that the reliable design data on the wave force could be obtained. In order to fulfil this purpose, the periods of the test waves were controlled in such a manner that the relative depth, h/L_A[1], or the ratio of the water depth to the lenght of small amplitude wave, would be one of seven values of 0.05, 0.07, 0.10, 0.14, 0.2, 0.3, and 0.5. Since several water depths from 1.00 m to 2.00 m were employed to compare the data at different depths, the wave period was varied at different water depths to give the same relative depth; the range of the wave period tested was from 1.5 to 7.9 sec. The wave height was also varied from the minimum values of about 10 cm to the highest ones possible without breaking; the maximum wave height tested was 80 cm. Such arrangements of wave periods, wave heights and water depth warranted the full investigation of the pile force problem.

---

1) As first shown by Airy, the length of small amplitude wave, L_A, with a period of T at the water depth of h is given by:

$$L_A=\frac{g}{2\pi}T^2\tanh 2\pi\frac{h}{L_A} \qquad (A)$$

Among several features of wave characteristics and forces on a cylinder, the followings were of the primary interest: the height of wave crest elevation, the magnitude and distribution of horizontal particle velocity, the drag coefficient, and the maximum wave force on a cylinder. The question of limiting wave height was also investigated as the breaking wave height on a gently inclined bottom with a slope of 1 to 100. The increase of wave length with the increase of wave height was not sought because it is only of minor importance on the wave force on a single pile. The measurement of water particle accelerations was not possible with the instrumentation available. Although the experiment produced the systematic data on wave profiles, these are not discussed in this report; the readers are requested to refer to the report by Tsuruta 1961.

2.2 Experimental Apparatus

The wave channel employed in the test is 105 m in length, 3.0 m in width and 2.5 m in depth, constructed in 1956 with reinforced concrete. Waves are generated with a pendulum-type wave paddle (which was set at the position of piston-type motion) driven by a high-voltage motor of 75 HP, and are absorbed on a rubble mound with a slope of 1 to 8 located at the other end of the channel. The reflected waves from the absorber are estimated as several per cent of incident waves in height at most unfavorable conditions.

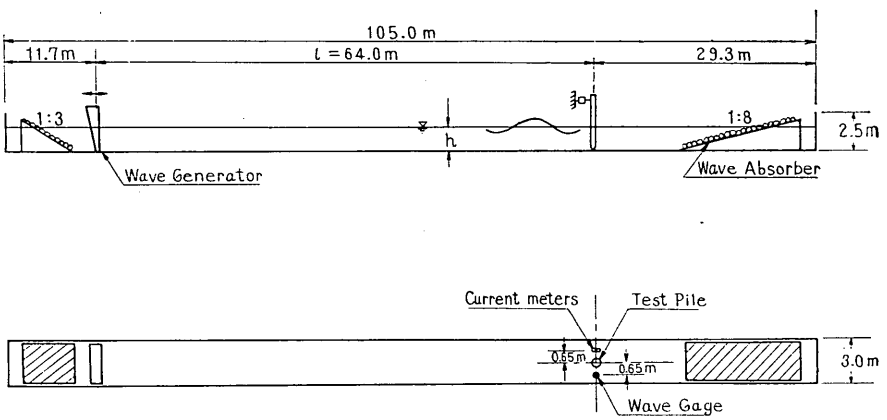

Fig. 2. Sketch of Wave Channel and Instrumentations

For most of the experiments (Case No. 1 through 54) the channel bottom was kept horizontal, but the rest of the experiments were conducted on a sloped bottom of 1 to 100. In the former tests, a test pile, a wave gage, and six current meters were located at the position 64 m away the wave generator as shown in Fig. 2. In

the latter tests the test pile and instrumentations were set at the location of 50 m from the wave generator.

The slope was constructed from the location of 29.8 m through the location of 75 m from the wave paddle, rising 50 cm from the original bottom at its end. (In the first 1.2 meter, the slope rises by 6 cm.) This slope was to produce test waves of large heights which had been unstable on the horizontal bottom. Since the slope was so gentle, the characteristics of these waves on the slope were regarded as the same with those on the horizontal bottom.

The wave gage is of resistant type gage with two parallel nickel wires. The variation of the water level varies the imersion length of nickel wires into the water, of which resistance is varied accordingly. The variation of resistance of the water between the wires is then picked up as the unbalanced current of a Wheatstone bridge, which is amplified and recorded with electro-magnetic oscillographs.

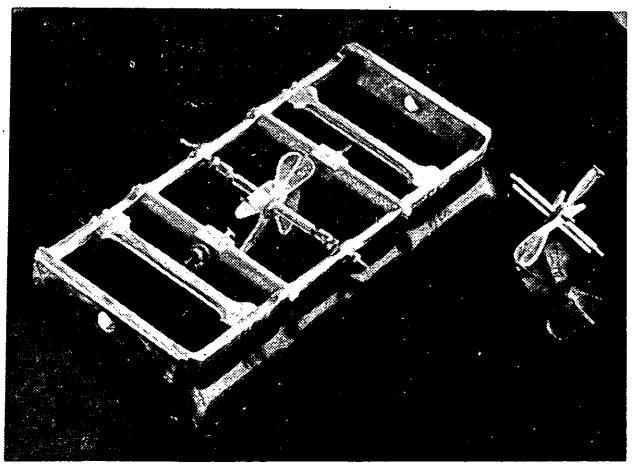

Photo. 1. Miniature Current Meter and Holding Frame

The current meters are of propeller-type with four blades made of acrylic plastics as shown in Photograph 1. The outer diameter of the propeller is 3.5 cm. In order to detect the rotation of the propeller, four electrodes connected with each other are mounted at the outer ends of the blades and two other electrodes are attached to the holding frame. A minute electric current flows one electrode of the holding frame, through the water and the electrodes of the propeller, to the opposite electrode of the holding frame. The magnitude of this current is varied as the distance between an electrode of the propeller and the electrode of the holding frame varies with the rotation of the propeller; thus each rotation of the popeller produces four pulse signals. Since the number of rotation per unit time is linearly

proportional to the velocity of current for the range of current velocity from 10 to 200cm/sec, the instantaneous velocities of water particles under wave action were obtained from the time intervals of two or four pulses.

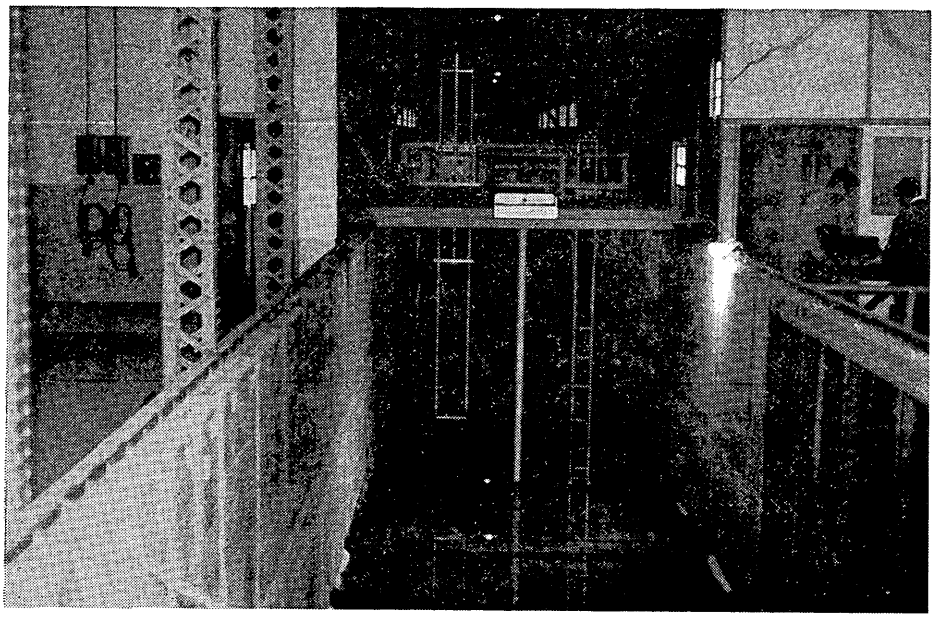

Photo. 2. Arrangement of Wave Gage, Test Pile, and Current Meters

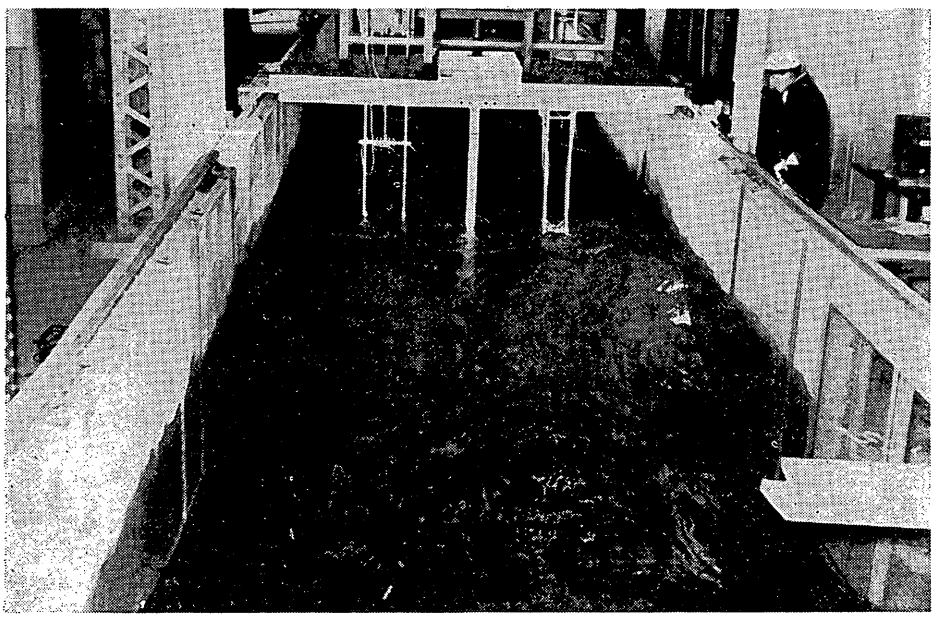

Photo. 3. A View of Experimental Run

In the experiments six of these miniature current meters were fixed at a vertical beam at intervals of 20 to 40 cm so as to measure the distributions of water particle velocities. These current meters and the wave gage were so arranged as to come into a line with the test pile at a distance of 65 cm from it towards the walls as shown in Photographs 2 and 3 (which shows the wave gage, a test pile, and current meters with a vertical beam from the left to the right).

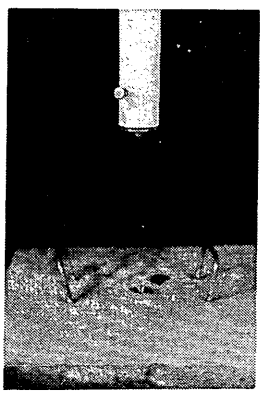

Photo. 4. Pivot Bearing for Test Pile

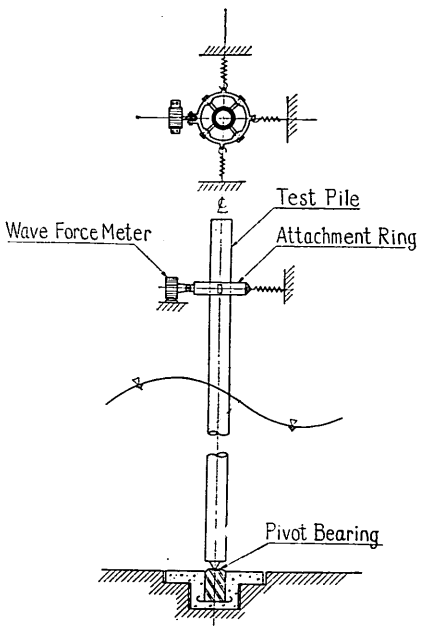

Fig. 3. Test Pile Arrangement

The test piles are steel pipes of a length of 3.2 m with diameters of 7.62 cm and 13.98 cm. The lower ends of the test piles were rested on a pivot bearing as shown in Photograph 4 so as to act as an ideal hinge, and the upper ends were connected to a load cell through an attachment ring at the height of 2.913 m from the channel bottom (see Fig. 3). The product of the measured force and the distance from the pivot to the load cell gives the moment of wave force around the bottom. The load cell utilizing resistance strain gages has a capacity of 20 kg for the tension side. To make ready for the negative forces at the time of wave troughs, an initial tension of 5 kg was introduced with a spring-screw system at the opposite side of the attachment ring to the load cell. Two more springs were also stretched laterally to prevent excessive lateral motions without interfering the measurement of the wave force moment.

All the data, the wave profile, pulse signals for orbital velocities at various elevations, and the moment of wave force, were recorded on photographic papers of

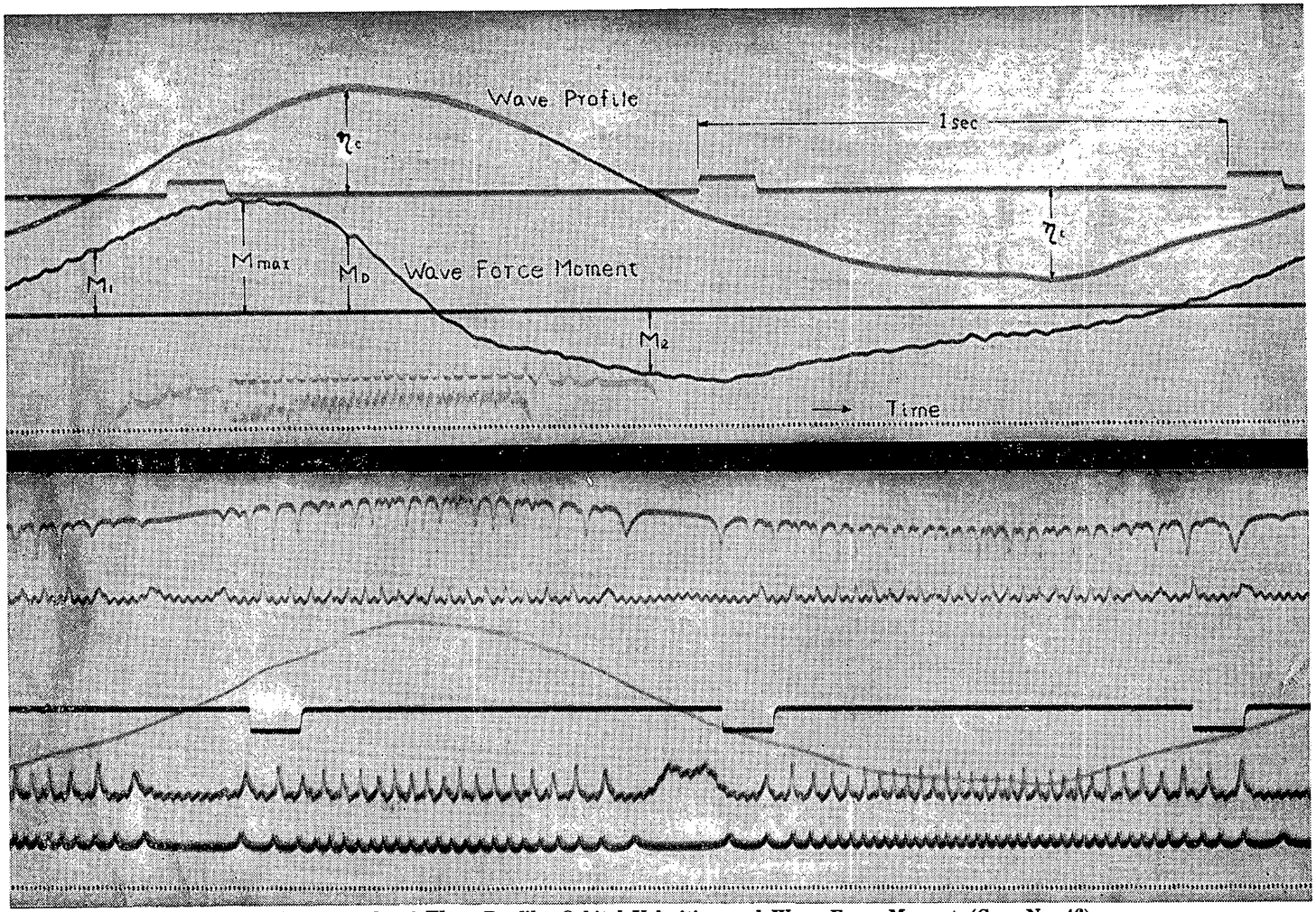

Photo. 5. Records of Wave Profile, Orbital Velocities, and Wave Force Moeut (Case No. 46)

two electro-magnetic oscillographs each having six recording elements. Photograph 5 is a typical record of experimental runs. In order to correlate the records of the two oscillographs, the records of wave profiles were made drawn on both the oscillographs at the same time.

2.3 Experimental Runs and Procedure of Data Analysis

The experiments were carried out for 80 different combinations of wave characteristics and test piles. Additional tests of 26 runs were also conducted to obtain supplementary data on wave profiles and orbital velocities. The experimental conditions and results are listed in Table A-1. In each run, the recording of the data was made for ten consecutive waves after the waves became steady since it took a few minutes to bring the motor into full rotation. The data shown in Table A-1 are the averages of these ten consecutive waves.

From the records of the experimental runs such as shown in Photogrph 5, the heights of wave crests and the depths of wave troughs are easily determined, giving the wave heights as their sums. The maximum orbital velocities at various elevations are evaluated from the closest time intervals of pulse signals. With six measurements of orbital velocities under the wave crests and troughs, the velocity distribution curves from the bottom up to the crest were drawn with a relative ease. Then, the drag coefficient being assumed constant along a cylinder (or representing the average value over the cylinder) is determined by numerically integrating Eq. 1 and comparing with the measured moment of drag force : i. e.,

$$C_D = \frac{M_D}{\frac{w}{2g} D \int_0^{h_c} u^2 z \, dz} \qquad \cdots\cdots (4)$$

where h_c is the height of the wave crest from the bottom and M_D is the moment of wave force at the passage of a wave crest. This numerical integration and the evaluation of the drag coefficient was carried out for each wave of ten consecutive waves, because of large variations in velocity distributions and wave force moments even though the wave heights did not vary more than a few per cent. The values of the drag coefficient C_D listed in Table A-1, however, are the averages of these drag coefficients for each run, not the calculated one with the average velocity distributions and the average moments.

The evaluation of the drag force moment with the moment under the crest is justified because the orbital velocity at every elevation reaches the maximum values under the crest, indicating no acceleration being present. Since the wave force is assumed to be described with the sum of the drag force and virtual mass force in the analysis, the record of the wave force moment under the crest is regarded as that of the drag force. Likewise at the times when the water surface traverses the

mean water level, the velocity is zero at every elevation as seen in Photo. 5, indicating the presence of the acceleration only. Hence the records of the wave force moment at these times, M_1 and M_2, are regarded as those of the virtual mass force. The average of these two measurements, one for rising time and the other for the falling time, is listed as the moment of the virtual mass force M_M in Table A-1. The difference between M_1 and M_2 were small: about 20 per cent for the largest ones.

Because of no available measurements on the magnitudes of water particle accelerations, the virtual mass coefficient was evaluated with the accelerations of the small amplitude waves. The small amplitude wave theory was also utilized to evaluate the apparent drag coefficient so as to make the comparison between the actual and apparent drag coefficients possible.

III. PRESENTATION AND DISCUSSION OF EXPERIMNTAL RESULTS

3.1 Breaking Wave Heights on Gently Inclined Bottom

One of the problems related to the present subject is the maximum wave height possible at a given location, since the offshore structures must be so designed to withstand the attack of the maximum waves. The limitation on the maximum wave height is imposed from two sources. The first one is the meteorological conditions which govern the growth and developement of wind waves. The second one is the kinematic condition of wave breaking. The meteorological conditions, or the maximum wind speed and its duration time, may not have the upper limit from the standpoint of the probability distribution. But the kinematic condition of wave breaking can impose the definite limit on the maximum wave height at a given location, although the limit is dependent upon the slope of the bottom, the water depth, and the wave period.

Since most of offshore structures are to be located on continental shelves, the bottom slopes at the sites of the structures are regarded to be very gentle, less than 1/100. The informations on the limiting wave heights on such gentle slopes are rather few however, although many experiments have been conducted on the wave breaking on steep slopes. In an attempt to determine the limiting wave heights for the designs of offshore structures, laboratory tests were made on the sloped bottom of 1 to 100. The water depth in front of the wave paddle was set at 1.00 m and 1.50 m. Wave gages were located at the section of uniform depth, at the location of wave breaking, and 1 m offshore of the wave breaking point. The first one was fixed at the location of 25 m from the wave paddle, but the other two were carried to and fro in seeking for breaking points for each run. These arrangements of wave gages are sketched in Fig. 4.

The judgement of the location of wave breaking was a crucial one in the experi-

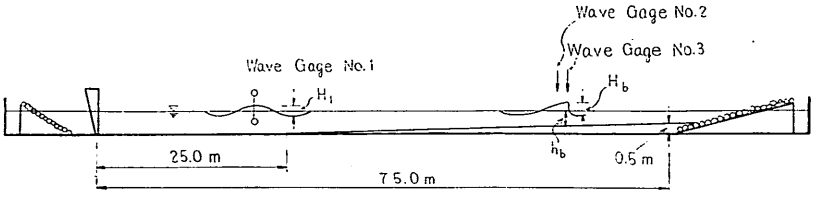

Fig. 4. Wave Gages Arrangement for Test of Breaking Waves

ments. The breaking points were not fixed but fluctuated from wave to wave over a distance of a few meters even if the offshore waves were uniform in the wave height and period. The wave records at the location of apparent wave breaking sometimes showed a variation of $\pm$ 5 % from the average in wave height: smaller wave heights seemed to belong to th waves which did not break at the site of the wave gage. Thus the average wave height even at the location of apparent wave breaking did not seem to represent the true breaking wave height. Hence one-tenth-maximum wave height of three wave records, each with ten consecutive waves, were employed as the breaking wave heights. When the wave gage No. 2 (located 1 m offshore of the breakig points) recorded larger wave heights than the wave gage No. 3 at the breaking points, the location of the gage No. 2 was judged as the breaking point and the one-tenth-maximum wave height of the gage No. 2 was taken as the breaking wave height. All the data of breaking wave characteristics are listed in Table A-2.

Examples of wave records at breaking points are shown in Fig. 5 with the results of the harmonic analysis. These wave records show the almost symmetric wave profiles with a slight leaning forward. Actual forms of breaking waves also held their symmetric profiles in most cases. Thus the breaking waves in tests were of spilling wave types with a small curling near the crests as shown in Photograph 6. Breaking waves of plunging type were not observed in the tests on a gentle slope of 1 to 100.

The results of the experiment are compiled in Fig. 6 which shows the relation of the breaking wave height H_b to the water depth at breaking point h_b against the relative water depth at the breaking point, h_b/L_A. The wave length has been calculated with Eq. A for the breaking water depth. This type of presentation was chosen because it indicates a small difference in breaking wave heights most critically, especially in the range of shallow water waves. For the same reason, the data show a rather wide scatterring. But there is little effect of the initial water depth, h_1; the data with h_1=100 cm and 150 cm follow the same trend of increasing H_b/h_b with the decreasing h_b/L_A.

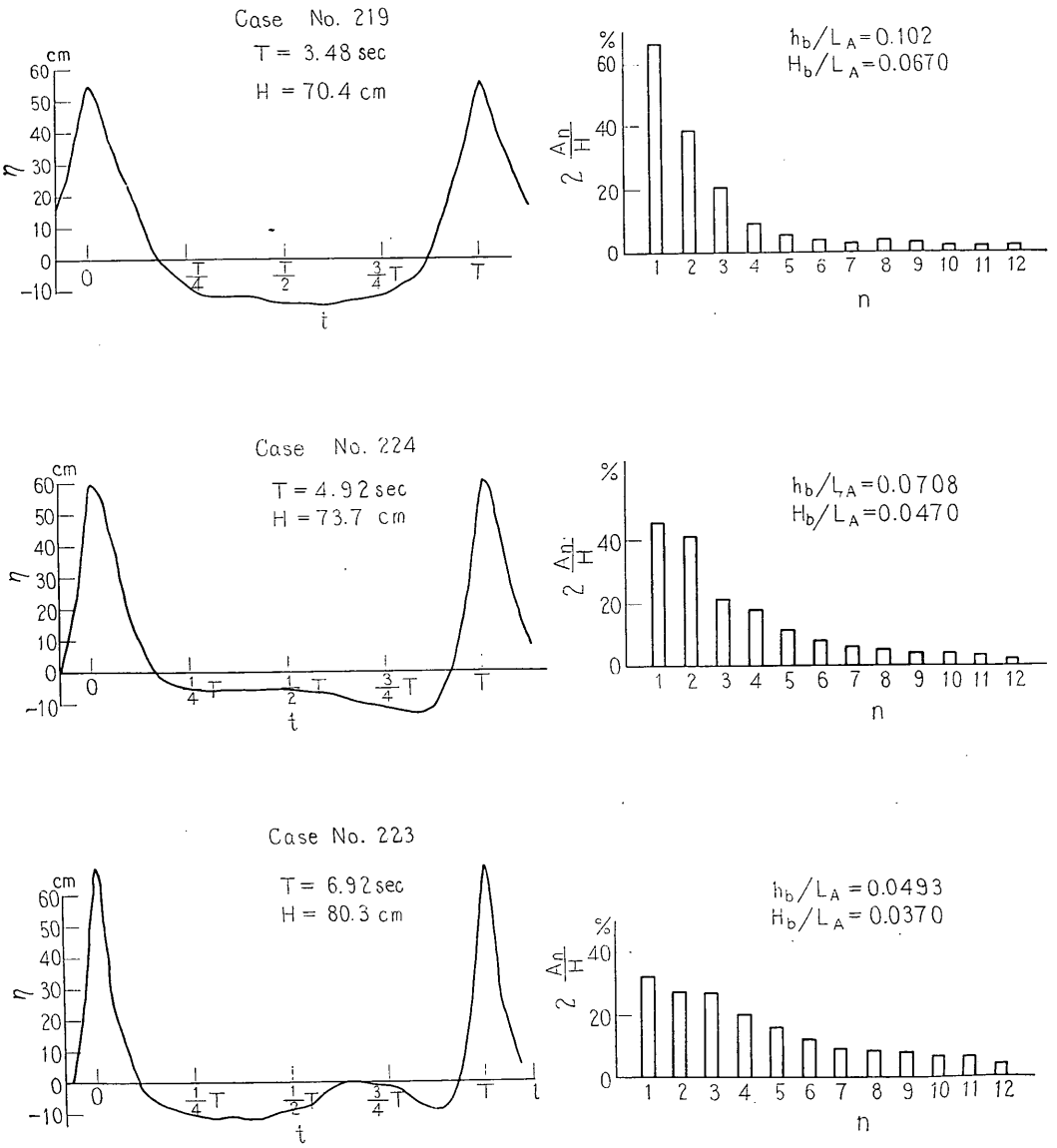

Fig. 5. Profiles of Breaking Waves

As for the theoretical values of breaker heights, those of deep water waves were investigated by Michell 1893, Havelock 1913, Yamada 1957(a) and Chappelear 1959. All the investigators employed the Stokes' criterion on wave breaking that the particle velocity at the wave crest must be equal to the wave celerity. The criterion results in the sharp crest of breaking waves with an angle of 120°. The breaking

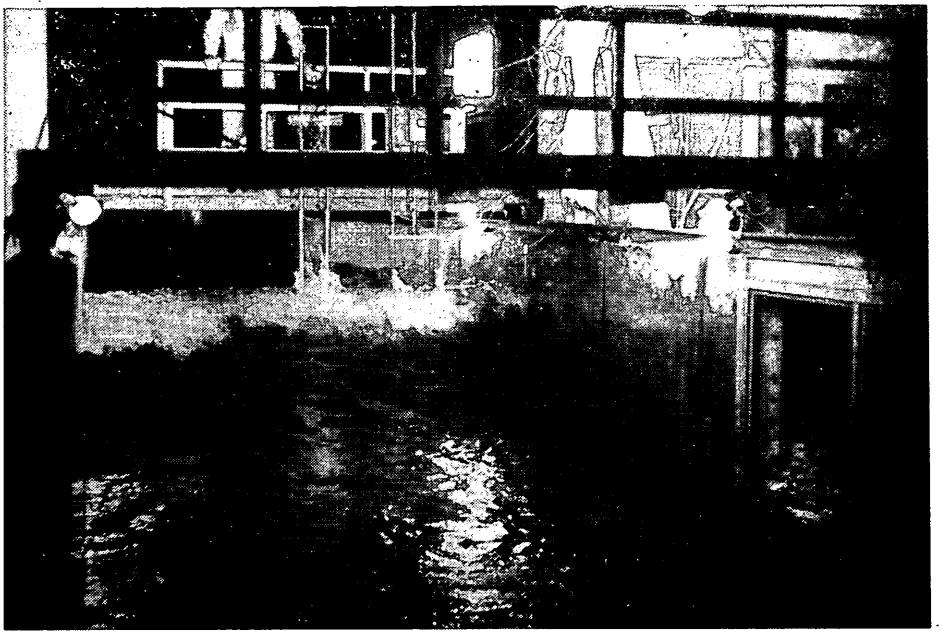

Photo. 6. Breaking Wave of Spilling Type with a Small Curling

wave heights for deep water waves thus calculated by the above investigators were about 0.142 times the wave length, and the length of breaking waves was calculated about 1.20 times that of small amplitude waves (or Airy's waves) calculated with Eq. *A*. As for the solitary wave, or the limiting wave of shallow water waves, McCowan 1894 obtained the breaking height of 0.78 times the water depth using the Stokes' criterion (see Munk 1949). Yamada 1957(b), however, improved the accuracy of the approximation and obtained the value of 0.828 for the ratio of the breaking wave height to the water depth. Laitone 1960 used a different criterion for wave breaking based upon the vertical velocity variation and obtained the limiting value of 0.727 for H_b/h_b. As for the intermediate depth waves, the Stokes' criterion was used by Chappelear 1959 and Yamada 1958. Chappelear's computation was carried out to the waves with the relative depth of $h/L_A=0.0819$ and the results are shown in Fig. 6. But the data at the shallower portion seem to be not accurate enough. Yamada's computation is for the wave with the relative depth of $h/L_A=0.337$; the limiting wave height for this wave was found to be 0.440 times the water depth.

Taking these theoretical breaker heights into consideration, a proposed breaker index has been determined as shown with the dashed line in Fig. 6. Since the experimental data show much higher breaker heights than the theoretical value of Laitone, his criterion for the limting wave height was not considered acceptable and

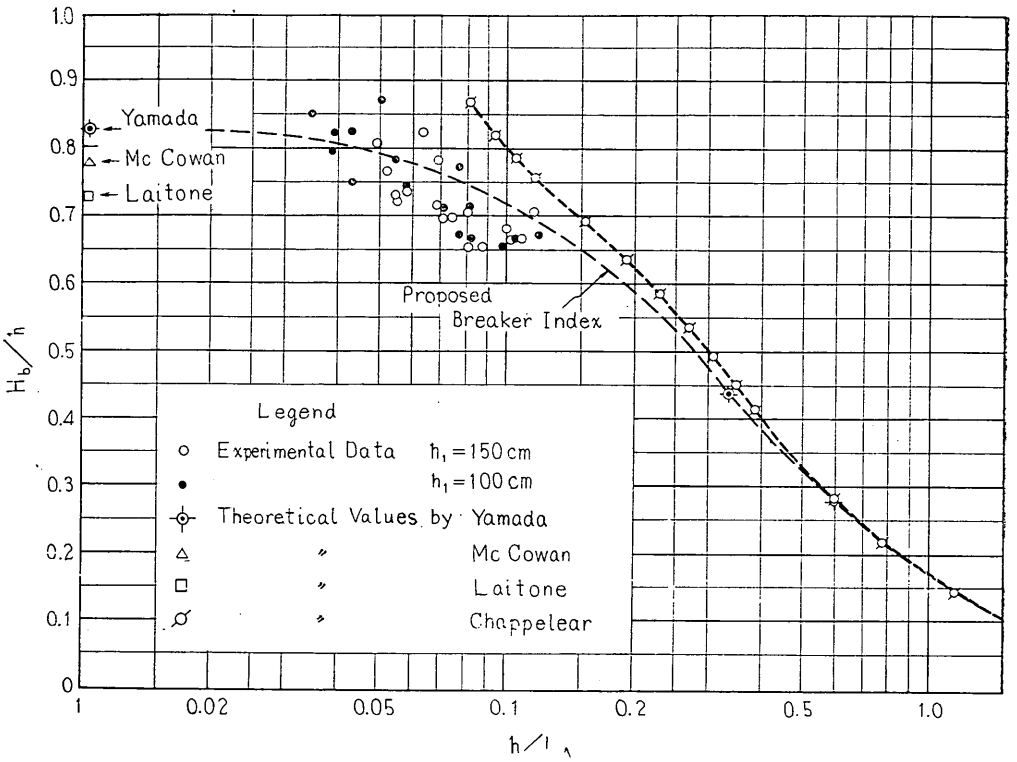

Fig. 6. Relative Breaking Wave Height H_b/h_b vs. Relative Depth h_b/L_A

the computations with the Stokes' criterion were referred to in drawing the proposed breaker index. As for the region of very shallow water, the result by Yamada was taken as the reference. In the range of h/L_A from 0.03 to 0.12, the experimental data provided the basis of the breaker index. From the range of h/L_A deeper than 0.12, the theoretical values of Yamada and Chappelear were referred to. The breaker index proposed herein is slightly larger in the shallow water region than that proposed by Bretschneider 1958, since he employed the value of $H_b/h_b=0.78$ by McCowan as the reference. The present breaker index should be used for the waves on the sea with the bottom slope smaller than 1 to 100. The breaker heights on steep slopes are expected to be larger than those given by the present breaker index. For such cases, Iversen's experimental data 1952 should be referred to, instead.

3.2 Height of Wave Crest Elevation

The experimental data on the wave crest height were obtained from the wave records at the site of the test piles and from the records of breaking waves. Since the calibration of the wave gages were taken from the still water level as the datum

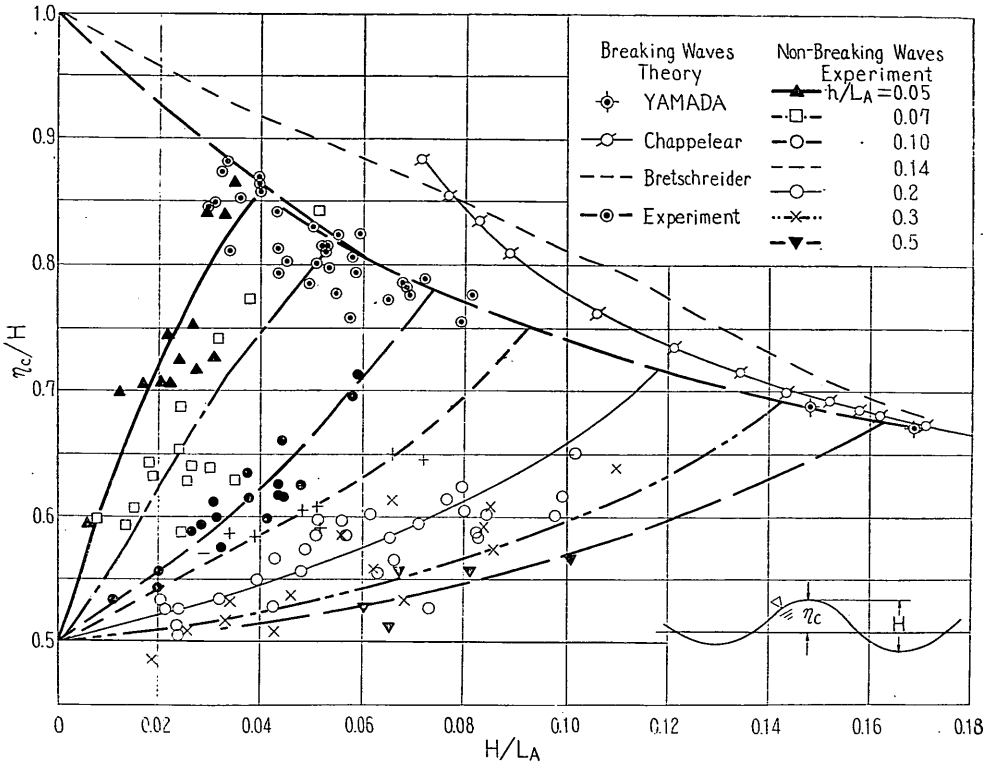

Fig. 7. Ratio of Wave Crest Height to Wave Height $\eta c/H$ vs. Wave Steepness H/L_A

line, the heights of wave crest elevations were easily obtained from the wave records. Figure 7 shows the ratio of wave crest height above the mean water level to the wave height against the wave steepness. The parameter is the relative depth, h/L_A. Although the data show some scattering, each group of data with the same relative depth indicates a common trend of increasing η_c/H with increasing wave steepness, thus enabling to construct a design diagram for the wave crest elevation. The data of breaking waves were also employed to determine the breaker index.

The breaker index for the crest elevation presented herein is smaller than those of Bretschneider's calculation and Chappelear's computation. The reason for the smallness of experimental crest elevations of breaking waves is considered as due to the small breaker heights in comparison to their breaker indexes in Fig. 6. The formation of the secondary wave crests at the troughs of some test waves in the shallow water region might have reduced the relative crest height of η_c/H; the wave height H is the sum of the crest height η_c and the trough depth η_t which would have been deepened at the lowest point of wave profile with the formation of secondary wave crest. The crest elevations of non-breaking waves tested were about the

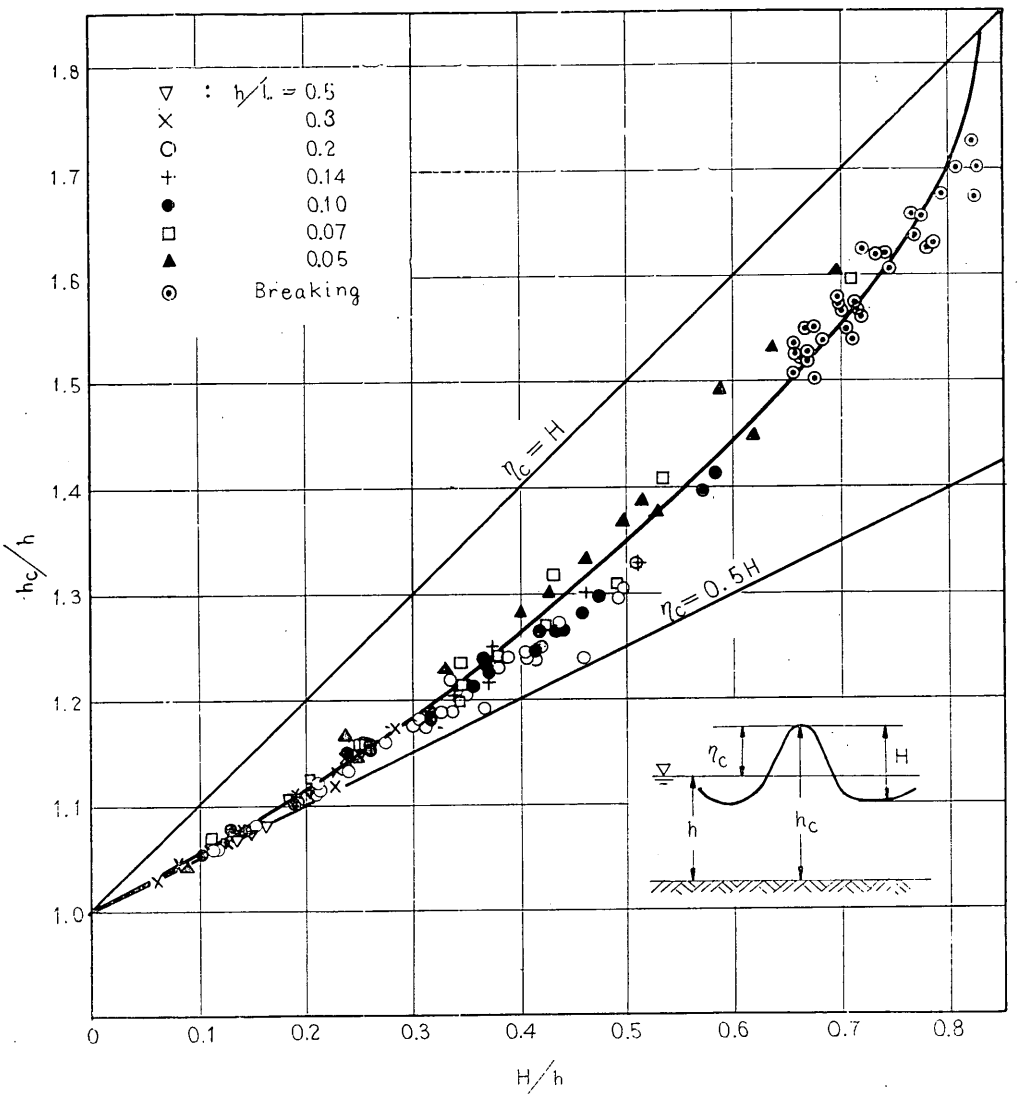

Fig. 8. Relative Height of Wave Crest above Bottom h_c/h vs. Relative Wave Height H/h

same with the experimental data obtained in a large wave channel of the Beach Erosion Board of the U.S. Army, Corps of Engineers, reported by Bretschneider 1958. But the data obtained at B. E. B. had rather large scatterings; thus a detailed comparison of the two experimental data was not possible.

Although the nature of the wave crest elevation is best seen in the form of Fig. 7, a more convenient form of presentation may be constructed for the practical use of piling design because the absolute height of the wave crest above the bottom

rather than the ratio of the wave crest to the wave height is sought in actual designs of piling. Figure 8 has been prepared for this purpose; the height of the wave crest above the bottom in terms of the mean water depth is plotted aginst the wave height in terms of the mean water depth. In this form of presentation, all the experimental data gather themselves around one curve regardless of the relative depth. Thus, the height of the wave crest above the botom may be estimated with only the informations of the wave height and the water depth.

Such an uniformity of the experimental data is partly due to the fact that the ratio of h_c/h must be located between the two extreme lines of $(1+H/h)$ for the solitary wave and of $(1+H/2h)$ for the Airy's waves, or the small amplitude waves. Since the difference between the two extreme lines is not so large, the magnitude of scattering of the experimental data is diminished accordingly, thus giving an uniform look of the experimental data. But another reason might be attributed to an important role of the parameter H/h in the regions of the intermediate depth water and shallow water.

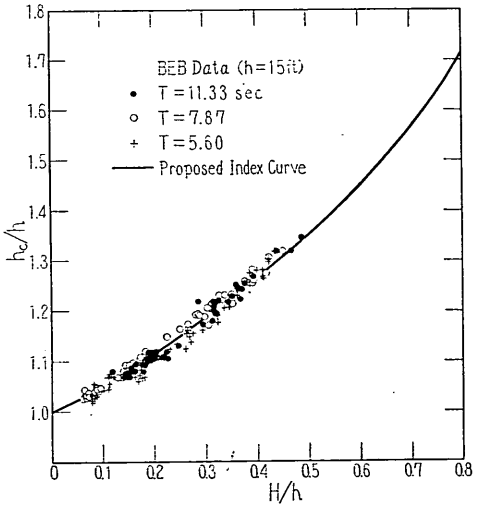

Fig. 9. **Comparison of Proposed Index for Wave Crest Elevation with BEB Data (after Bretschneider 1958)**

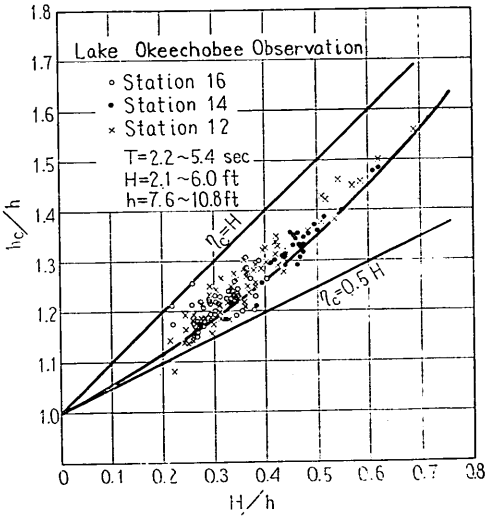

Fig. 10. **Lake Okeechobee Data on Wave Crest Elevation (after Bretschneider 1958)**

The empirical relation between h_c/h and H/h determined in Fig. 8 as a solid line was then compared with the experimental data of B. E. B. as shown in Fig. 9. Although the effect of wave periods is noticed slightly, the effect is practically negligible and the data agree well with the empirical curve. The irregularity of actual ocean waves and the effect of wind action would make it meaningless to

debate over minute differences in the ratio of η_c/H. Figure 10 is the re-plotting of Lake Okeechobee data quoted by Bretschneider. The scattering of the data is very large, but in the average the agreement is good.

Based on these figures, the index curve for the wave crest elevation above the bottom shown in Fig. 8 is recommended for the determination of the crest elevation in piling design problems in the region of the intermediate depth waves. For the deep water waves, Fig. 7 or the theory of the Stokes waves should be referred to. For this purpose, Skjelbreia and Hendrickson's table 1962 is very helpful. It should be also cautioned that the index curve and all the data presented herein are for progressive waves with the same direction of propagation; the superposition of waves with different directions of propagation, or the pheonomenon of triangular waves and others, should be considered in the determination of the elevation of a deck of an offshore structure to be free from the wave action.

3.3 Magnitudes and Distributions of Horizontal Particle Velocities

Tne minuature current meters mounted on a vertical beam at various elevation yielded the pulse records of orbital velocities at these elevations as shown in Photo. 5. From these records, it was clear that a maximum horizontal velocity takes place at the time of a wave crest passage or of a wave trough passage, regardless of the particle elevation. It was also noticed that the horizontal velocity becomes null and changes its direction about at the time when the water surface traverses the mean water level. The water particles moved shoreward while the water surface was above the mean water level and moved seaward while the water surface was below the mean water level. Such changes of the directions of particle movements were observed even for secondary wave crests if they were large enough to appear above the mean water level.

From the pulse records of orbital velocities, the analysis was made for only the particle velocities under the wave crests and wave troughs, since the current meters had been calibrated only with the uniform flow perpendicular to it. The lower portion of Fig. A-1 through A-18 in the appendix show typical records of orbital velocities under the wave crests and troughs. These velocities are the averages of ten consecutive waves; velocities of individual waves have deviations of as much as 10 per cent. The velocities plotted are presented in non-dimensional form being devided by a velocity term of $\pi H/T$. This velocity term was so chosen that the measured velocities could be easily compared with those of small amplitude waves. The upper portions of Fig. A-1 through A-18 are the profiles of corresponding waves.

Such distribution curves of particle velocities under the wave crests and troughs have been obtained for 106 waves. From these curves, the following characteristics

were observed:

1) The small amplitude wave theory provides a good approximation for the orbital velocities under the wave crests and troughs, when wave height is as small as one tenth of the water depth or less.
2) As a wave height increases, the orbital velocities under the wave crest becomes larger than those of small amplitude waves; the rate of deviation becomes large as the relative depth becomes small.
3) For waves in relatively deep water with the water depth being larger than one fifth of the wave length, the difference between the measured velocities and theoretical ones of small amplitude waves is less than 15 per cent. For such waves, the orbital velocities do not increase continuously but begin to decrease after some increases, as the wave height increases.
4) The orbital velocities under the wave troughs are larger than those under the wave crests for waves with $h/L_A \geq 0.2$, about equal to for waves with $h/L_A = 0.14$, and smaller for waves with $h/L_A \leq 0.1$.

The last characteristics is considered as due to the presence of return flow in an experimental flume to compensate the mass transport by waves. Thus in the actual sea where the return flow is not present except in the offshore current zone, the orbital velocities under wave crests may be larger than those expected from the experimental velocities in a laboratoy flume.

As for the orbital velocities of waves near breaking, experimental data were not available. Such data, however, are indispensable to construct the whole regime of the velocity variation pattern of water waves. Therefore, the following estimate of the orbital velocities of finite amplitude waves including breaking waves has been attempted. First, the orbital velocities of the small amplitued wave are adopted as the reference velocities (applying the expression for the velocity up to the height of wave crest) and a velocity factor K which is to be a function of h/L_A, H/h, and z/h is introduced so as to represent the finite amplitude effect; thus the velocities under the wave crests are expressed as:

$$U_{crest} = K \frac{\pi H}{T} \frac{\cosh kz}{\sinh kh} \quad \cdots\cdots (5)$$

where: $K = K(h/L_A,\ H/h,\ z/h)$

$k = 2\pi/L_A$

For the breaking waves, the particle velocity at the wave crest has to be equal to the wave celerity. This equality leads to the following expression for the maximum value of the velocity factor K:

$$K_{max} = \frac{L_b}{\pi H_b} \frac{\sinh kh}{\cosh kh_c} \quad \cdots\cdots (6)$$

where : h_c=height of wave crest form the bottom at breaking point

$_b$=subscript referring to breaking waves

The maximun velocity factor, K_{max}, has been computed with the breaker index listed in Table 1, and shown in the same table. The breaker index was estimated with the aid of the experimental data and theoretical works of Michell, Yamada and Chappelear. The breaker index presented herein is to be revised in the future with the developement of theoretical and experimental investigation of breaking waves.

Table 1. Proposed Breaker Index and Maximum Velocity Factor

h/L_A	H_b/h	$(h_c/h)_b$	H_b/L_A	L_b/L_A	K_{max}	α
0.03	0.820	1.775	0.0246	1.26	2.93	1.50
0.05	0.795	1.700	0.0397	1.24	2.77	1.50
0.07	0.765	1.645	0.0535	1.21	2.56	1.43
0.10	0.720	1.581	0.0720	1.18	2.28	1.25
0.14	0.665	1.517	0.0931	1.15	1.94	0.97
0.20	0.592	1.438	0.1184	1.15	1.60	0.68
0.30	0.479	1.330	0.1436	1.16	1.34	0.49
0.50	0.330	1.223	0.1650	1.18	1.12	0.25
0.70	0.243	1.163	0.1700	1.20	1.10	0.27

The velocity factor, K, while having the maximum values listed in Table 1, has a limiting value of unity for waves with very small heights. The examination of the velocity distribution curves such as Figs. A-1 through A-18 also indicates that the velocity factor should increase as the position of a water particle is elevated and that the velocity factor is not far from unity near the bottom. Taking these characteristics into consideration, the functional form of the velocity factor has been assumed in the following form :

$$K=\sqrt{1+\alpha\left(\frac{H}{h}\right)^{\frac{1}{2}}\left(\frac{z}{h}\right)^{3}} \qquad \cdots\cdots(7)$$

where a factor α is to represent the effect of the relative depth, h/L_A, and its value has been calculated with the characteristics of breaker index as shown in the last column of Table 1.

The orbital velocities under wave crests estimated with Eqs. 5 and 7 tend to be a little higher than those obtained in the experiments. Figure 11 shows the comparison of the measured and calculated velocities under the wave crests at the height of the mean water level. The ordinate is non-dimensional velocity, $uT/\pi H$, and the abscissa is the wave steepness, H/L_A. The calculated values are larger in the average than the measured ones, but the difference is not so great. Since the measured velocities are considered to be decreased by some extent by the presence of the return

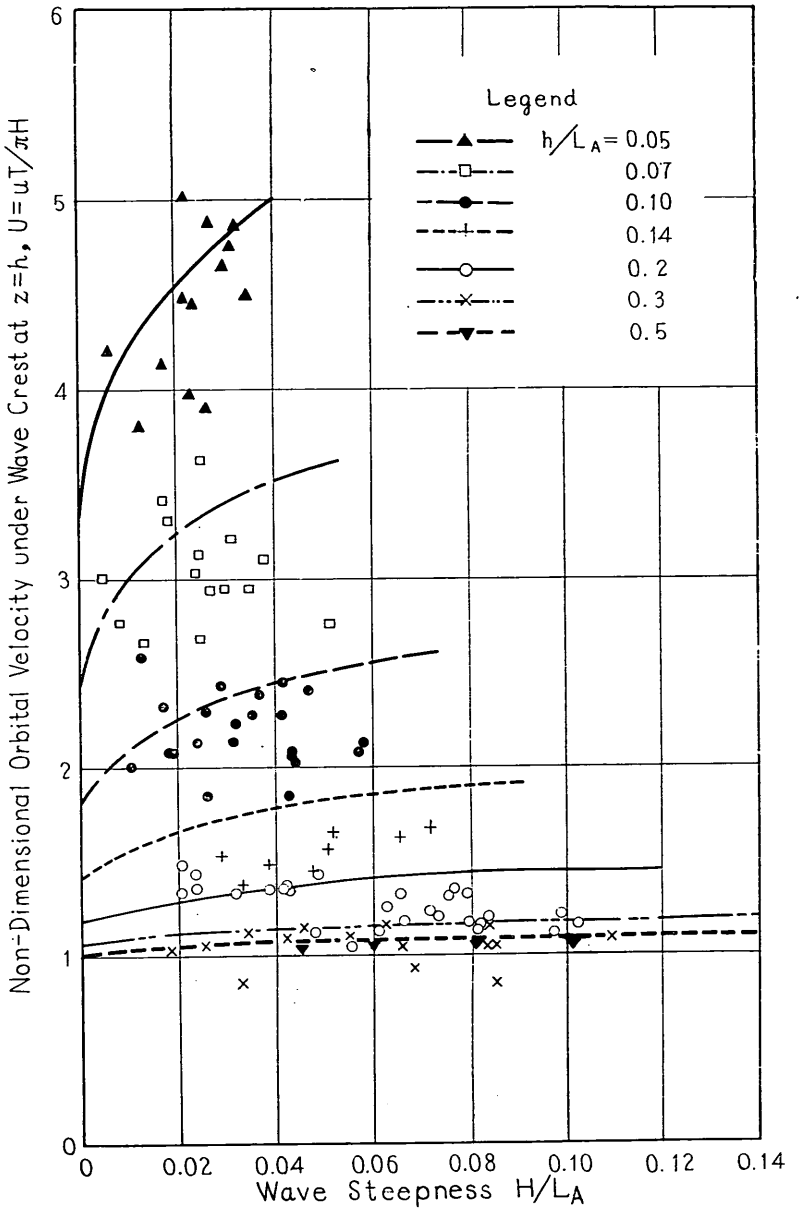

Fig. 11. Comparison of Measured Orbital Velocities with Calculated Ones under Wave Crests at Mean Water Level

flow in the wave channel, the use of Eqs. 5 and 7 for the estimate of the orbital velocities under the wave crests is suggested for practical purposes. The velocity distribution curves estimated with Eqs. 5 and 7 are also shown in Figs. A-1 through

A-18 with dashed lines.

3.4 Drag Coefficient of a Circular Cylinder

The drag coefficient C_D of a test pile has been computed from the moment of wave force measured and the velocity distribution curve directly obtained under a wave crest, as described in Section 2.2. The values of drag coefficient thus calculated are plotted in Fig. 12 against a Reynolds number which is based on the pile diameter and the orbital velocity under the wave crest at the mean water level. The open circles indicate the data for the test pile with a diameter of 7.62 cm (3 in.), while the solid circles indicate the data for the test pile with diameter of 13.98 cm (5.5 in.). Each point indicated in the figure is the average of ten values of the drag coefficient for ten consecutive waves in one run; the range of individual values is shown with two dashed lines for the upper and lower limits. As indicated with

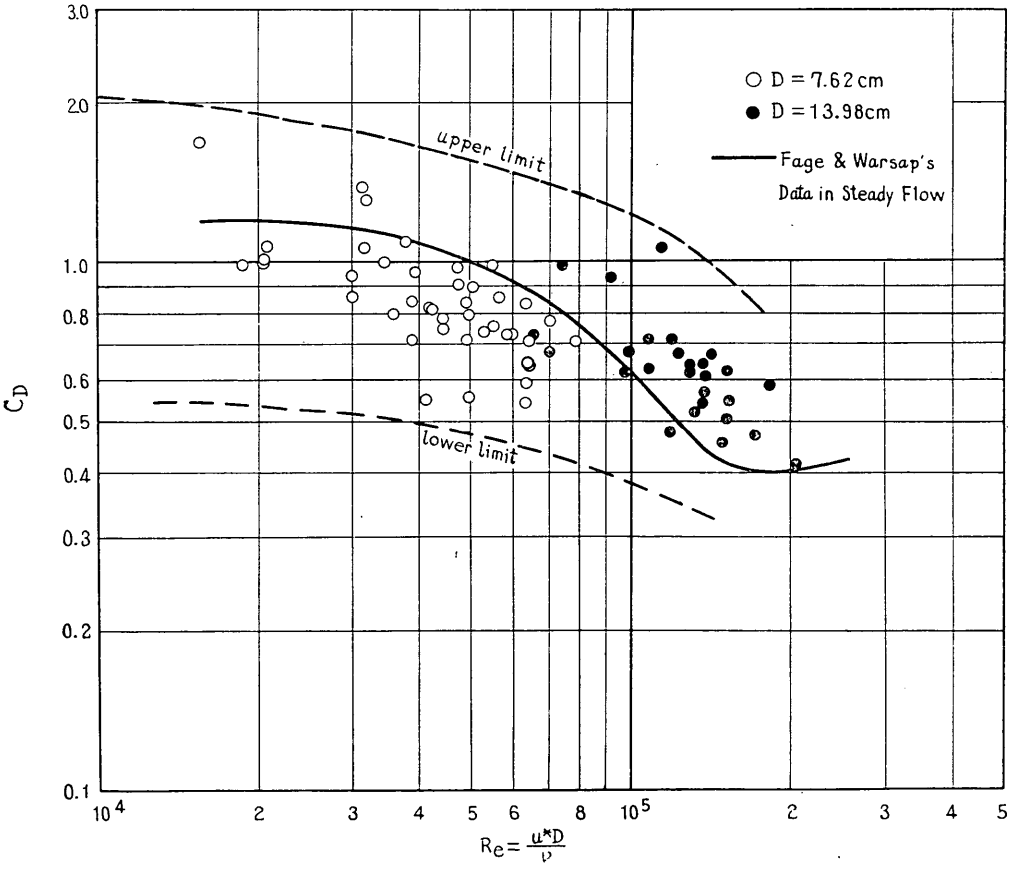

Fig. 12. Drag Coefficient Based on Actual Velocity Distributions C_D vs. Reynolds Number R_e

these lines, the scatter of the calculated values of the drag coefficient is large, even though the calculation has been based on the actual velocity distribution curves. The average value of the drag coefficient, however, shows a gradual decrease from a value of 1.3 to that of 0.4 over the range of Reynolds number from 1.5×10^4 to 2×10^5. These values of the drag coefficient agree well with the steady flow data obtained in wind tunnel tests. The solid line in Fig. 12 is that of Fage and Warsap's data 1930 in a wind tunnel with artifificial turbulence originated by means of a lattice made of ropes, and has been re-plotted from Goldstein 1938.

The comparison of the drag coefficient in the wave motion and that in a steady flow with turbulence was so made, since the oscillating flow around a cylinder under wave action is considered to contain high degree of turbulence. Thus from Fig. 12, it may be concluded that the drag coefficient of a circular cylinder under the wave action can be taken at the same value with that in a steady flow at the same Reynolds number, provided that the actual orbital velocities of water particles are known.

Then, a qusetion may be raised to what value the drag coefficient in a steady flow would take in the range of the Reynolds number higher than 10^6, since most of the wind tunnel experiments had been conducted in the range of the Reynolds number below 10^6. The experiment by Fage and Warsap 1930 with artificially roughened circular cylinders, quoted by Goldstein 1938, suggests the behavior of the drag coefficient in the higher Reynolds number region. When they tested a smooth cylinder, the drag coefficient dropped sharply from the value of 1.1 to 0.4 at the Reynolds number of 1×10^5 to 2.3×10^5. As they increased the roughness of the test cylinder by sticking various roughness of sand papers on it, the drop of the drag coefficient occurred at smaller values of the Reynolds number with a less amount of drop. The drag coefficient then increased again toward some constant values which depended upon the relative roughness of the cylinder surface; the roughest one tested has an asymptotic value of 1.0. It has also been reported that Blumberg and Rigg 1961 carried out a large scale test on the drag coefficient by towing a 3-ft. diameter cylinder of varying surface roughness in water (see Harleman and Dean 1963, and Wilson and Reid 1963). Their result confirmed the trend of Fage and Warsap's data. The drag coefficient does not vary in the range of the Reynolds number from 5×10^5 through 6×10^6, but shows an increasing trend with increasing roughness to a value of 1.02 for the roughest cylinder tested. Since prototype cylinders in the sea are subject to corrosion, coating of marine fauna or flora, and other changes in their surface conditions, the experimental data on rough cylinders should be referred to in the design of test piles. Hence the employment of $C_D=1.0$ is recommended for prototype pile designs.

When the orbital velocities of water particles are to be calculated by means of wave theory, the drag coefficient is not only governed by the Reynolds number and the surface roughness of a cylinder, but also affected by the wave characteristics, because the effect of the difference between the actual velocities and estimated ones has to be included in the term of the drag coefficient. Since the simplest wave theory is that of small amplitude waves, or the Airy's wave theory, it has often been employed as the first approximation. The apparent drag coefficient associated with the small amplitude wave theory has been calculated for the present data and plotted in Fig. 13 as a function of the relative depth, h/L_A. In this figure, the apparent drag coefficient C_D' shows an increasing trend with decreasing relative depth. This is well understood as the the effect of increasing wave crest elevation and of increas-

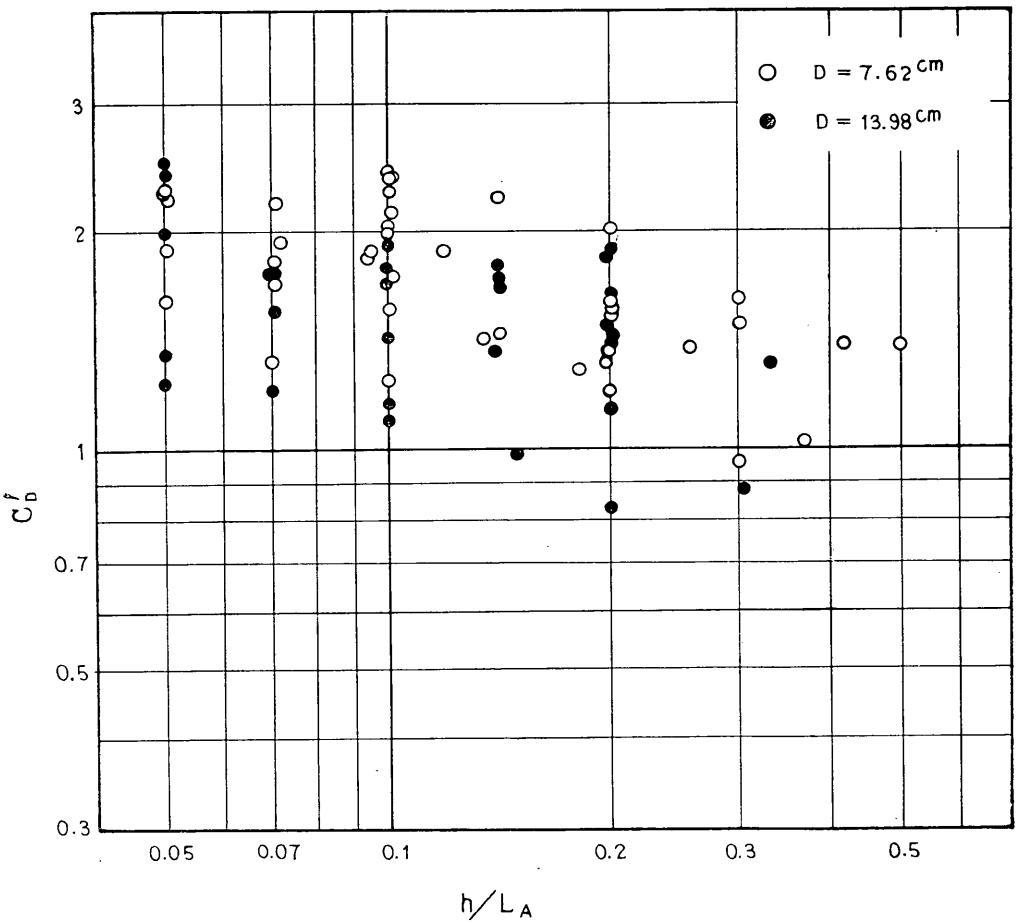

Fig. 13. Apparent Drag Coefficient Associated with Small Amplitude Wave Theory C_D' vs. Relative Depth h/L_A

ing deviation of the orbital velocities from the small amplitude wave theory. The apparent drag coefficient also increases almost linearly with the increase of the wave height for the same relative depth. Although the maximum value of C_D' in the experiment is 2.49, the real drag coefficient for that test waves is 0.59; if the real drag coefficient is to be taken as $C_D=1.0$, then the apparent drag coefficient must be taken as $C_D'=4.2$.

As for the reason of the large scatter in the calculated values of the drag coefficient as seen in Fig. 12, several factors may be cited as the major causes. The first one is the fact that the measurement of the orbital velocity had an inherent inacurracy of reading time intervals between pulse signals. Since the drag force is proportional to the square of the velocity, an error in the measurement of the velocity produces twice the error in the evaluation of the drag coefficient. The second factor is the difficulties to determine the exact instant when the orbital velocities reach at their maximum; a small difference at the determination of the instant caused a considerable change in the moment of the drag force read on wave force records. The third one is the presumtion of the uniform value of the drag coefficient over the length of a test pile, or the calculation of the drag coefficient as an average value over a test pile. Actually, the drag coefficient must have been different from an elevation to another depending upon the local Reynolds number. This variation must have acted to moderate the decrease of the drag coefficient with the Reynolds number. The fourth one is the use of the orbital velocity at the height of the mean water level as the reference velocity of the Reynolds number; this method is considered to have caused some inaccuracy in the effective Reynolds number. The elimination of these factors is a difficult task as long as a pile is tested directly with oscillating waves.

3.5 Virtual Mass Coefficient of a Circular Cylinder

The virtual mass coefficient has been calculated with the measured moment of the virtual mass force and the theoretical accelerations of small amplitude waves, since no information was available for the magnitudes of the actual water particle accelerations. The result of the calculation is shown in Fig. 14 which shows the virtual mass coefficient as a function of relative depth. Although the calculated values of the virtual mass coefficient varies from the minimum of 1.17 to the maximum of 2.94, there is a tendency to increase with decreasing relative depth. This tendency is regarded as due to the increase of the actual particle acceleration compared to the theoretical one of small amplitude waves. The effect of wave height or wave steepness on the virtual mass coefficient is not clear however, because of the scatter of the data. There is a slight indication that the value of C_M' decreases

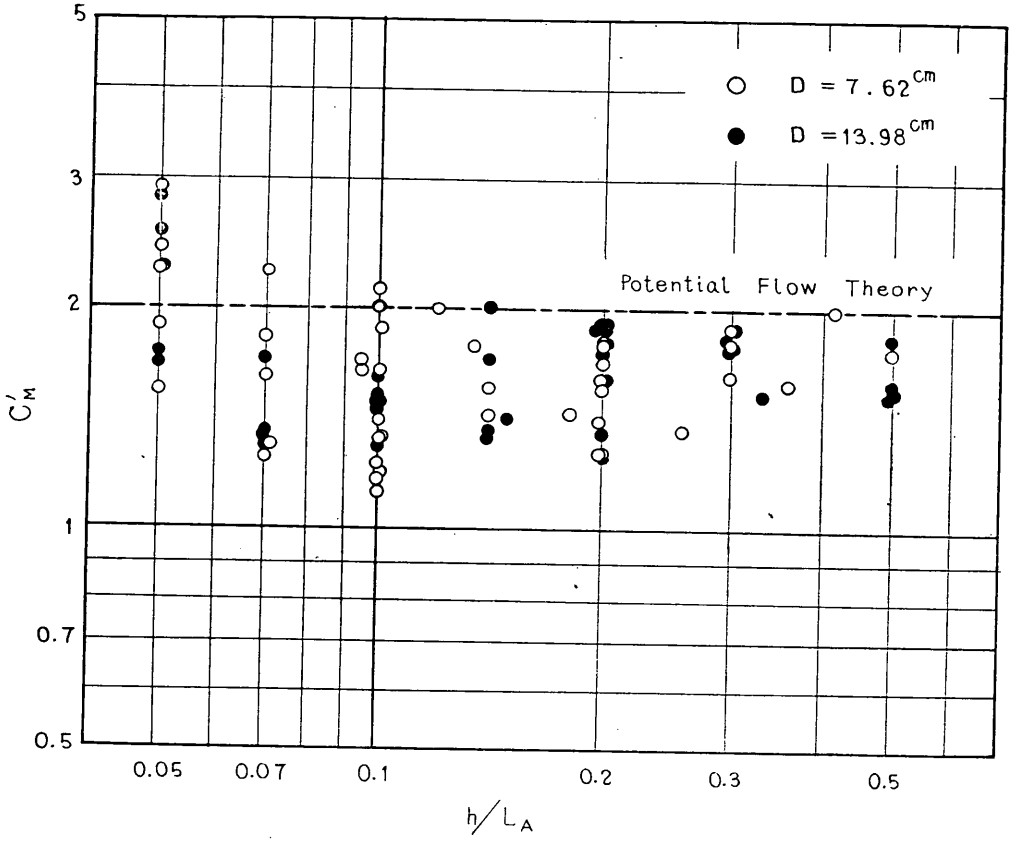

Fig. 14. Vitual Mass Coefficient C'_M vs. Relative Depth h/L_A

with increasing wave steepness for $h/L_A \geq 0.2$ but increases for $h/L_A \leq 0.1$. The effect of the Reynolds number or the cylinder diameter was not noticed on the values of the virtual mass coefficient. The over-all average of the virtual mass coefficient was 1.66 with a standard deviation of 0.39, i.e.,

$$C_M' = 1.66 \pm 0.39$$

Since this average value is inclusive of all the effects of the wave characteristics, special arrangements have been made for the test waves, Case No. 70 through 80. They were so chosen to satisfy the requirement of small amplitudes waves as far as possible; the ratio of the wave height to the water depth was kept below 0.2. The wave profiles were not so different from the sinusoidal curves; the height of a wave crest above the mean water level was less than 57 per cent of the wave height. Even with such relatively small amplitudes, the test waves had some amounts of higher harmonic components. The wave profiles were therefore analysed in a form of the Fourier series:

$$\eta=a_0+\sum_{n=1}^{\infty} a_n \cos n\sigma t+\sum_{n=1}^{\infty} b_n \sin n\sigma t \quad \cdots\cdots(8)$$

where the starting point of time is taken at the instant when the rising water surface traverses the mean water level, and σ is the angular frequency of $2\pi/T$. The results of the analysis with 12 equally spaced points are listed in Table A-3. The third and eighth waves of ten consecutive waves recorded were utilized in the analysis. As seen in the table, the first coefficient for the sine series is predominant, indicating wave profiles being nearly sinusoidal.

The result of the Fourier analysis of the wave profiles was then applied to more exact evaluation of water particle accelerations. Based on the form of wave profiles, the velocity potential ϕ has also been assumed in a form of the Fourier series with the same coefficients as those for the wave profiles listed in Table A-3: i.e.,

$$\phi=\sum_{n=1}^{\infty}\frac{a_n g}{n\sigma}\frac{\cosh k_n z}{\cosh k_n h}\sin(n\sigma t-k_n x)-\sum_{n=1}^{\infty}\frac{b_n g}{n\sigma}\frac{\cosh k_n z}{\cosh k_n h}\cos(n\sigma t-k_n x)$$

$$\text{where: } \sigma^2=\frac{k_n g}{n^2}\tanh k_n h \quad \cdots\cdots(9)$$

Then the orbital velocities and water particle accelerations at $t=0$ and $x=0$ are given by:

$$\eta=a_0+\sum_{n=1}^{\infty} a_n=0$$

$$u=-\frac{\partial\phi}{\partial x}=\sum_{n=1}^{\infty} n a_n \frac{\cosh k_n z}{\sinh k_n h} \quad \cdots\cdots(10)$$

$$\frac{\partial u}{\partial t}=\sum_{n=1}^{\infty} b_n n^2 \sigma^2 \frac{\cosh k_n z}{\sinh k_n h} \quad \cdots\cdots(11)$$

Since the orbital velocities are very small at $t=0$, the wave force acting at this instant is almost entirely that of virtual mass force. By comparing the measured moment of the wave force at $t=0$ and the integration of the water particle accelerations of Eq. 11, new values of the virtual mass coefficient have been obtained as shown in the last column of Table A-3. These values have a higher average with a smaller deviation than the results of the previous calculations such as:

$$C_M=1.71\pm0.12$$

This value is considerd as the most reliable one for a circular cylinder under the wave action, because of the computation method described in the above. The virtual mass coefficient of circulat cylinder in the ideal fluid is known to be 2.0. The smaller value of C_M obtained in the test than the value in the ideal fluid may be attributed to a possibility that a small portion of wakes remains behind a cylinder under the wave action even at the time of no velocity. Such a presence of wakes

prevents the realization of symmetric flow pattern around a cylinder and decreases the rate of the stream line deformation in the rear part of the cylinder, thus reducing the magnitude of the virtual mass force. The theoretical value of 2.0 for the potential flow, however, seems to be the most practical estimate for a circular cylinder when the scatter of the experimental data such as shown in Fig. 14 is taken into consideration.

3.6 Maximum Moment of Wave Force on a Circular Cylinder

The analysis and discussions of the wave force on a circular cylinder presented herein are all based upon the presumption that the wave force may be separated into two parts of the drag force and the virtual mass force. One possible test of this presumption is to see how a maximum wave force may be reconstructed from the drag force and the virtual mass force. If the velocities and accelerations of water particles are assumed to vary sinusoidally with respect to time for the sake of simplicity, the total wave force is represented with the maximum drag force $(F_D)_{\max}$ and the maximum virtual mass force $(F_M)_{\max}$ as :

$$F_T=(F_D)_{\max}\cos^2\frac{2\pi t}{T}+(F_M)_{\max}\sin\frac{2\pi t}{T} \quad \cdots\cdots(12)$$

The maximum value of the total force is derived from the above expression after a little manipulation as;

for $(F_M)_{\max}\geq 2(F_D)_{\max}$

$$(F_T)_{\max}=(F_M)_{\max} \quad \text{at } t=-T/4 \quad \cdots\cdots(13.1)$$

for $(F_M)_{\max}<2(F_D)_{\max}$

$$(F_T)_{\max}=(F_D)_{\max}+\frac{(F_M)_{\max}^2}{4(F_D)_{\max}} \quad \text{at } t=\frac{T}{2\pi}\sin^{-1}\left[\frac{(F_M)_{\max}}{2(F_D)_{\max}}\right] \quad \cdots\cdots(13.2)$$

These relations may also be assumed to be hold for the moment of the wave force as well as the wave force itself.

In order to examine the assumption of Eq. 12, the experimental data of the moments of wave forces around the bottom were analysed. The ratio of a maximum moment to the moment of the maximum drag force of the same wave, $M_{\max}/M_D$, is plotted in Fig. 15 against the ratio of the moment of the maximum virtual mass force to that of the maximum drag force, M_M/M_D. The relation of Eq. 13 is represented with a solid line. As seen in the figure, the actual values of the maximum moments are larger than those estimated with Eq. 13; the relations of Eq. 13 give the lower limit to the maximum moment. The difference between the actual maximum moments and those calculated with Eq. 13 is about 50 per cent of the latter for the largest one; the difference is greatest in the range of M_M/M_D from 0.4 to 2.5. Outside of this range, the difference is less than 30 per cent of the value

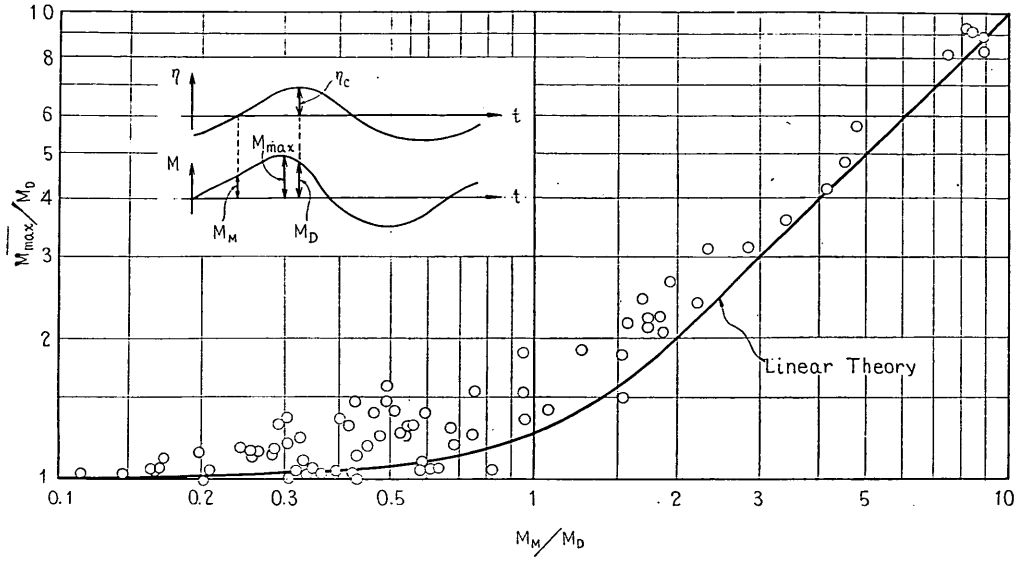

Fig. 15. Comparison of Maximum Moment with Moments of Maximum Drag and Virtual Mass Forcee

estimated with Eq. 13. Therefore, although the assumption of Eq. 12 is not true from the theoretical point of view, it may be concluded that the relations of Eq. 13 are the useful formulas for the estimate of maximum forces and moments.

IV. A COMPUTATION METHOD OF WAVE FORCE ON A VERTICAL CIRCULAR CYLINDER

4.1 Selection of Design Wave and Water Depth

Based on the results of the experiments described in the foregoing chapters and of other theoretical and experimental works, it may be possible to present a method to compute the wave forces on a vertical circular cylinder. The method is intended to serve for the need of a reliable computation method for the wave force problems on pile structures, and thus it is open to the refinements in the future as more data and informations will become available.

The first step in a design of an offshore structure is to determine a design wave and water depth. Although the employment of significant wave is common in designs of breakwaters and may be justified for the over-all stability consideration of an offshore structure, the highest possible wave should be used for the design of component members of an offshore structure or for the design of vertical piles driven

into the foundation. This is so because the attack of only one high wave may destroy the component members or vertical piles if the wave force is large enough to produce internal stresses greater than the breaking strength of the material used. In the case of a breakwater, one big wave may slide it over some distance, but it is unlikely that it will lead to the collapse of the breakwater.

The highest possible wave also should be considered at the largest water depth possible at a given location. An increased water depth makes it possible to bring forth a higher wave than before and also increases the length of a pile which is exposed to the wave action. The largest possible water depth at a given location is determined as the depth at the time of high water level plus the height of the meteolorogical tide caused by a design typhoon. Bretschneider 1958 has presented an empirical relation between the storm surge height and the magnitude of a hurricane along the coast of the Gulf of Mexico. As for the storm surges along the coasts of Japan, many studies have been done, especially after the disaster of the Ise-Bay Typhoon. Along the shores of major bays of Japan, such as Tokyo, Osaka, and Ise, the results of numerical computations for possible storm surges are available (see references 21 and 33). As for other parts of the coasts of Japan, an statistical investigation of available tide records will give useful informations for the height of possible surges.

Once a design water depth is determined, the largest possible wave height will be estimated from Fig. 6, which shows the limiting relative wave height $(H/h)_b$ for a given relative depth, h/L_A. The breaker index in Fig. 6 is also utilized to construct the diagram of Fig. 16 for the limiting wave height for a given water depth and wave period. This limiting wave height only gives the upper limit to the possible wave height at a given location. The question whether a wave with this limiting height can really be generated must be answered from the meteorological conditions and the statistical characteristics of ocean waves. For further informations readers should refer to Bretschneider 1958 and others.

Another caution for the use of the breaker index in Fig. 6 or the diagram of Fig. 16 is the fact that the limiting wave height presented in the figures should be applied for waves on flat ocean bed where the bottom slope is less than 1 to 100. Where the bottom slope is steep, waves may plunge into breaking. The breaking wave heights on steep slopes have been found to be larger than those on gentle slopes; Iversen's data 1952 on breaking waves show a maximum value of $(H/h)_b=1.0$ on 1 to 10 slope.

The next step is to estimate the height of the wave crest elevation. For this purpose, the use of Fig. 8 is recommended as discussed in Section 3.2. The crest height thus estimated, however, is only applicable for the design purpose of wave

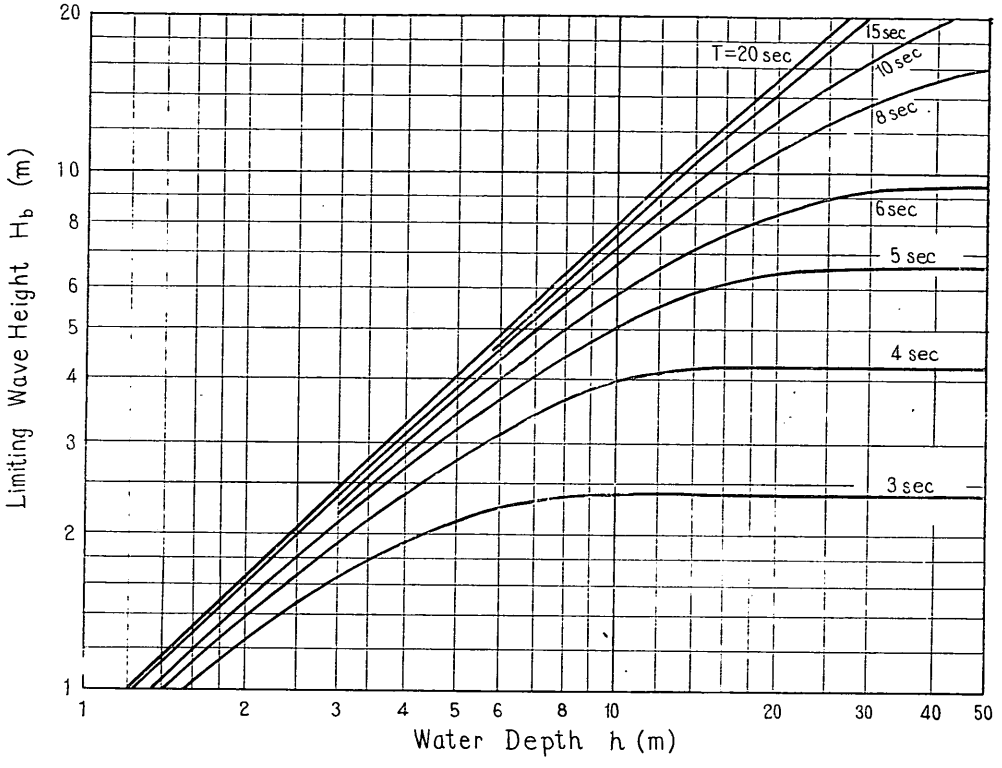

Fig. 16. Limiting Wave Height for a Given Wave Period at a Given Water Depth

forces on a vertical cylinder since the figure is constructed for progressive waves only. When two trains of waves come from different directions, a three-dimensional, partial standing wave system thus formed may produce wave crests higher than those estimated with Fig. 8. Such high wave crests caused by partial standing waves are not so dangerous for a vertical cylinder because the resultant horizontal velocities would be smaller than those of a single train of progressive waves. In a design of upper parts of an offshore structure, however, it is better to have a clearance between the bottom of upper structure and the sea level larger than the design wave height.

4.2 Drag Force and Its Moment

With a design wave and water depth thus determined, the maximum drag force is computed in the following manner. First the water particle velocities under the wave crests may be estimated with Eqs. 5 and 7, i.e.

$$u_{\text{crest}} = \frac{\pi H}{T}\sqrt{1+\alpha\left(\frac{H}{h}\right)^{\frac{1}{2}}\left(\frac{z}{h}\right)^{3}}\ \frac{\cosh kz}{\sinh kh} \qquad \cdots\cdots(14)$$

This equation has been computed for four elevations of $z=0$, $0.5h$, h, and h_c. The results of the computation are compiled in Figs. 17, 18 and 19 in a form of $uT/\pi H$ versus H/h with a parameter of h/L_A.

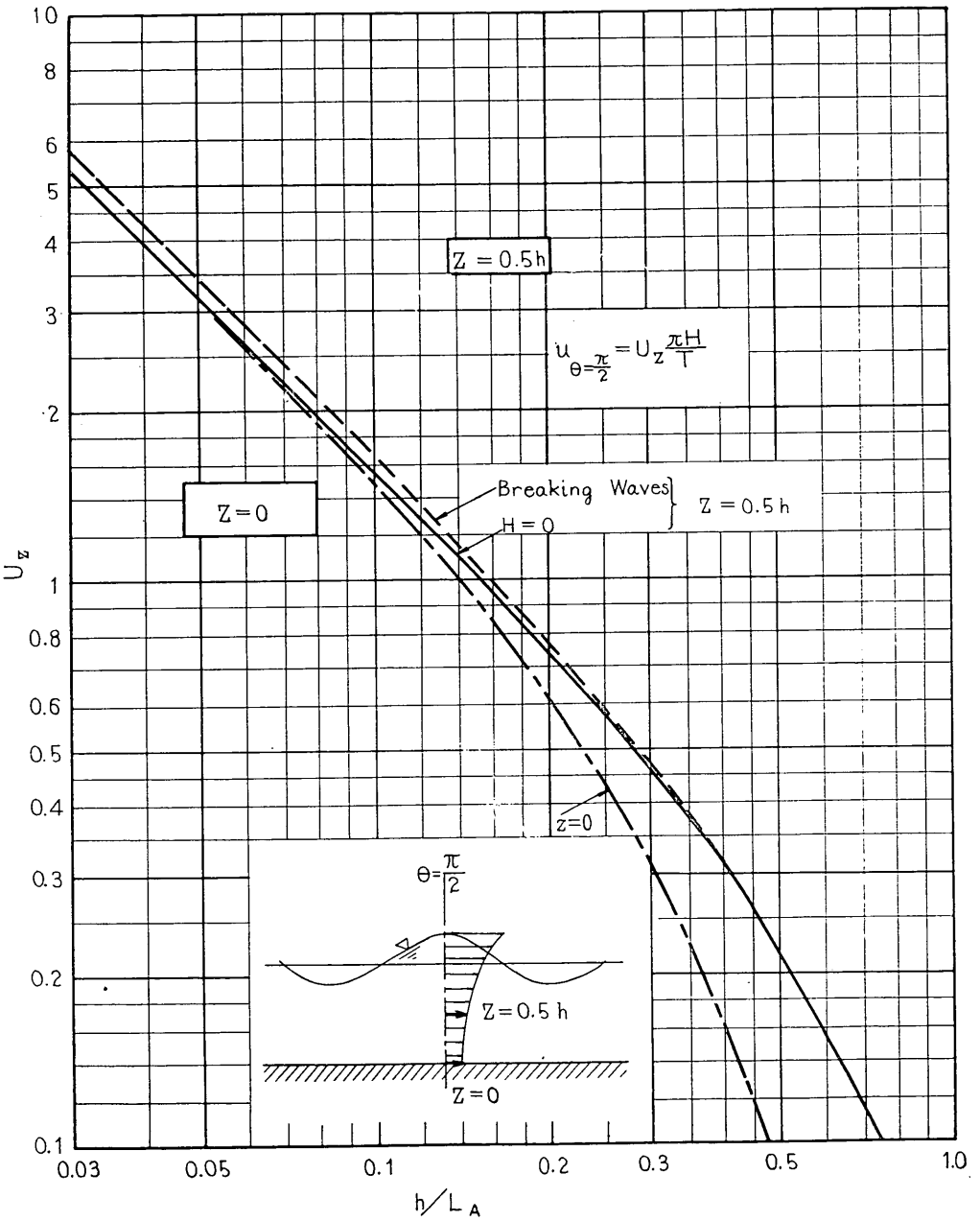

Fig. 17. Design Diagram for Orbital Velocity under Wave Crest at $z=0$ and $0.5h$

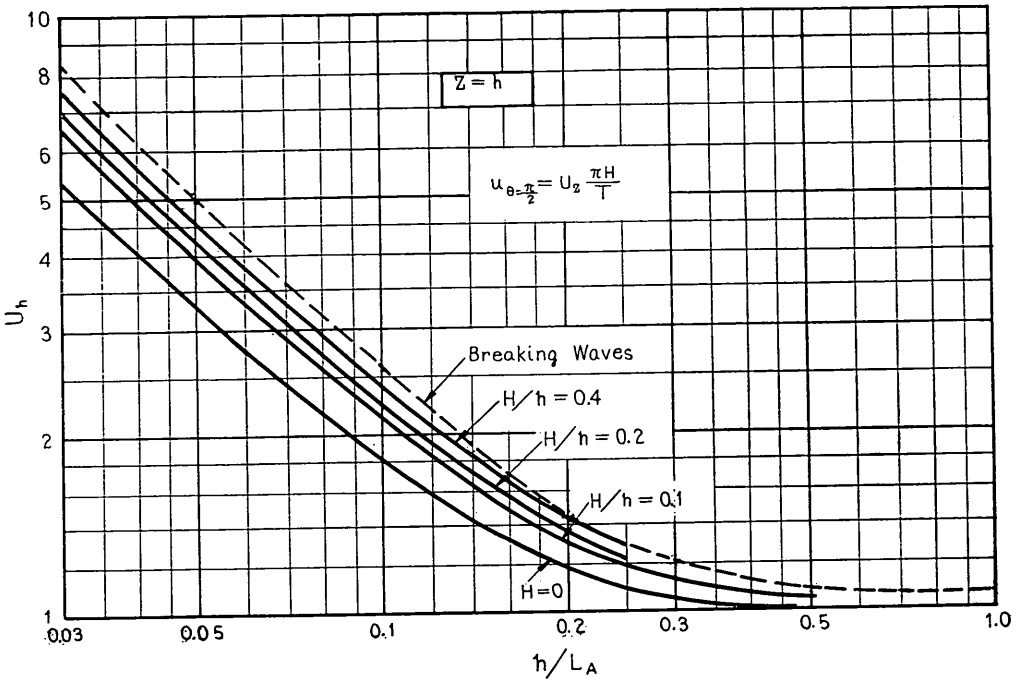

Fig. 18. Design Diagram for Ortital Velocity under Wave Crest at $z=h$

Then the drag force is obtained by substituting the above velocities into Eq. 1 and by executing the calculation. The total drag force from the bottom to the wave crest for a vertical cylinder of uniform section is given with the integration of Eq. 1 as:

$$(F_D)_{\max} = \frac{w}{2g} C_D D \int_o^{h_c} u^2 \, dz = w \, C_D D \, H^2 \, K_D \quad \cdots\cdots (15)$$

where: K_D=non-dimensional factor for maximum drag force.

The moment of the maximum drag force is also given by the following integration:

$$(M_D)_{\max} = \frac{w}{2g} C_D D \int_o^{h_c} u^2 \, z \, dz = w \, C_D D \, H^2 \, K_D \, S_D \quad \cdots\cdots (16)$$

where: S_D=arm length of maximum drag force measured from sea bottom.

The drag force factor K_D and the arm length S_D are computed with the following equations:

$$K_D = \frac{\sinh 2kh_c}{16 \sinh 2kh} (F_1 + AF_2) \quad \cdots\cdots (16)$$

$$S_D = h_c \frac{G_1 + AG_2}{F_1 + AF_2} \quad \cdots\cdots (17)$$

where:

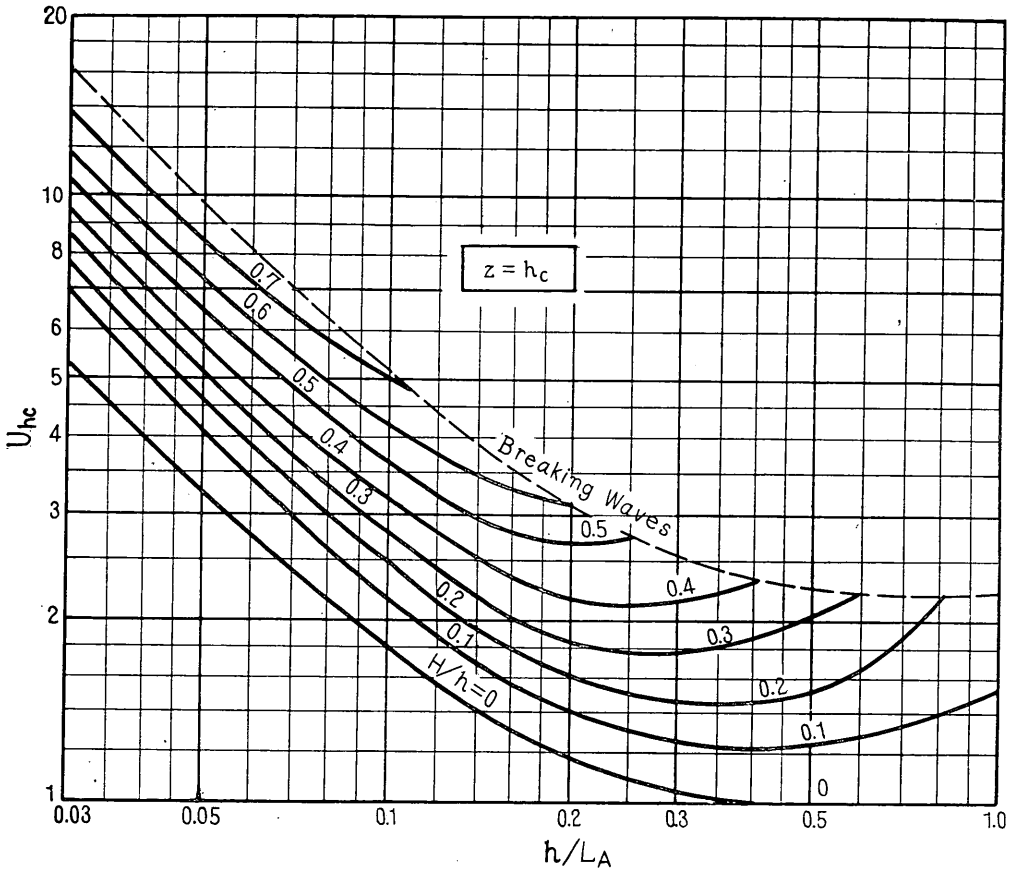

Fig. 19. Design Diagram for Orbital Velocity at Wave Crest. $z=h_c$

$$A=\alpha\left(\frac{H}{h}\right)^{\frac{1}{2}}\left(\frac{h_c}{h}\right)^3 \quad \cdots\cdots(18)$$

$$F_1=1+\frac{2kh_c}{\sinh 2kh_c} \quad \cdots\cdots(19)$$

$$F_2=1+\frac{kh_c}{2\sinh 2kh_c}+\frac{3}{2(kh_c)^2}\left[1-\frac{kh_c}{\tanh 2kh_c}-\frac{\tanh kh_c}{2kh_c}\right] \quad \cdots\cdots(20)$$

$$G_1=1+\frac{kh_c}{\sinh 2kh_c}-\frac{\tanh kh_c}{2kh_c} \quad \cdots\cdots(21)$$

$$G_2=1+\frac{2kh_c}{5\sinh 2kh_c}+\frac{1}{(kh_c)^2}\left[3-\frac{2kh_c}{\tanh 2kh_c}\right]+\frac{3}{2(kh_c)^4}\left[1+\frac{2kh_c}{\tanh 2kh_c}\right] \quad \cdots\cdots(22)$$

The computation of these equations has been carried out for various values of h/L_A and H/h so as to yield the design diagrams for K_D and S_D/h. The results of

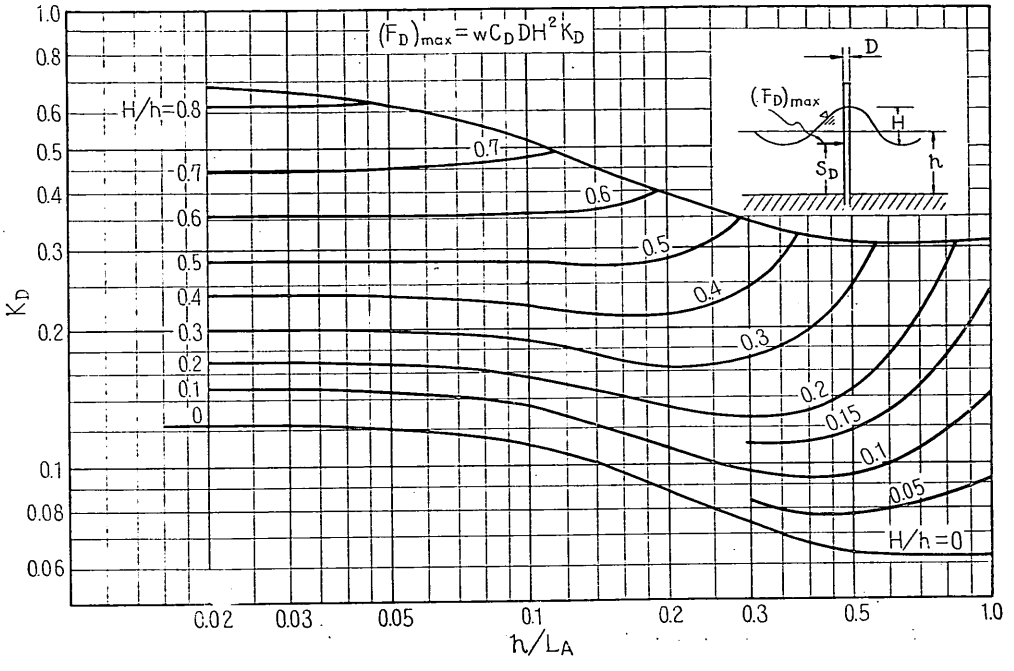

Fig. 20. Drag Force Factor K_D for a Uniform Vertical Cylinder

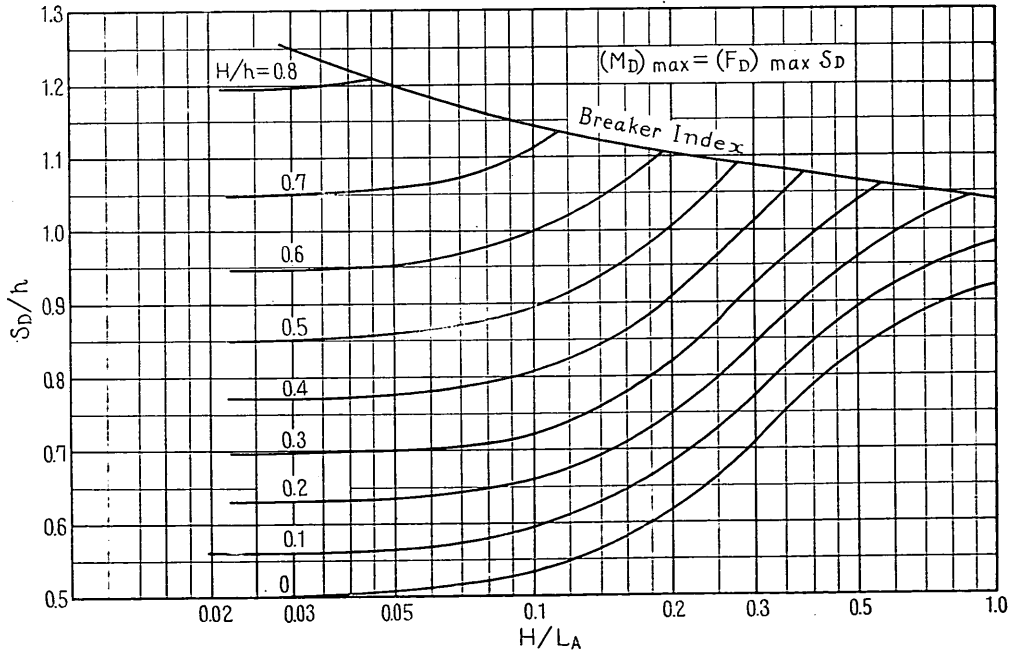

Fig. 21. Effective Lever Arm S_D for Maximum Drag Force

the computation are compiled in Figs. 20 and 21. These figures are to be regarded as the revision of the similar diagrams constructed by Reid and Bretschneider 1953. The drag corefficient C_D should be taken 1.0 for a cylinder of circular section as discussed in Section 3.4. For a cylinder of rectangular section of H-shaped section, the drag coefficient may be taken as 2.0 with a diameter D being measured diagonally based on the wind-tunnel data for steady state flow.

Figures 20 and 21 indicate an interesting feature of the wave force on a pile. The largest value of K_D is seen to be about 0.7. The maximum arm length S_D is 1.25 h. From the forms of Eqs. 15 and 16, it can be said therefore that the maximum drag force on a circular pile may safely be replaced with an uniform pressure of 0.7 w H acting from 0.9 h to 1.6h. This magnitude of wave force is far smaller than that of the breaking wave pressure on a vertical wall, as might be imagined from the natures of two wave forces. The wave force on a rectangular pile, however, should be taken twice that on a circular pile.

As for a vertical cylinder with a varying diameter, the diagrams of Figs. 20 and 21 are not available. The wave force must be computed with Eqs. 1 and 14 by numerical integrations. The diagrams of Figs. 7, 18 and 19 for horizontal velocities under wave crests will be useful to estimate the velocity distribution.

4.3 Virtual Mass Force and Its Moment

In order to compute the virtual mass force, the water particle accelerations of small amplitude waves are employed here as the first approximation. The water particle accelerations of actual waves with large amplitudes are somehow different from those of small amplitude waves, but the difference is considered to be small compared to the difference in horizontal particle velocities. The nature of virtual mass force which is proportional to the acceleration also allows the approximation of small amplitude waves; the drag force is proportional to the square of the orbital velocities and the error involved in the estimate of the velocities is multiplied accordingly.

The water particle accelerations of small amplitude waves have the following maximum values at the time when the water surface crosses the mean water level:

$$\left(\frac{\partial u}{\partial t}\right)_{\max}=\frac{2\pi^2 H}{T^2}\ \frac{\cosh kz}{\sinh kh} \qquad (23)$$

This acceleration has been calculated for the points of three elevations, $z=0$, 0.5 h and h, and has been compiled in Fig. 22 which shows the non-dimensional acceleration, $\left(\frac{\partial u}{\partial t}\right)_{\max} T^2/H$ as a function of the relative depth, h/L_A.

The maximum virtual mass force is then computed by substituting Eq. 23 into Eq. 2 and by integrating it from the bottom to the water surface. For a vertical

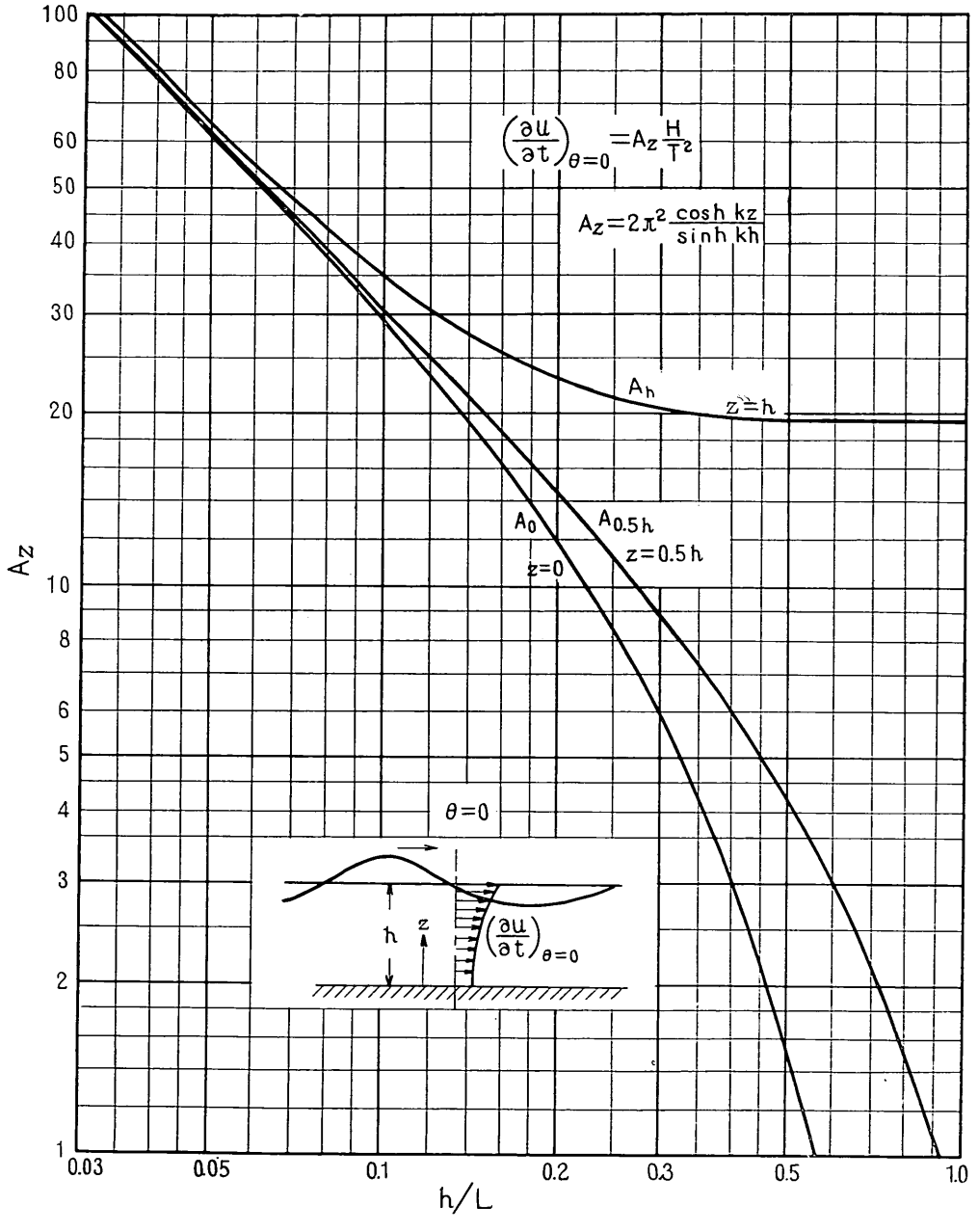

Fig. 22. Design Diagram for Water Particle Accleration

circular cylinder of uniform diameter, the integration is easily carried out, yielding the following formula:

$$(F_M)_{max} = \frac{w}{g} C_M \frac{\pi D^2}{4} \int_o^h \left(\frac{\partial u}{\partial t}\right)_{max} dz = wC_M D^2 H K_M \cdots\cdots (24)$$

where : K_M=non-dimensional factor for maximum virtual mass force

$=(\pi/8)\tanh kh$

The moment of this maximum virtual mass force is also obtained by the following integration :

$$(M_M)_{max} = \frac{w}{g} C_M \frac{\pi D^2}{4} \int_o^h \left(\frac{\partial u}{\partial t}\right)_{max} z\, dz$$

The substitution of Eq. 23 into the above equation yields the following formula for the maximum moment :

$$(M_M)_{max} = w\, C_M D^2\, H\, K_M\, S_M \cdots\cdots (25)$$

where : S_M=arm length of maximum virtual mass force measured from sea bottom

$$= h\left[1 - \frac{1}{kh \sinh kh}(\cosh kh - 1)\right]$$

The virtual mass force factor K_M and the effective lever arm S_M have been computed and compiled in Figs. 23 and 24 as functions of the relative depth, h/L_A. Being different from the drag force factor K_D which has a decreasing tendency

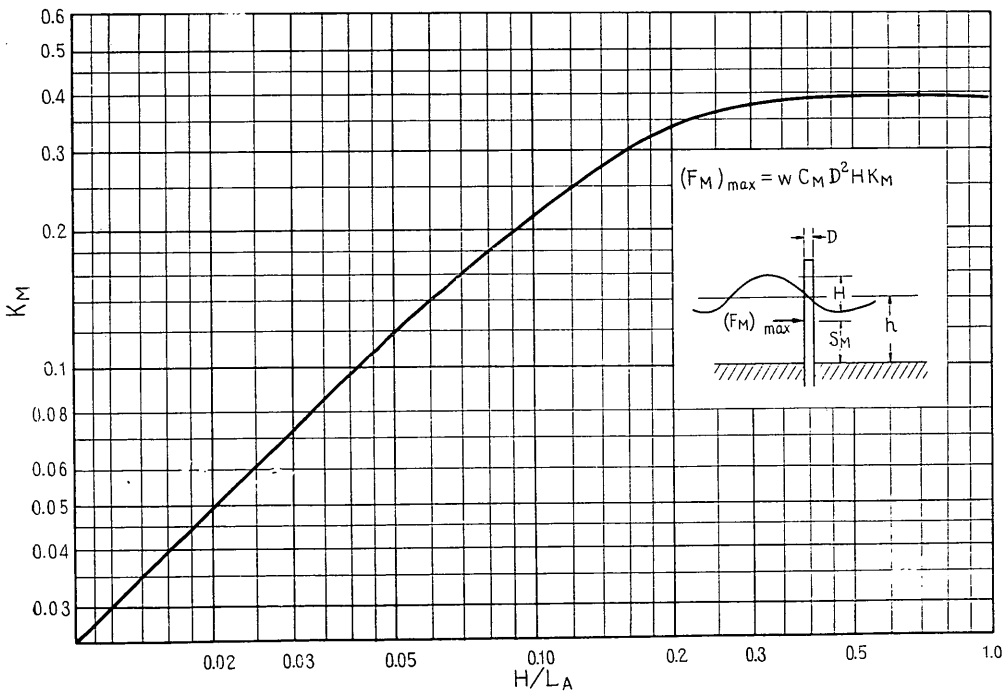

Fig. 23. Vitual Mass Force Facter K_M for a Uniform Vertical Cylinder

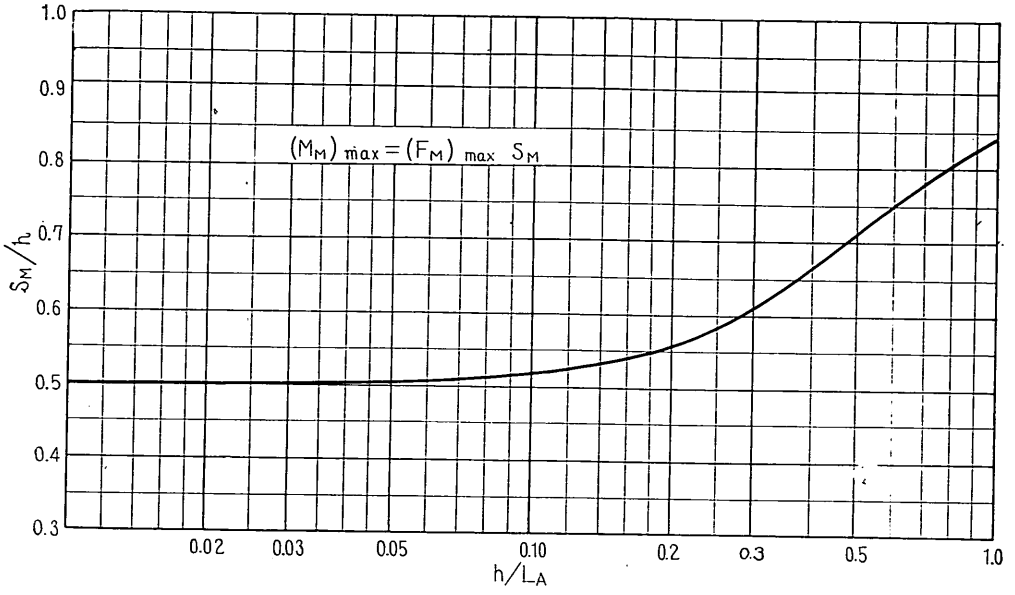

Fig. 24. Effective Lever Arm S_M for a Maximum Virtual Mass Force

with increasing relative depth, the virtual mass force factor K_M increases as the relative depth increases.

The virtual mass coefficient C_M in the above formulas should be taken at 2.0 as discussed in Section 3.5. Until more reliable informations become available for the accelerations of the actual waves and the virtual mass coefficient based on the actual accelerations, the value of 2.0 seems to be a reasonable one for the practical design purpose.

4.4 Total Wave Force and Its Moment

As discussed in Section 3.6, the total wave force may be estimated with Eq. 12 with the maximum drag force and virtual mass force computed by Eqs. 15 and 24. The total moment may also be estimated with Eq. 12 in co-operation with Eqs. 16 and 25. The maximum values of the total force and its moment is evaluated with Eq. 13.

This computation method of the total wave force and its moment is not a rigorous one to describe every phase of wave force variation. It is rather a conventional method intended for a solution of actual design problems of wave forces on piles. The best way to evaluate its validity is to compare the measured wave forces or moments to the computed ones. For this purpose, the maximum moments of wave forces on test piles were compared in Fig. 25 to those computed by the present

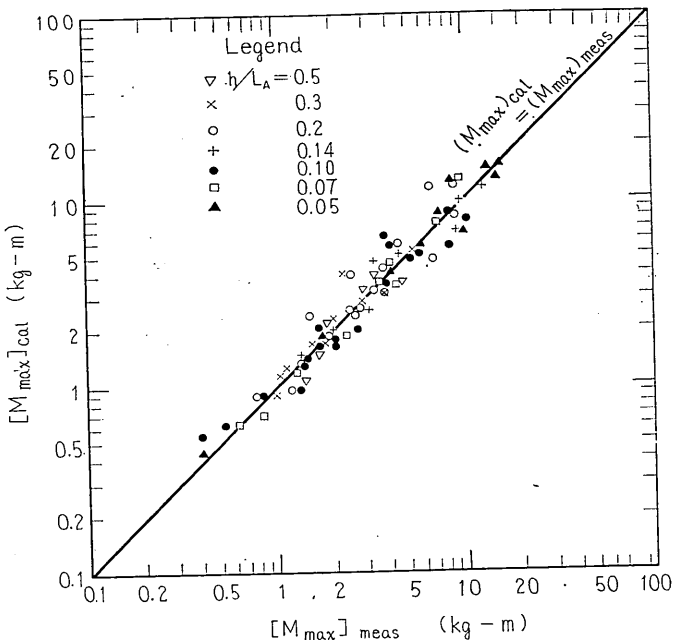

Fig. 25. Comparison of Calculated Maximum Moments with Measured Ones

method. The wave height, wave period, pile diameter, and water depth employed in the computation are the same as those listed in Table A-1. The drag coefficient C_D of Table A-1 was also used to compute the maximum moment of wave force, since the test was mostly conducted at the region of the critiral Reynolds number and the constant value of 1.0 recommended for prototype piles was apparently not practical for this case. As seen in Fig. 25, the computed maximum moments are located between the values 0.66 times and 1.75 times the measured ones, from the smallest value of 0.4 kg-m to the largest value of 16 kg-m. But in the average, the computed values agree with the measured ones fairly well. The ratio of the computed value to the measured one is expressed as:

$$[M_{\max}]_{cal}=(1.04\pm0.24)[M_{\max}]_{meas}$$

Another verification for the validity of the present method is seen in Fig. 26 which shows the comparison of computed and measured maximum wave forces. The experimental data were obtained by Harleman and Shapiro 1955 in a wave channel 27 m long and 0.76 m wide for several test piles with diameters ranging from 1.3 to 15.2 cm. The wave heights were varied from 12.2 to 25.5 cm and the water depth from 29.2 to 60.9 cm. But the relative depth, h/L_A, and the relative wave height, H/h, were kept constant at the values of 0.2 and 0.42, respectively. Thus

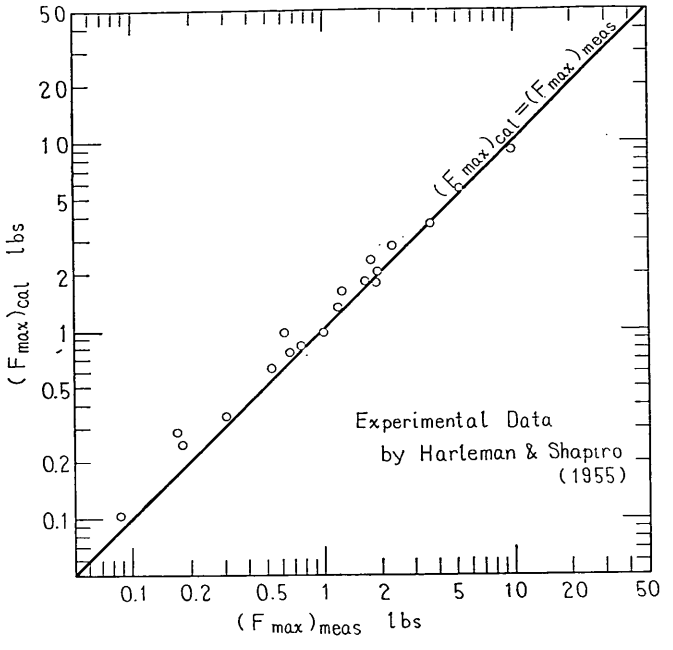

Fig. 26. Comparison of Calculated Maximum Forces with Experimental Ones (after Harleman and Shapiro 1955)

the comparison of the computed wave forces with the measured ones in Fig. 26 serves as a validity test of the present method for various pile diameters and water depths rather than for various wave characteristics. The results are very encouraging; the average value for the ratio of the computed maximum forces to the measured ones is 1.15 with a standard deviation of 0.16, or:

$$[F_{\max}]_{cal}=(1.15\pm0.16)\ [F_{\max}]_{meas}$$

This average value of 1.15 indicates that the present method tends to forecast rather larger maximum wave force than the actual one; hence the error is on the safe side.

4.5 An Example of Wave Force Computation

In order to illustrate the proposed computation method for the maximum wave force on a vertical pile, an example of wave force computation will be helpful. As for the design conditions the followings are selected:

water depth : $h=12$ m

bottom slope : $i=0.007$

wave period : $T=14$ sec

wave height : $H_{1/3}=6$ m

pile diameter : $D=0.9$ m

Since the bottom slope is very gentle, the present method is applicable. The first step is to calculate the relative depth h/L_A. This is obtained from Fig. 27 as:

$h/L_A=0.068$

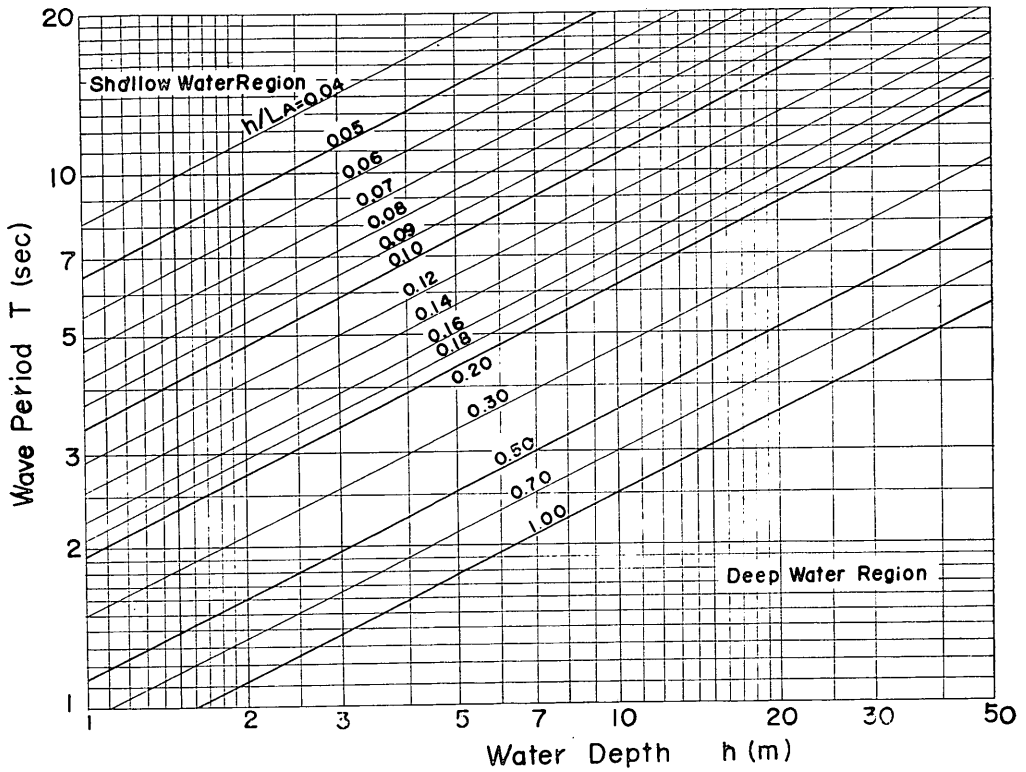

Fig. 27. Design Diagram for Relative Depth, h/L_A

For this relative depth, the limiting wave height is read from Fig. 5 as

$$\frac{H_b}{h}=0.77$$

hence,

$$H_b=0.77\times 12.0=9.25 \text{ m}$$

This wave height of 9.25 m can occur under the given conditions, because the significant wave height of 6.0 m would be associated with the maximum wave height of 11.2 m or more in the deep water. Therefore the wave height of 9.25 m is used for the computation of the design wave force on the pile.

The next step is to estimate the maximum drag and virtual mass forces. From Figs. 20 through 24, the non-dimensional factors K_D and K_M, and the arm lengths ot these forces, S_D and S_M, are obtained for $h/L_A=0.068$ and $H/h=0.77$ as:

$K_D = 0.58$

$K_M = 0.157$

$S_D = 1.17\ h = 14.0$ m

$S_M = 0.51\ h = 6.1$ m

The maximum drag and virtual mass forces and their moments are thus evaluated with Eqs. 15, 16, 24 and 25 as:

$$(F_D)_{max} = 1.0 \times 1.0 \times 0.9 \times 9.25^2 \times 0.59 = 44.6 \text{ ton}$$

$$(M_D)_{max} = 44.6 \times 14.0 = 626 \text{ ton-m}$$

$$(F_M)_{max} = 1.0 \times 2.0 \times 0.9^2 \times 9.25 \times 0.146 = 2.2 \text{ ton}$$

$$(M_M)_{max} = 2.2 \times 6.1 = 13.4 \text{ ton-m}$$

The maximum design wave force and its moment are estimated from Eq. 13 with the above values at hand as:

$$F_{max} = 44.6 + \frac{2.2^2}{4 \times 44.6} = 44.6 \text{ ton}$$

$$M_{max} = 626 + \frac{13.4^2}{4 \times 626} = 626 \text{ ton-m}$$

As for more detailed informations, the height of wave crest is estimated from Fig. 7 as:

$$h_c = 1.655h = 1.665 \times 12.0 = 19.9 \text{ m}$$

The horizontal orbital velocities beneath the crests are obtained with the aid of Figs. 17, 18 and 19 as:

$$z = h_c = 19.9 \text{ m} : U = 7.4 \times \frac{\pi H}{T} = 7.4 \times \frac{3.14 \times 9.25}{14} = 15.4 \text{ m/sec}$$

$$z = h = 12.0 \text{ m} : U = 3.7 \times \frac{\pi H}{T} = 3.7 \times \frac{3.14 \times 9.25}{14} = 7.7 \text{ m/sec}$$

$$z = 0.5h = 6.0 \text{ m} : U = 2.5 \times \frac{\pi H}{T} = 2.5 \times \frac{3.14 \times 9.25}{14} = 5.2 \text{ m/sec}$$

$$z = 0 \text{ m} : U = 2.3 \times \frac{\pi H}{T} = 2.3 \times \frac{3.14 \times 9.25}{14} = 4.8 \text{ m/sec}$$

The intensity of wave force per unit length beneath the wave crest is derived from Eq. 1 for the above four elevations as:

$$z = 19.9 \text{ m} : q = \frac{dF_D}{dz} = 1.0 \times \frac{1.0}{2 \times 9.8} \times 0.9 \times 15.4^2 = 10.9 \text{ t/m}$$

$$z = 12.0 \text{ m} : q = 1.0 \times \frac{1.0}{2 \times 9.8} \times 0.9 \times 7.7^2 = 2.7 \text{ t/m}$$

$$z = 6.0 \text{ m} : q = 1.0 \times \frac{1.0}{2 \times 9.8} \times 0.9 \times 5.2^2 = 1.2 \text{ t/m}$$

$$z = 0 \text{ m} : q = 1.0 \times \frac{1.0}{2 \times 9.8} \times 0.9 \times 4.8^2 = 1.1 \text{ t/m}$$

From this example, it may be well understood that the most of the drag force acting on a vertical pile are concentrated near the wave crest well above the mean

water level.

4.6 Remarks on the Design of Piling Subject to Wave Action

As indicated in the foregoing sections, the present study covers only a limited portion of the wave force problems on pilings. A rigid vertical pile with an uniform circular section erected on a flat or gently sloping bottom is treated in this report. Effects of group pillings, impact forces of breaking waves on a steep slope, and effects of flexibility are a few examples of the problems which engineers will certainly encounter in their actual designs. Although the author is in no position to answer these questions, a survey of previous investigations can reveal the natures of these problems to some extent as seen in the following paragraphs.

1) Effect of group piling on the wave force on individual piles

When more than a single pile are erected in a narrow area, the wave forces on individual piles are expected to be different from that on a single pile. The effect of neighboring pile on the wave force on a pile may be considered in two ways: the blocking effect and sheltering effect. The blocking effect of neighboring piles in sides tends to increase the wave force, while the sheltering effect of front and rear piles tends to decrease the wave force. The amount of these effects are mainly dependent upon the ratio of the spacing between the piles and the pile diameter. Laboratory tests by Morison, Johnson, and O'Brien 1953 on one inch diameter piles have shown that the blocking effect increased the maximum moment two times compared to that on an isolated pile for the relative spacing of $S/D=0.5$, but the increase in the moment for the relative spacing of $S/D=1.5$ was only about ten per cent. As for the sheltering effect the reduction in the wave force moment for piles with the relative spacing of 1.5 was about 20 per cent. These effects have also been studied by Ross 1959 and Laird, Johnson, and Walker 1960. The results of both studies show the same nature of blocking effect and sheltering effect with the study of Morison, Johnson and O'Brien, but there are some differences in the magnitudes of these effects among these studies.

Taking the large amount of variation in actual wave forces into consideration, it may be considered that the blocking and sheltering effects will be negligible if the relative spacing S/D is greater than 2 (center-to-center distance to be more than three pile diameters). As for the group pilings with the relative spacing samller than 2, the blocking effect should be taken into account in the actual pile design.

2) Impact forces of breaking waves

In the previous discussions, the wave force on a pile is treated as a statical force or a gradually varying force. When breaking waves, especially of plunging

type on steep slope, attack a pile, such a treatment may not be applicable and the consideration of an impact force due to sudden accelerations may become necessary. Experiments by Hall 1958 on a slope of 1 to 10 showed a breaking wave force factor of C_B in the following expression

$$F_B = C_B \, w \, D \, H_B^2$$

to be 1.2 to 3.0 for the maximum breaking wave force. Since the maximum drag force factor K_D in Fig. 20 is about 0.7, this value of C_B indicates that the impact of breaking waves causes the wave forces two to four times larger than the forces by non-breaking waves with the same wave heights, assuming the drag coefficient C_D to be 1.0 for Hall's data. Some experiments are also being conducted by the author on the breaking wave forces on a pile erected on a gentle slope of 1 to 100. Preliminary results have shown that a pile attacked by breaking waves experiences a wave force about two times larger than that by non-breaking waves with identical wave heights. Since these impact forces have very short durations, there is a question whether a prototype pile may respond to such a high frequency force especially when a prototype pile has some flexibility. Nevertherless, the nature and magnitude of impact forces by breaking waves on pile have to be studied in full detail.

3) **Flexibility of a pile or an offshore structure**

A prototype pile or offshore structure is not a rigid body but a flexible one with a some range of natural frequency. When the natural frequency of a structure is the same or nearly the same with the predominant wave frequency, a high degree of resonant oscillation may occur for the structure and introduce large stresses in structural members. Such a resonant oscillation may not be a dangerous one for a single vertical pile, since the natural period of a sigle pile is mostly less tha a few seconds. But for a platform with slender legs in fairly deep sea, the wave periods and the natural periods may coincide. Harleman, Nolan, and Honsinger 1962 measured the displacement of a model platform and showed the largest displacement being associated with relatively small wave height and short wave period. By replacing the model platform with an equivalent spring-mass system, they have also analysed the behavior of the platform numerically and obtained a good agreement with the experimental data. Based on this study, they suggest a selection of the design wave with a wave period which will cause resonant oscillations in the structure.

On the other hand, if a structure is a very flexible one with a natural period of a minute or so, then the resultant force will be much smaller than that for a rigid structure. Such an occasion might appear in the operation of oil-drilling in the sea a few hundred meters deep, as the exploration of petroleum resources moves from the shallow continental shelf to the deeper portion as seen in the cases of the Gulf

of Mexico.

4) **Wave force on large diameter pile**

As the diameter of a cylinder becomes large, the interference of the cylinder with the wave system must be taken into consideration. For waves of small amplitudes in the water of finite depth, MacCamy and Fuchs 1954 have solved the wave pattern around a vertical circular cylinder with the diffraction theory and computed wave force (virtual mass force) acting on the cylinder. When their result is interpreted in terms of the virtual mass coefficient C_M after Reid 1960, the coefficient varies with the ratio of the cylinder diameter to the wave length as shown in Table 2:

Table 2. Virtual Mass Coefficient Based on Diffraction Theory

D/L	C_M	D/L	C_M
0.048	2.03	0.478	0.842
0.096	2.06	0.573	0.653
0.143	2.04	0.669	0.523
0.191	1.92	0.764	0.436
0.239	1.73	0.859	0.353
0.287	1.53	0.955	0.308
0.334	1.30	1.000	0.288
0.382	1.12		

These values are computed from the following equation

$$C_M = \frac{16\ L^2}{\pi^3\ D^2\ \sqrt{[J_1'(\pi D/L)]^2+[Y_1'(\pi D/L)]^2}}$$

in which J_1 and Y_1 are Bessel functions of the first and second kind, of the first order. From this table it is seen that a pile is considered as a small diameter pile when D/L is less than 0.15. For a larger pile diameter, a correction for the virtual mass coefficient is necessary.

Another information on the definition of a large diameter pile is the relative magnitude of the virtual mass force compared to the drag force. Based on Figs. 20 and 23 the critical value of H/D which gives the equal magnitude of virtual mass force and drag forces is calculated and plotted in Fig. 28. The drag coefficient C_D and the virtual mass coefficient C_M are taken as 1.0 and 2.0, respectively. Since the magnitude of the drag force increases as the relative wave height H/h increases, the critical value of H/D for $(F_D)_{max}=(F_M)_{max}$ depends upon the relative wave height H/h as well as the relative depth h/L_A. In Fig. 28, two extreme cases of infinitesimal wave height and of maximum wave height of breakers are presented. The figure may serve as a handy reference to estimate relative magnitudes of drag force and virtual mass force.

5) **Protection against the scouring at the foot of a pile**

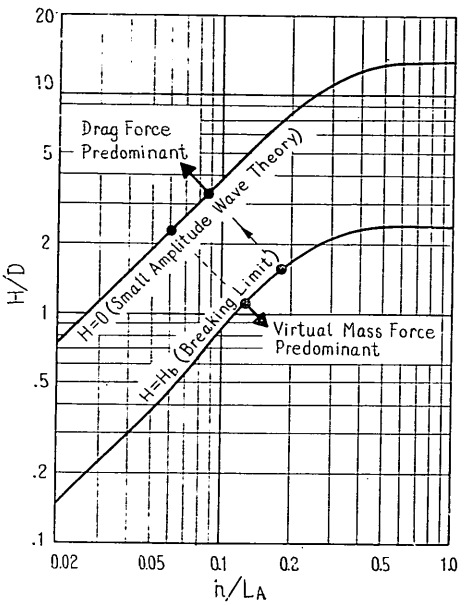

Fig. 28. Critical Value of H/D For $(F_D)_{max}=(F_M)_{max}$

In a design of a single pile driven into the foundation, the predominant design factor will be the bending moment of wave force at the foot of piling. Unless the foundation is made of rocks, some kind of protection works is necessary to prevent the scouring at the foot of a pile, since any scouring causes an increase in the bending moment. The area which requires the scouring protection works may be determined from the size of bed materials and the orbital velocity pattern around the pile. The first approximation for the velocity field is that of two-dimensional potential flow around a circular cylinder, although wakes and eddies are present in the rear of the cylinder in the actual flow. The velocity field around a circular cylinder placed in an uniform flow is described as:

$$q=U\left(1-2\frac{a^2}{r^2}\cos 2\theta+\frac{a^4}{r^4}\right)^{\frac{1}{2}}$$

where q is the resultant velocity, U is the uniform flow velocity, r is the distance from the center of the cylinder, and a is the radius of the cylinder. The maximum velocity is observed at the sides of the cylinder where the velocity is twice the uniform flow velocity. In the case of a small diameter pile, the horizontal orbital velocity at the bottom $u_{z=0}$ can be taken as U.

V. CONCLUSIONS

Summing up the results of the study described above, the followings are the major conclusions:

1. The height of a wave crest above the sea bottom in term of the mean water depth is most closely related to the ratio of the wave height to the water depth. An index curve proposed for the relation between h_c/h and H/h seems to be satisfactory for practical design purposes.
2. The horizontal velocities of water particles under wave crests have been expressed with the orbital velocities of small amplitude waves and a velocity factor which varies from 1.0 to 3.0 depending upon the relative wave height, the relative

elevation of water particle, and the relative depth. A formula for the velocity factor has been given to cover the whole range of progressive waves. The resultant orbital velocity shows a good agreement with experimental data.

3. The drag coefficient of a circular cylinder under the wave action has been determined, based upon the actual distribution of water particle velocities. The actual drag coefficient showed a scatter in its value from 0.34 to 2.0 for the range of the Reynolds number from 1.0×10^4 to 2.1×10^5, but the average value and tendency of the actual drag coefficient agreed fairly well with the drag coefficient in steady state flow.
4. The most reliable value of the virtual mass coefficient is 1.71 with a standard deviation of 0.12. For the practical purpose of a pile design, however, the value of 2.0 is recommended in co-operations with the water particle accelerations of small amplitude waves.
5. Based upon the experimental data and theoretical considerations, a calculation method of wave forces on a vertical cylinder has been presented. The calculation method has been calibrated with the experimental data by the author and by Harleman and Shapiro, showing a tendency to forecast a little larger wave forces and moments than the actual ones. Since the error is on the safe side, the calculation method can be used for the actual wave force designs.

ACKNOWLEDGEMENT

The study presented herein was conducted at the Hydraulics Division of the Port and Harbour Technical Research Institute under the supervision of Dr. Senri Tsuruta, Head of the Division. He also granted the use of the experimental data to the author which he obtained with the assistances of Mr. Suketo Haranaka, Mr. Shusaku Kakizaki, and the author, and presented in a part of his report in Japanese. The author sincerely wishes to express his appreciation to Dr. Senri Tsuruta for his helpful supervision and generous grant for the publication of the experimental data.

The author also wishes to express his heartful thanks to Dr. Hisashi Mitsuyasu, Chief of the Wave Laboratory, for his critical review of the manuscript and suggestions to it.

REFERENCES

1. Beach Erosion Board (1961): "Shore Protection Planning and Design," Technical Report No. 4, U. S. Government Printing Office, 241 pp.
2. Blumberg, R. and Rigg, A. M. (1961): "Hydrodynamic Drag at Super-Critical Reynolds Numbers" Paper presented at ASME meeting, Los Angels,

California, June 14, Petroleum Session.

3. Bretschneider, C. L. (1958) : "Selection of Design Wave for Offshore Structures," Journal of the Waterways and Harbors Division, Proc. ASCE, WW 2, Paper No. 1568, March, 37 pp.
4. Chappelear, J. E. (1959) : "On the Theory of the Highest Waves," Beach Erosion Board, Technical Memorandum No. 116, July, 28 pp.
5. Crook, R. C. (1955) : "Re-analysis of Existing Wave Force Data on Model Piles," Beach Erosion Board, Technical Memorandum No. 71, April, 19 pp.
6. Dean, R. G. and Harleman, D. R. F. (1963) : "Interaction of Structures and Waves," Chapter H of Estuary and Coastline Hydrodynamics edited by A. T. Ippen, MIT Hydrodynamics Laboratory.
7. Fage and Warsap (1930) : A. R. C. Reports and Memoranda. No. 1283, quoted by Goldstein (1938).
8. Goldstein, S. (1938) : "Modern Development in Fluid Dynamics," Oxford, New York.
9. Hall, M. A. (1958) : "Laboratory Study of Breaking Wave Forces on Piles," Beach Erosion Board, Technical Memorandum No. 116, August, 24 pp.
10. Harleman, D. R. F. and Shapiro, W. C. (1955) : "Experimental and Analytical Studies of Wave Forces on Offshore Structures Part I," MIT Hydrodynamics Laboratory, Technical Report No. 19, May, 55 pp.
11. Harleman, D. R. F., Nolan, W. C., and Honsinger, V. C. (1962) : "Dynamic Analysis of Offshore Structure," Proc., Eighth Conference on Coastal Engineering, Chapter 28, pp. 482-499.
12. Havelock, T. H. (1919) : "Periodic Irrotational Waves of Finite Height," Proc. Roy. Soc., London, Ser. A. Vol. 95, pp. 38-51.
13. Iversen, H. W. and Balent, R. (1951) : "A Correlating Modulus for Fluid Resistance in Accelerated Motion," Jour. Applied Physics, Vol. 22, No. 3, pp. 324-328.
14. Iversen, H. W. (1952) : "Laboratory Study of Breakers," National Bureau of Standard, Circular 521, Gravity Waves, Chapter 3, pp. 9-32.
15. Laitone, E. V. (1960) : "The Second Approximation to Cnoidal and Solitary Waves," Jour. Fluid Mech., Vol. 9, Part 3, pp. 430-444.
16. Laird, A. D. K., Johnson, C. A., and Walker R. W. (1959) : "Water Forces on Accelerated Cylinders," Journal of the Waterways and Harbors Division, Proc., ASCE, WW 1, Paper No. 1982, March, pp.99-119.
17. Laird, A. D. K., Johnson, C. A., and Walker, R. W. (1960) : "Water Eddy Forces on Oscillating Cylinders," Journal of the Hydraulics Division, Proc. ASCE, HY 9, Paper No. 2652, Nov., pp. 43-54.

18. MacCamy, R. C. and Fuchs, R. A. (1954) : "Wave Forces on Piles : A Diffraction Theory," Beach Erosion Board, Technical Memorandum No. 69, Dec., 17 pp.
19. McCowan, J. (1894) : "On the Highest Wave of Permanent Type," Philosophical Mag., Series 5, Vol. 38, pp. 351-358.
20. Michell, J. H. (1893) : "On the Highest Waves in Water," Philosophical Mag., Series 5, Vol. 36, pp. 430-435.
21. Miyazaki, M., Unoki, S., and Ueno, T. (1961) : "On Storm Surges Caused by the Ise Bay Typhoon and Theoretical Computations," Coastal Engineering in Japan, Vol. 4, pp. 11-22.
22. Morison, J. R., O'Brien, M. P., Johnson, J.W., and Schaaf, S.A.(1950) : "The Force Exerted by Surface Waves on Piles," Petroleum Tans., Amer. Inst. Mining and Metal Engr., Vol. 189, 149-154.
23. Morison, J. R. (1951) : "Design of Piling," Proceedings of First Conference on Coastal Engineering, Chapter 28, pp. 254-258.
24. Morison, J. R., Johnson, J. W., and O'Brien, M. P. (1953) : "Experimental Studies of Forces on Piles," Proceedings of Fourth Conference on Coastal Engineering, Chapter 25, pp. 340-370.
25. Munk, W. H. (1949) : "The Solitary Wave and Its Application to Surf Problems," Annals New York Acad. Sci., Vol. 51, Art. 3, pp. 376-424.
26. Quinn, A. DeF. (1961) : "Design and Construction of Ports and Marine Structures," McGraw Hill, New York, 531 pp.
27. Reid, R. O. and Bretschneider, C. L. (1953) : "Surface Waves and Offshore Structure : The Design Wave in Deep or Shallow Water, Storm Tide, and Forces on Vertical Piles and Large Submerged Objects," Technical Report, Texas A. & M. Research Foundation, 36 pp.
28. Reid, R. O. (1957) : "Correlation of Water Level Variations with Wave Forces on a Vertical Pile for Nonperiodic Waves," Proc., Sixth Conference on Coastal Engineering, Chapter 46, pp. 749-786.
29. Reid, R. O. (1960) : "Estimation of Wave Forces on a Fixed Vertical Cylinder of Large Diameter," Department of Oceanography, A. and M. College of Texas, May (unpublished).
30. Ross, C. W. (1959) : "Large-Scale Tests of Wave Forces on Piling," Beach Erosion Board, Technical Memorandum, No. 111, May.
31. Skjelbreia, L. and Hendrickson, J. A. (1962) : "Fifth Order Gravity Wave Theory with Tables of Functions," National Engineering Science Company, Pasadena, California, 424 pp.
32. Tsuruta, S. (1961) : "Some Design Problems of an Oil-Drilling Platform,"

Transportation Technical Research Institute, Ministry of Transportation, 331 pp. (in Japanese, unpublished).

33. Unoki, S. and Isozaki, I. (1963) : "On the Effect of a Dike with Openings on the Storm Surge Caused by a Typhoon," Coastal Engineering in Japan, Vol. 6, pp. 58-65.

34. Wiegel, R. L., Beebe, K. E., and Moon, J. (1957) : "Ocean Wave Forces on Circular Cylindrical Piles," Journal of the Hydraulics Division, Proc. ASCE, HY 2, Paper No. 1199, March, 36 pp.

35. Wilson, B. W. and Reid, R. O. (1963) : A Discussion of "Wave Force Coefficients for Offshore Pipelines," Journal of the Waterways and Harbors Division, Proc. ASCE, WW 1, Feb., pp. 61-65.

36. Yamada, H. (1957a) : "Highest Waves of Permanent Type on the Surface of Deep Water," Reports of Research Inst. Applied Mech., Univ. of Kyushu, Vol. V, No. 18, pp. 37-52.

37. Yamada, H. (1957b) : "On the Highest Solitary Wave," Reports of Research Inst. Applied Mech., Univ. of Kyushu, Vol. V, No. 18, pp. 53-67.

38. Yamada, H. (1958) : "Permanent Gravity Waves on Water of Uniform Depth," Reports of Research Inst. Applied Mech., Univ. of Kysushu, Vol. VI. No. 23, pp. 127-139.

TABLE A-1 Characteristics of Test Waves and Data of Wave Forecs on a Pile

No	h (cm)	i	ℓ (m)	T (sec)	L_A (m)	H (cm)	h/L_A	H/L_A	η_c/Hu^* (%)	(cm/sec)	$2A_1/H$	$2A_2/H$	$2A_3/H$	$2A_4/H$	$2A_5/H$	D (cm)	H/D	R_e $\times 10^4$	M_{max} (kg-m)	M_D	M_M	C_D	C_D'	C'_M
1	130	0	64	2.24	6.61	43.9	0.197	0.0664	56.5	72.4	0.922	0.147	0.073	0.016	0.007	7.62	5.77	4.86	1.506	1.444	0.868	0.829	1.37	1.42
2				2.25	6.65	53.2	0.195	0.0800	60.5	87.2	0.898	0.215	0.074	0.032	0.009		7.00	5.85	2.47	2.105	0.937	0.726	1.38	1.27
3				4.06	13.72	59.0	0.0948	0.0284	59.3	73.8	0.998	0.295	0.028	0.029	0.054		5.13	4.96	1.697	1.697	0.520	0.790	1.88	1.70
4				4.10	13.86	59.8	0.0968	0.0431	61.8	98.0	0.889	0.263	0.110	0.052	0 024		7.86	6.37	3.80	3.80	0.775	0.823	1.80	1.65
5	100	0	64	1.950	5.03	36.8	0.1986	0.0733	52.6	73.9	0.917	0.192	0.055	0.034	0.021	7.62	4.83	4.93	0.959	0.739	0.498	0.551	1.32	1.26
6				3.38	9.97	23.9	0.1003	0.0239	52.7	47.0	0.843	0.078	0.137	0.073	0.064		3.14	3.14	0.519	0.509	0.182	1.061	1.99	1.17
7				3.27	9.90	31.8	0.1010	0.0321	57.6	65.9	0.867	0.132	0.098	0.062	0.031		4.18	4.41	0.796	0.781	0.261	0.749	1.74	1.24
8				3.38	9.95	35.6	0.1005	0.0358	59.7	76.5	0.863	0.278	0.097	0.022	0.016		4.68	5.06	1.740	1.351	0.444	0.893	2.36	1.89
9				3.37	9.93	41.3	0.1007	0.0417	59.8	96.7	0.809	0.229	0.117	0.075	0.032		5.42	6.46	2.000	1.813	0.363	0.703	2.36	1.33
10	150	0	64	1.527	3.60	23.5	0.417	0.0653	51.1	61.9	0.935	0.046	0.052	0.036	0.030	7.62	3.08	4.10	1.431	0.460	1.062	0.549	1.39	2.00
11				1.627	4.05	34.5	0.370	0.0852	57.3	56.6	0.934	0.160	0.051	0.008	0.022		4.53	3.78	1.632	0.730	1.263	0.709	1.03	1.69
12				1.829	4.98	22.5	0.301	0.0453	56.8	44.8	0.960	0.090	0.015	0.008	0.018		2.95	2.98	0.998	0.447	0.816	0.858	1.48	1.81
13				1.826	4.97	35.9	0.302	0.0653	61.4	63.4	0.943	0.245	0.068	0.019	0.018		3.08	4.10	1.743	1.243	1.351	0.806	1.61	1.88
14				2.02	5.86	51.7	0.256	0.0833	59.2	79.8	0.947	0.145	0.022	0.028	0.020		6.78	5.34	2.30	2.19	1.38	0.736	1.36	1.44
15				2.37	7.47	32.1	0.201	0.0430	56.5	58.0	1.032	0.156	0.042	0.020	0.014		4.21	3.86	1.338	1.297	0.937	0.939	2.03	1.79
16				2.38	7.50	46.2	0.200	0.0616	60.1	73.7	0.964	0.195	0.033	0.013	0.019		6.06	4.91	2.71	2.10	1.17	0.709	1.59	1.56
17				2.37	7.47	57.3	0.201	0.0767	61.3	95.2	0.966	0.223	0.041	0.016	0.018		7.51	6.38	3.71	3.71	1.59	0.641	1.56	1.70
18				2.54	8.22	65.7	0.1825	0.0798	62.3	94.8	0.925	0.215	0.073	0.014	0.030		8.62	6.33	4.53	3.50	1.44	0.543	1.29	1.44
19				3.11	10.66	30.5	0.1403	0.0286	57.0	49.4	0.954	0.123	0.046	0.030	0.011		4.00	3.16	1.362	1.346	0.563	1.314	2.22	1.44
20				3.11	10.64	41.2	0.1410	0.0387	58.6	66.4	0.960	0.171	0.019	0.018	0.010		5.40	4.43	1.975	1.586	0.842	0.779	1.44	1.59
21				3.22	11.13	56.4	0.1348	0.0507	60.7	83.6	0.957	0.221	0.047	0.022	0.010		7.39	5.52	3.34	2.96	1.25	0.753	1.42	1.78
22				3.52	12.58	54.9	0.1193	0.0436	66.0	95.9	0.871	0.218	0.091	0.018	0.028		7.20	6.41	3.78	3.60	1.24	0.629	1.88	2.00
23				4.13	14.89	15.3	0.1007	0.0103	53.2	23.5	0.838	0.038	0.162	0.047	0.041		2.01	1.55	0.390	0.357	0.210	1.678	2.27	1.40
24				4.12	14.85	28.5	0.1010	0.0192	54.3	46.8	0.899	0.050	0.093	0.039	0.019		3.74	3.13	1.348	1.166	0.335	1.369	2.12	1.19
25				4.13	14.91	39.2	0.1006	0.0263	50.8	58.8	0.940	0.116	0.090	0.026	0.028		5.14	3.92	1.689	1.618	0.514	0.961	1.56	1.33
26				4.14	14.94	38.7	0.1003	0.0259	61.1	70.2	0.932	0.206	0.080	0.028	0.055		5.08	4.72	2.71	2.46	0.63	0.945	2.43	1.65
27				4.15	14.98	65.7	0.1001	0.0439	61.5	94.3	0.867	0.265	0.087	0.035	0.003		8.62	6.32	4.17	3.66	0.73	0.586	1.25	1.13

u*: orbital velocity beneath the wave crest at the height of still water levol

$$R_e = \frac{u^* D}{\nu}$$

TABLE A-1 (2)

No	h (cm)	i	ℓ (m)	T (sec)	L_A (m)	H (cm)	h/L_A	H/L_A	η_c/H (%)	u* (cm/sec)	$2A_1/H$	$2A_2/H$	$2A_3/H$	$2A_4/H$	$2A_5/H$	D (cm)	H/D	R_e $\times 10_4$	M_{max} (kg-m)	M_D	M_M	C_D	C_D'	C'_M
28	150	0	64	5.74	21.35	30.8	0.0703	0.0145	60.5	51.4	0.805	0.265	0.177	0.080	0.035	7.62	4.04	3.42	1.345	1.205	0.341	0.997	1.83	1.54
29				5.70	21.19	38.1	0.0708	0.0180	63.1	71.1	0.803	0.248	0.168	0.064	0.023		5.00	4.74	2.33	2.21	0.344	0.903	2.19	1.25
30				5.62	20.86	52.2	0.0719	0.0251	62.8	85.3	0.811	0.213	0.192	0.091	0.021		6.85	5.69	3.77	3.68	0.50	0.855	1.94	1.30
31				5.71	21.24	52.1	0.0706	0.0245	58.7	89.1	0.896	0.167	0.104	0.072	0.033		6.85	5.97	3.62	3.19	0.84	0.726	1.69	2.25
32				7.97	30.06	18.7	0.0500	0.0062	59.4	30.7	0.700	0.345	0.119	0.047	0.076		2.55	2.05	0.407	0.391	0.152	1.004	1.60	1.55
33				7.91	29.84	36.0	0.0502	0.0121	69.8	54.8	0.598	0.479	0.216	0.100	0.027		4.72	3.75	1.794	1.723	0.358	1.079	1.89	1.88
34				7.96	30.03	49.6	0.0500	0.0165	70.1	81.7	0.469	0.538	0.249	0.115	0.056		6.50	5.48	4.10	3.86	0.63	0.978	2.28	2.43
35				7.96	30.05	60.2	0.0500	0.0201	70.8	104.2	0.396	0.600	0.238	0.127	0.076		7.90	7.01	6.03	5.80	0.93	0.765	2.27	2.94
36				7.90	29.79	60.4	0.0504	0.0233	72.3	117.8	0.325	0.638	0.188	0.172	0.076		9.10	7.89	7.68	7.47	0.83	0.700	2.21	2.26
37	200	0	64	1.603	3.99	27.0	0.501	0.0676	55.7	53.4	0.948	0.108	0.033	0.012	0.024	7.62	3.54	3.57	1.703	0.826	1.529	0.790	1.39	1.76
38				2.10	6.58	21.6	0.304	0.0328	51.7	28.1	1.010	0.076	0.019	0.041	0.022		2.83	1.87	1.045	0.336	0.941	0.987	0.96	1.63
39				2.74	9.99	20.3	0.200	0.0204	53.4	31.0	0.958	0.064	0.027	0.044	0.073		2.66	2.06	0.765	0.517	0.795	1.056	1.52	1.81
40				2.75	10.06	48.2	0.1988	0.0479	55.6	62.0	0.950	0.124	0.097	0.014	0.044		6.32	4.13	2.78	2.35	1.605	0.815	1.20	1.60
41				4.80	20.00	26.3	0.1000	0.0132	57.5	44.6	1.017	0.232	0.111	0.036	0.030		3.45	2.97	1.316	1.273	0.737	0.939	2.03	2.14
42				6.59	28.25	23.0	0.0707	0.0081	59.8	30.6	0.796	0.213	0.089	0.023	0.110		3.02	2.04	0.843	0.652	0.362	0.982	1.33	1.62
43	150	0	64	1.728	4.52	37.7	0.332	0.0833	59.3	74.1	0.920	0.140	0.017	0.045	0.028	13.98	2.70	10.73	5.58	2.08	4.01	0.620	1.33	1.53
44				2.38	7.51	36.0	0.1995	0.0490	57.7	67.5	0.966	0.143	0.016	0.007	0.099		2.58	9.75	4.56	2.17	3.73	0.614	1.47	1.90
45				2.36	7.41	52.7	0.203	0.0713	59.3	85.5	0.882	0.152	0.072	0.020	0.027		3.77	11.05	6.73	3.12	4.86	0.471	0.83	1.68
46				2.43	7.74	58.5	0.1940	0.0756	61.8	95.2	0.928	0.173	0.059	0.017	0.014		4.19	13.76	8.89	5.84	5.58	0.608	1.85	1.79
47				2.98	10.13	34.6	0.1480	0.0336	58.8	48.5	0.870	0.103	0.096	0.050	0.015		2.63	7.0	3.13	1.29	2.19	0.671	0.98	1.41
48				3.14	10.78	55.9	0.1391	0.0518	59.0	87.5	0.928	0.243	0.057	0.013	0.011		4.00	12.95	9.41	5.04	4.81	0.632	1.36	2.01
49				4.15	14.97	28.6	0.1002	0.0191	55.8	45.1	0.949	0.092	0.055	0.046	0.011		2.05	6.51	2.09	1.11	1.39	0.727	1.09	1.48
50				4.16	15.04	47.0	0.0997	0.0313	59.6	75.0	0.968	0.210	0.035	0.030	0.007		3.36	10.80	5.33	3.84	2.29	0.705	1.40	1.48
51				4.17	15.07	64.7	0.0995	0.0431	61.6	93.8	0.854	0.262	0.073	0.039	0.008		3.20	13.56	8.29	5.96	2.74	0.562	1.15	1.29
52				5.77	21.48	5.73	0.0698	0.0266	64.0	92.2	0.858	0.156	0.153	0.105	0.048		4.10	13.31	6.14	4.99	2.36	0.519	1.20	1.71
53				7.89	29.74	74.3	0.0505	0.0216	74.2	103.5	0.418	0.579	0.206	0.103	0.086		5.32	14.93	8.72	6.53	2.00	0.451	1.23	1.74
54				7.90	29.79	77.2	0.0503	0.0259	75.2	119.2	0.339	0.600	0.180	0.150	0.083		5.52	17.22	13.47	10.36	3.06	0.466	1.35	2.26

TABLE A-1 (3)

No	h (cm)	i	ℓ (m)	T (sec)	L_A (m)	H (cm)	h/L_A	H/L_A	η_c/H (%)	u* (cm/sec)	$2A_1/H$	$2A_2/H$	$2A_3/H$	$2A_4/H$	$2A_5/H$	D (cm)	H/D	R_e $\times 10^4$	M_{max} (kg-m)	M_D (kg-m)	M_M (kg-m)	C_D	C_D'	C'_M
55	130	1/100	50	2.21	6.47	35.6	0.201	0.0552	59.8	57.5	0.919	0.233	0.030	0.012	0.048	13.98	2.54	7.41	3.80	2.05	3.12	0.973	1.64	1.61
56				2.22	6.50	53.8	0.200	0.0825	58.5	88.4	0.940	0.248	0.037	0.020	0.014		3.84	11.42	6.53	5.29	3.95	1.065	1.86	1.35
57				2.21	6.48	63.5	0.201	0.0980	60.2	100.5	0.937	0.230	0.039	0.018	0.015		2.54	12.91	8.87	5.79	4.34	0.610	1.45	1.26
58				2.86	9.21	44.3	0.1411	0.0481	60.7	70.9	0.889	0.238	0.082	0.032	0.011		3.16	9.12	4.50	3.36	3.25	0.927	1.66	1.71
59				2.89	9.23	60.5	1.1407	0.0656	65.0	106.1	0.898	0.285	0.116	0.014	0.006		4.32	13.52	9.51	6.80	3.47	0.639	1.80	1.33
60				2.90	9.82	66.6	0.1400	0.0718	64.6	120.4	0.854	0.319	0.100	0.023	0.027		4.76	15.32	12.41	7.94	3.90	0.542	1.73	1.37
61				3.88	13.07	48.3	0.0995	0.0369	61.4	93.2	0.907	0.246	0.071	0.053	0.035		3.45	11.85	5.95	4.79	2.55	0.706	1.92	1.61
62				3.90	13.11	54.3	0.0992	0.0414	63.3	106.6	0.875	0.296	0.095	0.053	0.031		3.88	13.57	8.35	5.62	2.75	0.538	1.78	1.54
63				3.87	13.07	61.6	0.0995	0.0471	62.5	120.3	0.891	0.300	0.107	0.041	0.014		4.40	15.30	10.34	6.93	2.94	0.501	1.70	1.45
64				5.33	18.46	43.8	0.0704	0.0237	65.3	78.0	0.785	0.273	0.165	0.065	0.039		3.13	9.93	4.52	3.37	1.33	0.667	1.58	1.26
65				5.36	18.47	55.3	0.0704	0.0299	63.9	95.1	0.793	0.250	0.167	0.083	0.044		3.96	12.11	7.06	5.98	1.83	0.667	1.76	1.35
66				5.36	18.47	64.1	0.0704	0.0348	62.9	110.4	0.820	0.235	0.123	0.097	0.038		4.59	14.05	9.24	8.08	2.06	0.669	1.76	1.33
67				7.40	25.98	55.6	0.0500	0.0216	70.7	119.1	0.405	0.493	0.306	0.120	0.075		3.98	15.15	10.12	8.41	2.76	0.618	2.43	2.83
68				7.38	25.90	68.5	0.0502	0.0266	71.7	142.2	0.322	0.516	0.283	0.185	0.117		4.91	18.09	15.27	13.10	3.17	0.586	2.49	2.54
69				7.42	26.05	80.1	0.0496	0.0307	72.7	159.7	0.264	0.482	0.253	0.171	0.115		5.73	20.32	16.00	14.26	2.37	0.407	1.99	1.69
70	130	1/100	50	1.396	3.02	13.43	0.499	0.0444	45.7	31.4	0.977	0.090	0.023	0.029	0.012	13.98	0.96		1.910	0.135	1.999		0.67*	1.840
71				1.387	2.99	20.3	0.502	0.0600	52.9	47.1	0.944	0.116	0.053	0.018	0.013		1.45		2.77	0.58	2.61		1.26*	1.577
72				1.397	3.03	24.4	0.496	0.0807	55.6	57.7	0.924	0.167	0.055	0.009	0.014		1.75		3.40	0.37	3.07		0.56*	1.554
73				1.372	2.93	30.5	0.512	0.1041	56.8	73.3	0.952	0.186	0.055	0.047	0.011		2.18		4.57	0.80	3.82		0.77*	1.529
74				1.817	4.93	9.31	0.304	0.0189	48.5	16.3	1.017	0.064	0.024	0.016	0.017		0.67		1.122	0.126	1.133		1.33*	1.798
75				1.804	4.87	16.84	0.308	0.0346	53.2	32.5	0.990	0.067	0.008	0.020	0.017		1.21		1.97	0.24	2.14		0.78*	1.876
76				1.823	4.96	21.0	0.303	0.0424	50.9	39.5	1.006	0.023	0.025	0.024	0.012		1.50		2.84	0.35	2.61		0.73*	1.836
77				1.821	4.95	30.7	0.304	0.0621	55.8	60.7	0.985	0.132	0.021	0.021	0.007		2.20		3.78	0.90	3.72		0.88	1.796
78				2.38	7.50	17.29	0.200	0.0231	51.2	32.7	0.981	0.057	0.021	0.009	0.020		1.24		1.884	0.204	1.650		0.60*	1.750
79				2.36	7.44	23.6	0.202	0.0318	53.4	41.4	1.003	0.085	0.017	0.018	0.010		1.69		2.56	0.72	2.45		1.14*	1.909
80				2.37	7.49	29.3	0.201	0.0392	55.0	52.6	0.993	0.113	0.012	0.013	0.017		2.10		3.26	1.36	3.00		1.40	1.878

* : These data have little reliability due to small magnitudes of the records of M_D less than 10 mm.

TABLE A-1 (4)

No	h (cm)	i	ℓ (m)	T (sec)	L_A (m)	H (cm)	h/L_A	H/L_A	η_c/H (%)	u* (cm/sec)	$2A_1/H$	$2A_2/H$	$2A_3/H$	$2A_4/H$	$2A_5/H$
81	130	1/100	50	1.706	4.33	10.94	0.300	0.0253	50.7	21.3	0.964	0.075	0.015	0.032	0.011
82				1.702	4.32	23.9	0.301	0.0553	58.4	47.7	0.900	0.150	0.110	0.019	0.019
83				1.696	4.29	29.4	0.303	0.0684	53.3	49.2	0.958	0.108	0.037	0.019	0.013
84				1.705	4.33	36.8	0.300	0.0850	60.8	71.2	0.950	0.254	0.067	0.012	0.019
85				1.705	4.33	47.5	0.300	0.1097	63.9	95.2	0.910	0.244	0.050	0.030	0.015
86				2.21	6.47	13.30	0.201	0.0206	52.6	27.8	1.004	0.166	0.071	0.025	0.009
87				2.21	6.48	27.5	0.201	0.0424	54.6	53.0	1.007	0.118	0.040	0.019	0.048
88				2.22	6.51	40.9	0.200	0.0628	55.7	72.5	0.990	0.108	0.024	0.024	0.014
89				2.21	6.48	53.3	0.201	0.0821	58.9	86.8	0.907	0.188	0.057	0.019	0.017
90				2.21	6.49	64.6	0.200	0.0996	61.8	111.2	0.854	0.265	0.081	0.023	0.015
91	130	1/100	55	2.19	6.40	15.1	0.203	0.0236	50.3	29.3	1.024	0.046	0.019	0.055	0.022
92				2.21	6.49	27.4	0.201	0.0422	52.9	53.0	0.975	0.123	0.024	0.015	0.019
93				2.21	6.49	42.5	0.201	0.0655	58.1	79.3	0.938	0.158	0.037	0.014	0.014
94				2.22	6.50	54.6	0.200	0.0840	60.1	92.9	0.930	0.197	0.051	0.014	0.016
95				2.20	6.44	66.1	0.202	0.1025	65.1	110.0	0.881	0.277	0.117	0.041	0.014
96	110	1/100	65	3.52	10.87	62.5	0.1012	0.0575	69.7	116.4	0.766	0.405	0.166	0.057	0.018
97				3.54	10.98	64.0	0.1003	0.0583	71.4	120.8	0.790	0.369	0.180	0.064	0.026
98				4.91	15.54	20.3	0.0704	0.0130	59.1	34.4	0.802	0.164	0.138	0.022	0.048
99				4.91	15.64	27.0	0.0704	0.0172	64.2	58.5	0.833	0.237	0.183	0.048	0.017
100				4.91	15.61	38.0	0.0704	0.0243	68.9	88.4	0.695	0.313	0.187	0.070	0.042
101				4.82	15.31	47.5	0.0719	0.0311	74.1	98.8	0.624	0.372	0.294	0.137	0.049
102				4.88	15.53	58.7	0.0707	0.0377	77.4	117.5	0.525	0.476	0.286	0.131	0.066
103				4.84	15 37	78.1	0.0717	0.0509	84.4	140.0	0.387	0.409	0.257	0.189	0.117
104				6.90	22.30	64.5	0.0494	0.0290	84.1	136.5	0.351	0.373	0.311	0.194	0.123
105				6.82	22.02	69.8	0.0499	0.0322	84.0	156.1	0.343	0.359	0.287	0.180	0.132
106				6.81	21.99	76.4	0.0500	0.0347	86.7	158.3	0.347	0.299	0.303	0.181	0.147

TABLE A-2 Characteristics of Brearing Waves

No	h_1 (cm)	h_b (cm)	T (sec)	H_1 (cm)	H_b (cm)	$(h/L_A)_b$	$(H/L_A)_b$	$(H/h)_b$	η_c/H (%)	$2A_1/H$	$2A_2/H$	$2A_3/H$	$2A_4/H$	$2A_5/H$
201	100	62.9	2.30	38.8	42.5	0.117	0.0791	0.676	75.6	0.727	0.385	0.188	0.090	0.047
202		62.3	2.57	38.5	41.7	0.104	0.0696	0.669	77.8	0.813	0.380	0.196	0.098	0.061
203		69.8	2.89	38.5	45.8	0.0973	0.0645	0.656	77.4	0.626	0.386	0.184	0.132	0.042
204		60.8	3.19	36.4	43.5	0.0815	0.0583	0.715	79.5	0.540	0.414	0.255	0.189	0.123
205		70.8	3.43	41.9	47.3	0.0821	0.0549	0.668	82.5	0.442	0.383	0.231	0.146	0.102
206		68.5	3.55	39.8	46.3	0.0775	0.0523	0.675	81.3	0.541	0.286	0.252	0.142	0.092
207		62.2	3.68	34.6	44.3	0.0704	0.0501	0.713	80.1	0.451	0.362	0.282	0.164	0.121
208		67.6	3.55	46.4	52.3	0.0770	0.0594	0.773	82.5	0.461	0.370	0.233	0.157	0.140
209		68.3	4.67	45.0	51.0	0.0578	0.0432	0.747	81.2	0.382	0.326	0.294	0.172	0.131
210		65.0	4.83	43.8	51.0	0.0547	0.0429	0.785	79.7	0.385	0.266	0.275	0.197	0.150
211		60.3	5.03	39.9	52.9	0.0506	0.0444	0.877	80.2	0.317	0.257	0.239	0.197	0.171
212		67.4	6.14	40.2	50.5	0.0430	0.0322	0.750	87.4	0.289	0.247	0.288	0.223	0.215
213		61.4	6.41	35.7	50.6	0.0394	0.0325	0.824	88.2	0.272	0.222	0.266	0.223	0.182
214		72.5	6.42	44.4	59.9	0.0428	0.0353	0.826	85.2	0.264	0.332	0.327	0.171	0.191
215		68.0	6.88	43.4	54.1	0.0386	0.0307	0.795	85.0	0.168	0.366	0.208	0.209	0.174
216		61.1	7.30	37.7	53.0	0.0347	0.0296	0.854	84.7	0.148	0.356	0.196	0.243	0.195
217	150	112.5	3.17	64.9	79.5	0.115	0.0813	0.707	77.8	0.647	0.351	0.198	0.118	0.074
218		109.0	3.31	62.8	72.9	0.108	0.0723	0.668	79.0	0.628	0.365	0.197	0.121	0.079
219		107.0	3.48	60.1	71.1	0.102	0.0678	0.665	78.8	0.657	0.410	0.209	0.093	0.057
220		114.0	3.66	66.7	77.8	0.0990	0.0676	0.683	78.6	0.689	0.420	0.208	0.101	0.062
221		121.5	4.20	57.9	79.7	0.0875	0.0574	0.656	80.6	0.570	0.342	0.261	0.121	0.096
222		118.5	4.54	62.8	77.7	0.0801	0.0525	0.655	81.7	0.431	0.394	0.223	0.156	0.104
223		113.5	4.82	65.4	79.3	0.0738	0.0516	0.699	81.1	0.429	0.370	0.251	0.157	0.115
224		111.0	4.92	63.5	77.4	0.0708	0.0493	0.697	83.1	0.454	0.410	0.277	0.181	0.115
225		107.5	5.04	60.8	77.1	0.0682	0.0490	0.718	78.6	0.438	0.371	0.264	0.164	0.122
226		122.0	4.61	74.5	86.8	0.0804	0.0571	0.711	75.9	0.454	0.420	0.227	0.170	0.101
227		116.0	4.77	74.3	84.9	0.0742	0.0543	0.732	77.9	0.397	0.424	0.238	0.166	0.119
228		109.0	5.00	75.2	85.3	0.0687	0.0538	0.783	79.9	0.310	0.419	0.236	0.198	0.130
229		104.0	5.33	72.7	86.5	0.0633	0.0522	0.825	81.7	0.395	0.324	0.242	0.172	0.122
230		122.0	6.30	67.7	93.1	0.0580	0.0428	0.738	84.2	0.473	0.387	0.319	0.214	0.149
231		118.5	6.50	69.1	86.2	0.0550	0.0397	0.722	86.6	0.329	0.316	0.296	0.193	0.161
232		113.0	6.69	66.8	87.2	0.0520	0.0398	0.765	85.9	0.287	0.324	0.261	0.209	0.161
234		107.0	6.92	68.1	86.4	0.0493	0.0398	0.808	87.1	0.318	0.273	0.269	0.198	0.155

TABLE A-3 Harmonic Analysis of Test Wave for Determination of Virtual Mass Coefficient

Case No	Wave No	T (sec)	H (cm)	a_0	a_1	b_1	a_2	b_2	a_3 (cm)	b_3	a_4	b_4	a_5	b_5	M_1 (kg-m)	C_M
70	3	1.396	13.62	−0.85	0.95	6.69	−0.24	0.49	−0.04	0.02	0.16	0.13	−0.03	−0.03	1.910	1.575
	8	1.396	13.63	−0.88	1.40	6.54	−0.42	0.51	−0.19	−0.21	0.11	0.13	−0.09	−0.06	1.869	1.680
71	3	1.387	19.63	−0.56	2.01	9.05	−1.31	0.11	−0.21	−0.33	−0.06	0.11	−0.09	−0.12	2.53	1.757
	8	1.387	20.63	−0.51	1.40	9.72	−0.98	0.31	0.27	−0.63	0.10	0.20	−0.05	−0.09	2.62	1.694
72	3	1.397	25.00	−0.68	2.38	11.55	−1.94	−0.07	0	−0.73	−0.06	0.15	0	−0.22	2.88	1.664
	8	1.397	25.63	−0.49	2.91	11.49	−2.11	0.36	−0.38	−0.60	0.02	0.07	0.09	0.09	3.41	1.868
73	3	1.372	29.00	−0.85	5.04	13.03	−3.12	1.36	−0.36	−0.67	−0.47	−0.02	−0.12	0.12	4.18	1.860
	8	1.372	29.76	−1.00	4.78	13.29	−1.91	0.69	−0.88	−0.04	−0.91	−0.11	−0.24	−0.21	4.49	1.987
74	3	1.817	9.38	−0.26	0.25	4.71	−0.03	0.31	−0.06	0.08	0.07	−0.06	0	−0.06	1.086	1.555
	8	1.817	9.25	−0.33	0.48	4.75	−0.19	0.22	0	0.13	−0.04	0.04	0.08	−0.06	1.129	1.571
75	3	1.804	17.00	−0.11	0.40	8.42	−0.45	−0.07	−0.02	0.05	−0.12	0.11	0.25	0.02	2.041	1.755
	8	1.804	17.00	−0.06	0.60	8.39	−0.54	−0.25	0	−0.08	0	0.18	0.03	0.03	1.911	1.736
76	3	1.823	20.88	0.02	−0.12	10.55	−0.24	−0.13	0.37	0.25	0.07	0.16	−0.01	0.15	2.66	1.791
	8	1.823	21.01	−0.03	−0.34	10.50	−0.04	0.13	−0.04	0.06	0.31	0.14	0.06	0.07	3.53	1.700
77	3	1.821	30.26	0.12	1.51	14.91	−2.14	−0.05	0.37	0.06	0.07	0.34	0.06	−0.03	3.19	1.530
	8	1.821	31.01	−0.11	1.61	15.08	−1.83	−0.55	0.26	0.02	−0.02	0.30	0.13	−0.06	3.53	1.780
78	3	2.38	17.25	−0.14	0.18	8.47	−0.25	0.46	0.16	−0.10	0.03	0.08	0	0.07	1.780	1.850
	8	2.38	17.38	−0.04	−0.14	8.51	−0.21	0.39	0.15	−0.07	0.07	−0.01	0.24	0.10	1.760	1.782
79	3	2.36	22.38	0.05	1.36	11.69	−0.91	0.15	−0.23	0.11	−0.16	−0.11	−0.13	−0.11	2.27	1.743
	8	2.36	23.68	−0.10	1.36	11.75	−1.06	0.22	−0.12	0.08	−0.09	0.18	−0.05	0.02	2.23	1.615
80	3	2.37	29.38	−0.06	1.42	14.43	−1.61	0.43	0.11	−0.10	0.21	0.11	−0.27	0.10	2.53	1.532
	8	2.37	28.75	−0.03	1.60	14.28	−1.57	0.38	0	−0.19	−0.09	0.09	−0.10	−0.18	2.58	1.668

APPENDIX Figures of Typical Wave Profiles and Orbital Velocity Distributions under Wave Crests and Troughs

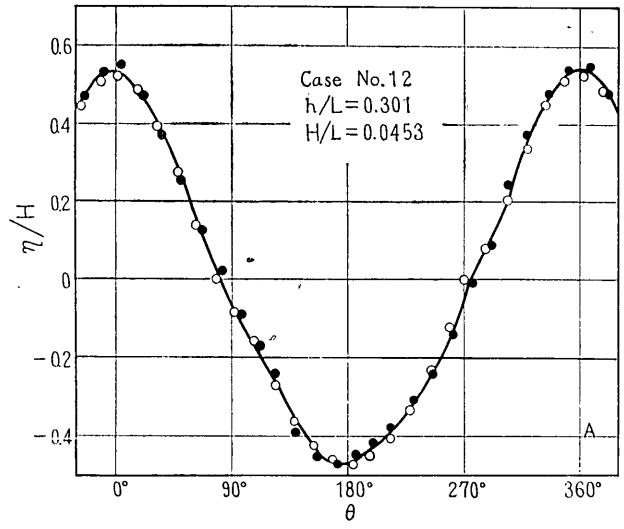

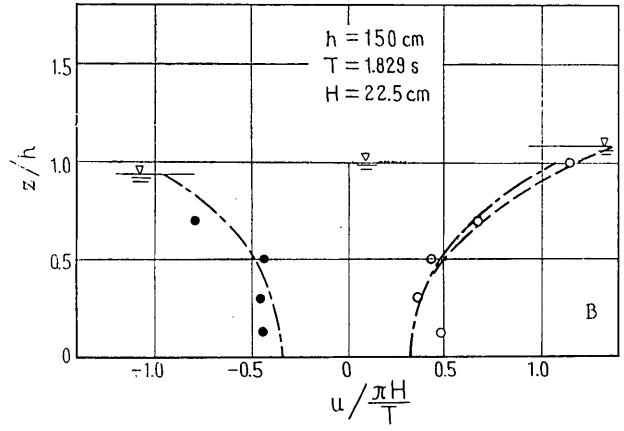

Fig. A—1

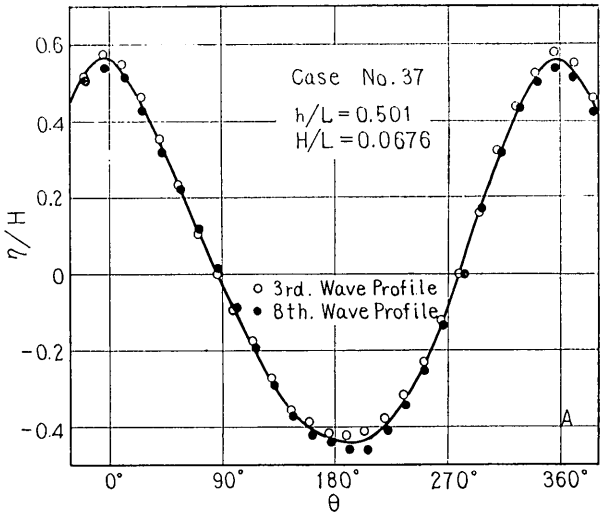

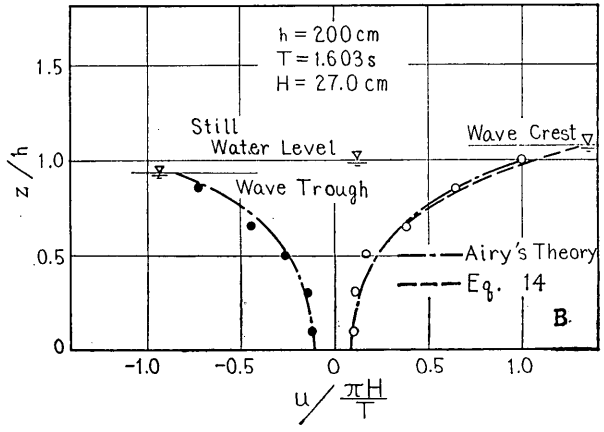

Fig. A—2

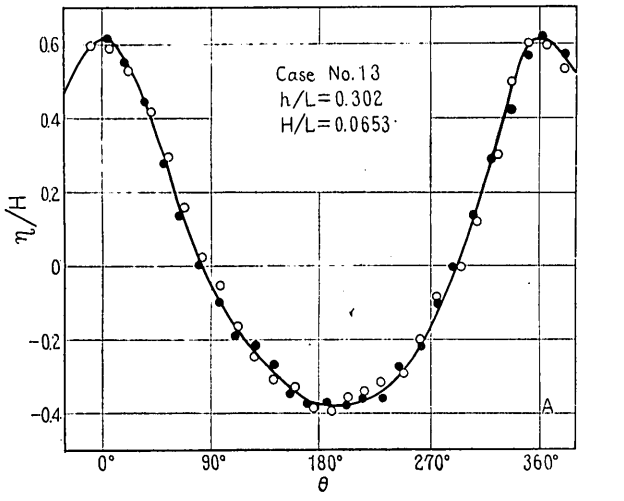
Case No. 13
h/L = 0.302
H/L = 0.0653
η/H
θ
A

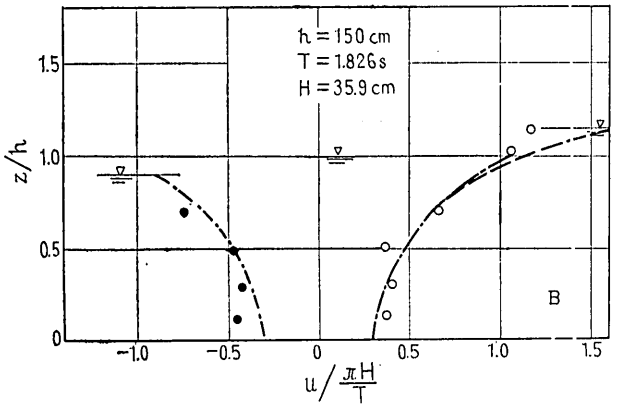
h = 150 cm
T = 1.826 s
H = 35.9 cm
z/h
u / πH/T
B

Fig. A—3

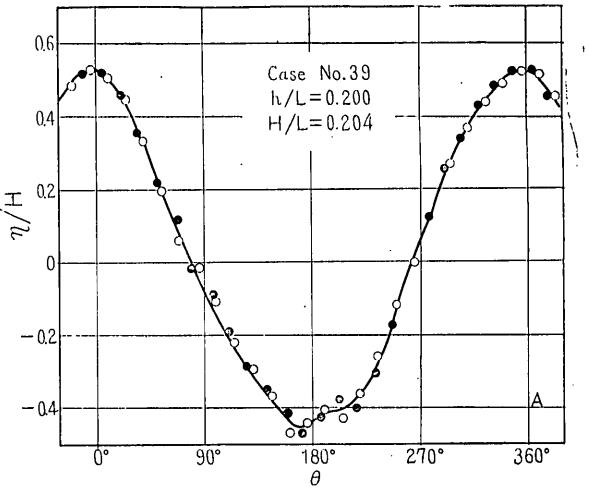
Case No. 39
h/L = 0.200
H/L = 0.204
η/H
θ
A

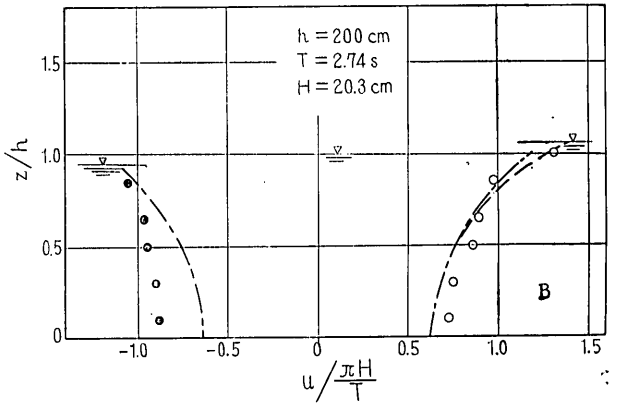
h = 200 cm
T = 2.74 s
H = 20.3 cm
z/h
u / πH/T
B

Fig. A—4

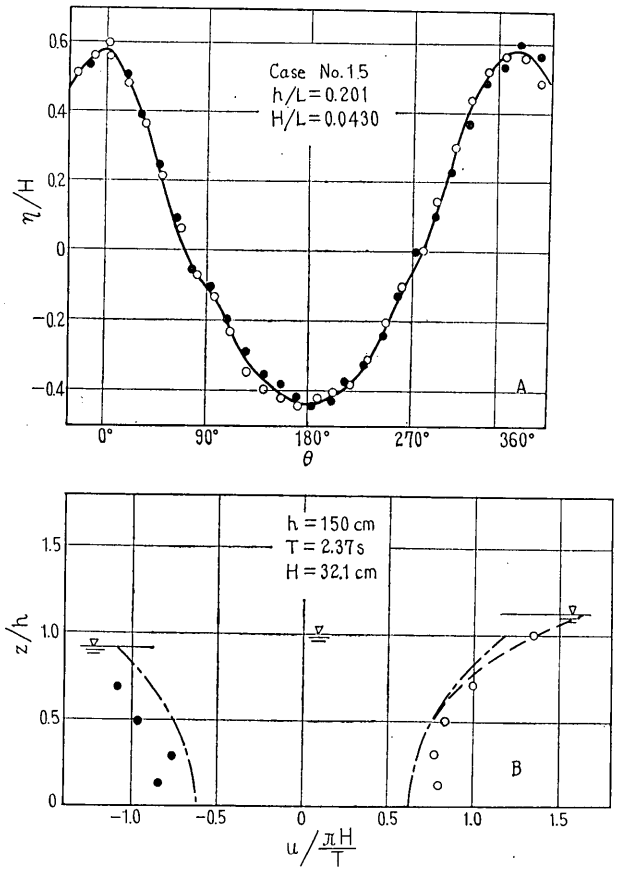
Case No. 15
h/L = 0.201
H/L = 0.0430
η/H
θ
A
h = 150 cm
T = 2.37 s
H = 32.1 cm
z/h
u/(πH/T)
B

Fig. A—5

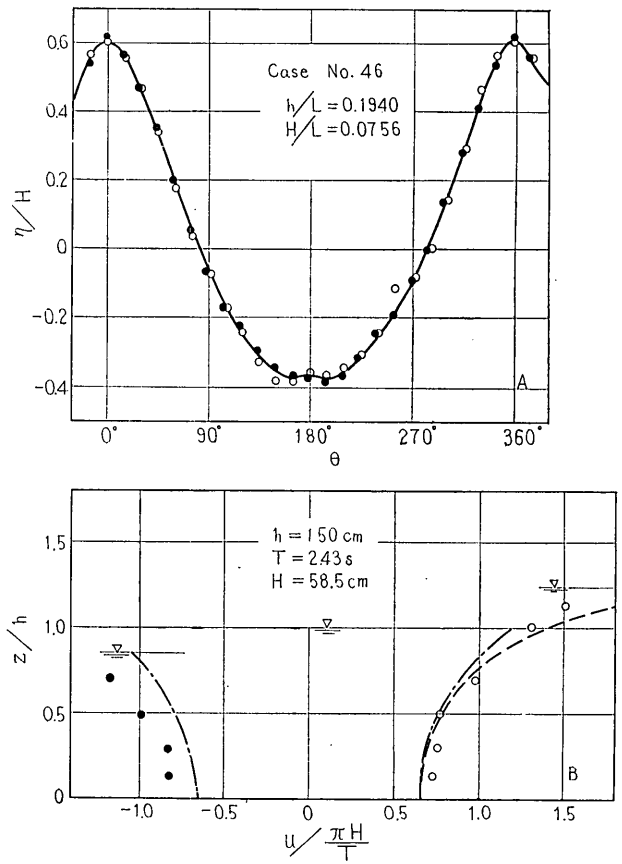
Case No. 46
h/L = 0.1940
H/L = 0.0756
η/H
θ
A
h = 150 cm
T = 2.43 s
H = 58.5 cm
z/h
u/(πH/T)
B

Fig. A—6

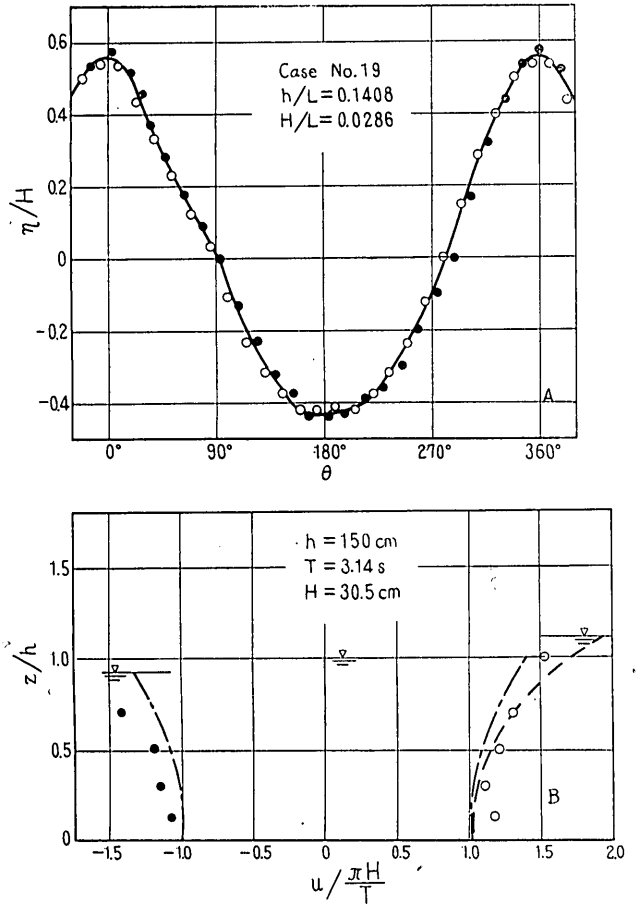
Case No. 19
h/L = 0.1408
H/L = 0.0286
η/H
θ
A
h = 150 cm
T = 3.14 s
H = 30.5 cm
z/h
u/(πH/T)
B

Fig. A—7

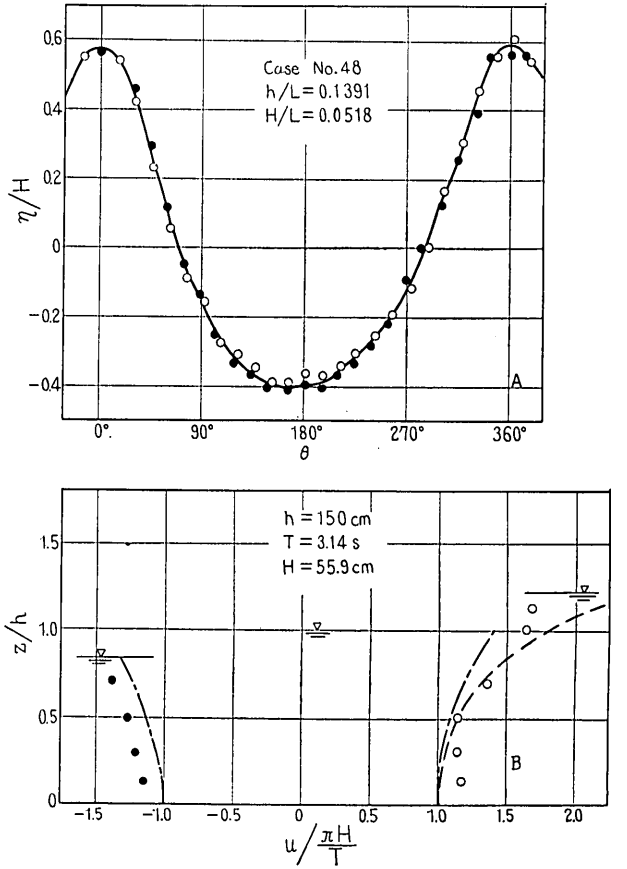
Case No. 48
h/L = 0.1391
H/L = 0.0518
η/H
θ
A
h = 150 cm
T = 3.14 s
H = 55.9 cm
z/h
u/(πH/T)
B

Fig. A—8

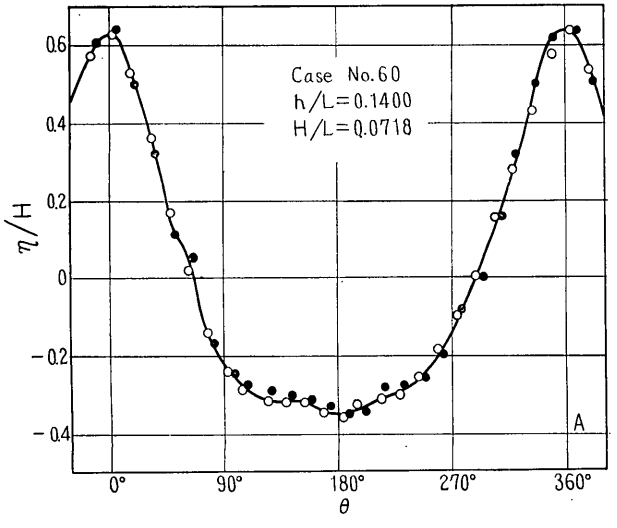

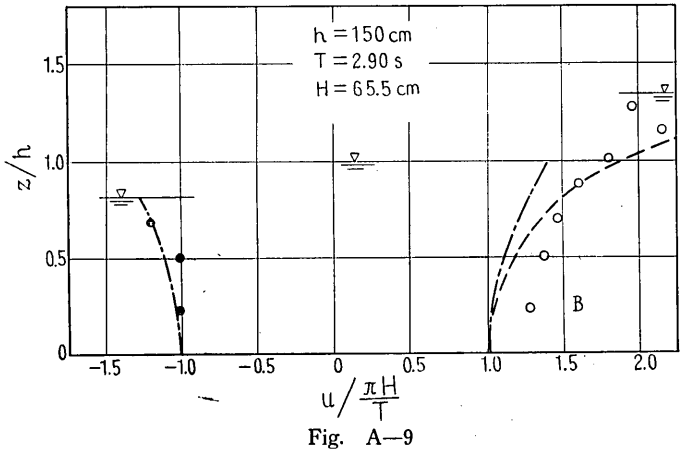

Fig. A—9

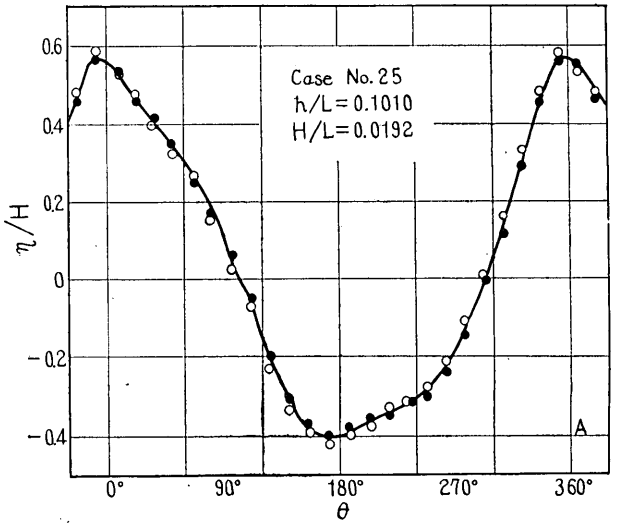

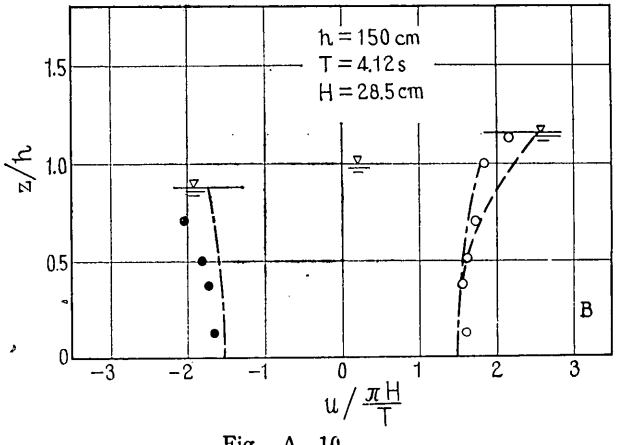

Fig. A—10

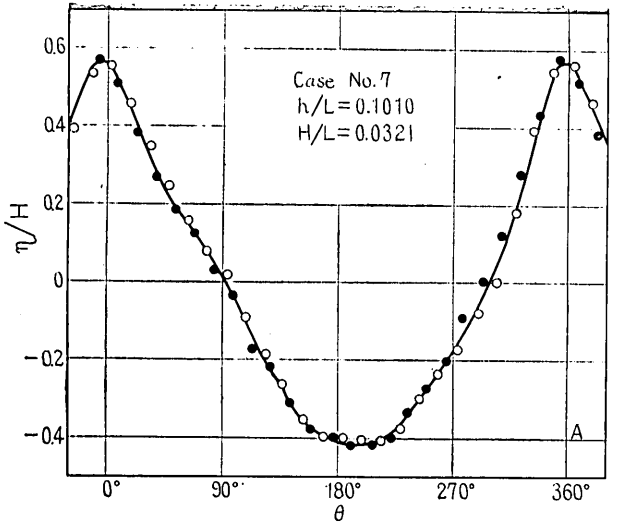

Fig. A—11

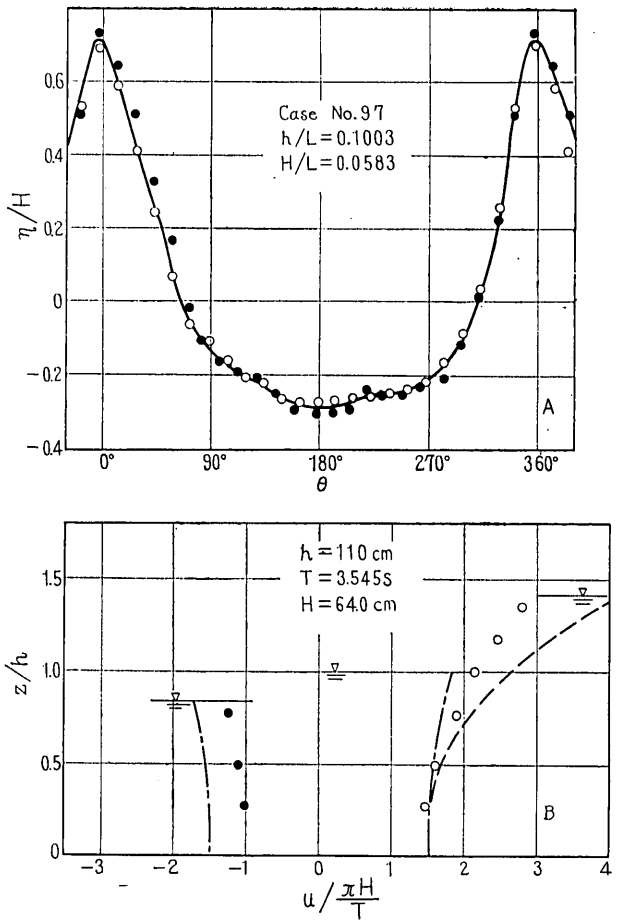

Fig. A—12

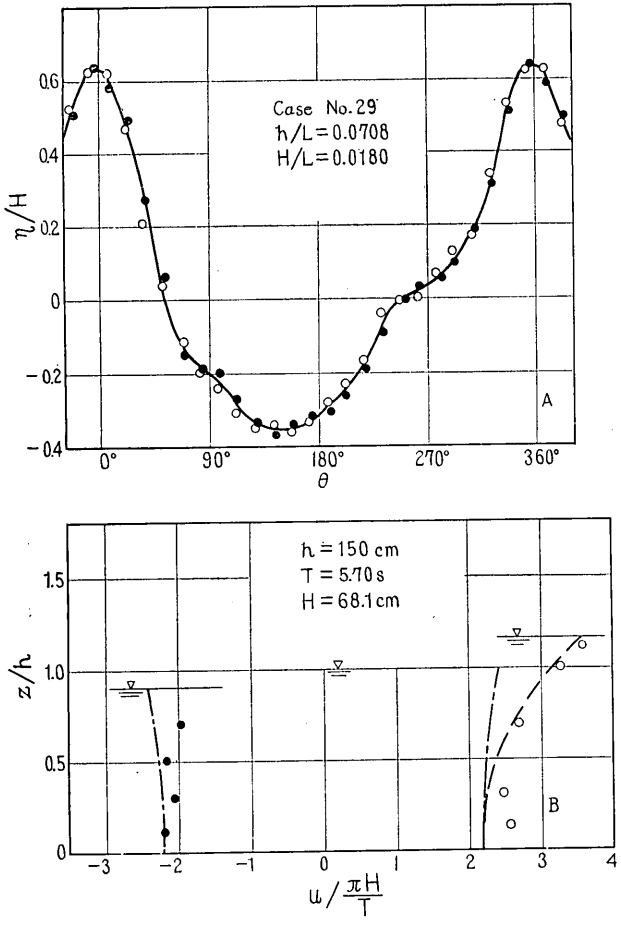

Fig. A—13

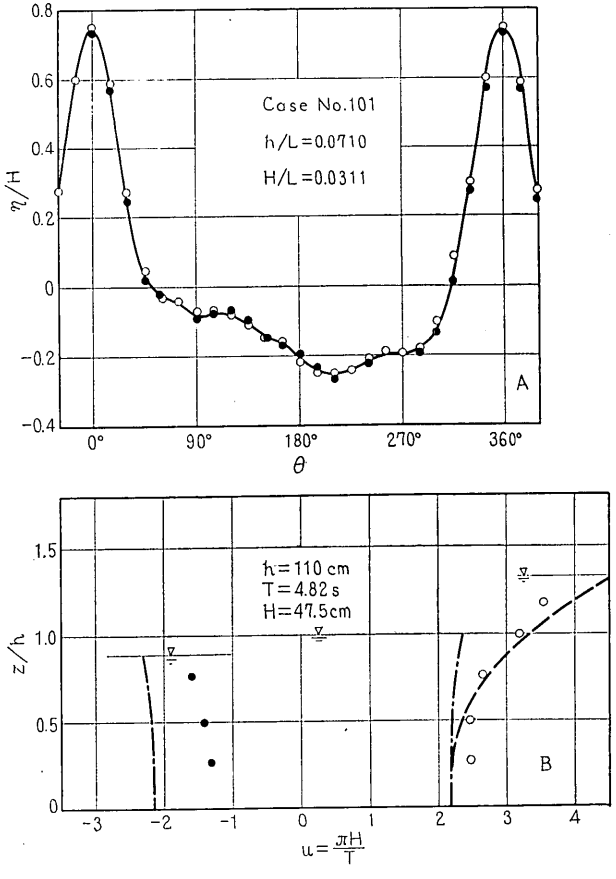

Fig. A—14

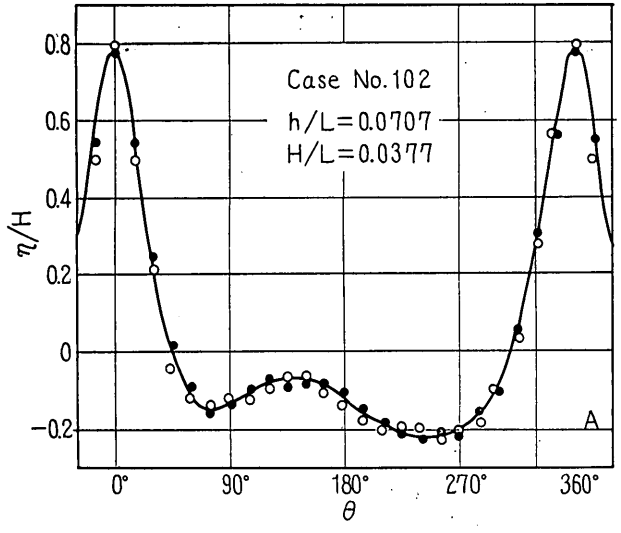

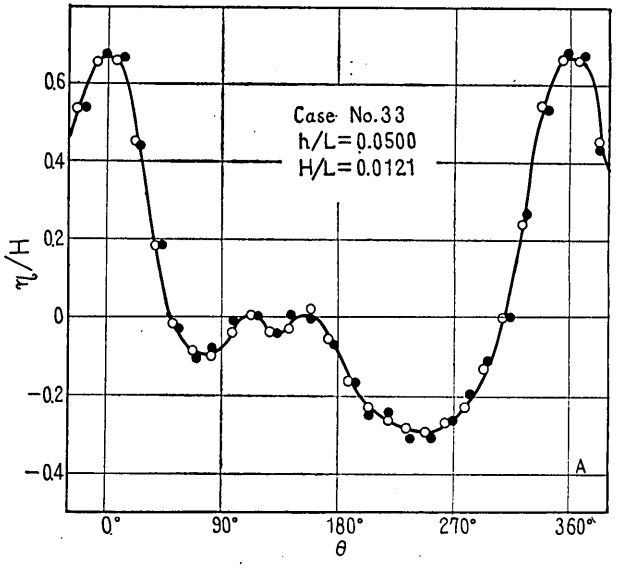

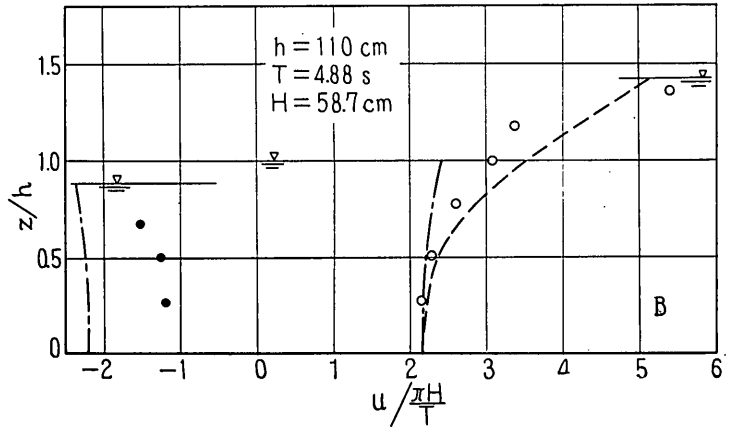

Fig. A—15

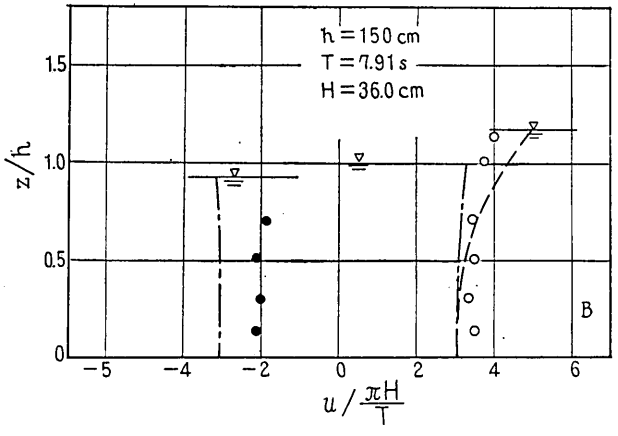

Fig. A—16

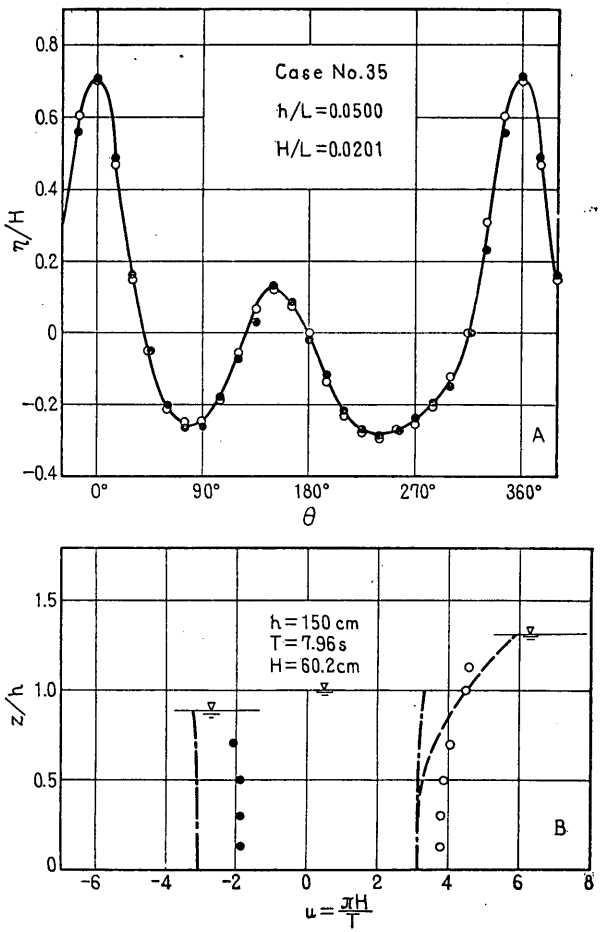

Fig. A—17

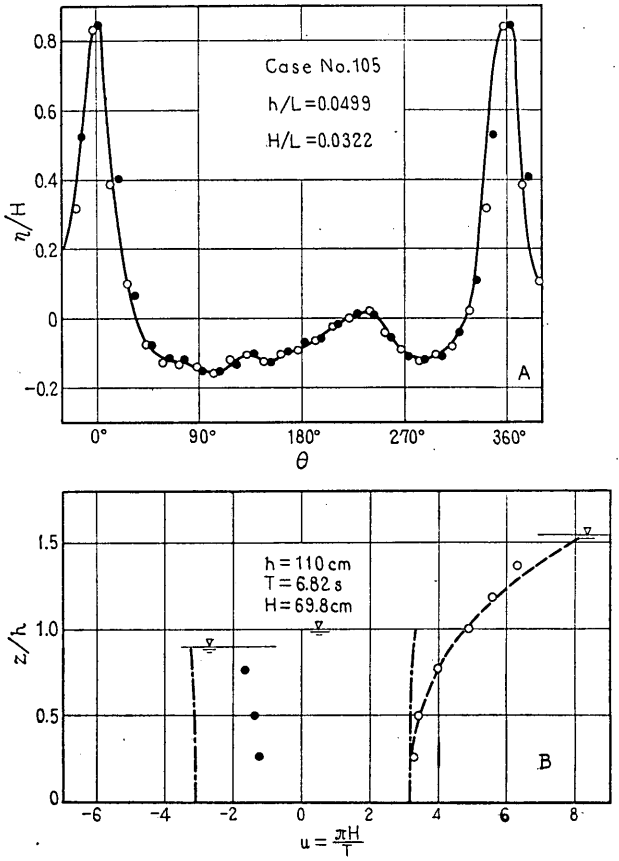

Fig. A—18